The role of paleogeography in Asian monsoon evolution: a review and new insights from climate modelling

D. Tardif, A.-C. Sarr, F. Fluteau, A. Licht, M. Kaya, J.-B. Ladant, N. Meijer, Y. Donnadieu, Guillaume Dupont-Nivet, C.T. Bolton, et al.

The role of paleogeography in Asian monsoon evolution: Associated a review and new insights from climate modelling

D. Tardif, A.-C. Sarr, F. Fluteau, A. Licht, M. Kaya, J.-B. Ladant, N. Meijer, Y. Donnadieu, G. Dupont-Nivet, C.T. Bolton, G. Le Hir, Q. Pillot, F. Poblete, P. Sepulchre, A. Toumoulin, W. Banfield

PII: S0012-8252(23)00153-8

DOI: https://doi.org/10.1016/j.earscirev.2023.104464

Reference: EARTH 104464

To appear in: *Earth-Science Reviews*

Received date: 23 January 2023

Revised date: 19 April 2023

Accepted date: 26 May 2023

Please cite this article as: D. Tardif, A.-C. Sarr, F. Fluteau, et al., The role of paleogeography in Asian monsoon evolution: Associated a review and new insights from climate modelling, *Earth-Science Reviews* (2023), https://doi.org/10.1016/j.earscirev.2023.104464

The role :of paleogeography in Asian monsoon evolution: associated a review:and new insights from climate modelling

D. Tardif[1,2,3,4], **A-C. Sarr**[1], **F. Fluteau**[4], **A. Licht**[1], **M. Kaya**[5], **J-B. Ladant**[3], **N. Meijer**[6], **Y. Donnadieu**[1], **G. Dupont-Nivet**[7,8], **C.T. Bolton**[1], **G. Le Hir**[4], **Q. Pillot**[1], **F. Poblete**[9], **P. Sepulchre**[3], **A. Toumoulin**[10], **W. Banfield**[1]

[1]Aix Marseille Univ, CNRS, IRD, INRAE, CEREGE, Aix-en-Provence, France

[2]IRD, DIADE, University of Montpellier, Montpellier, France

[3]Laboratoire des Sciences du Climat et de l'Environnement, LSCE/IPSL, CEA-CNRS-UVSQ, Université Paris-Saclay, 91191 Gif-sur-Yvette, France

[4]Université Paris Cité, Institut de physique du globe de Paris, CNRS, F-75005 Paris, France

[5]Department of Geological Engineering, Middle East Technical University, Ankara, Turkey

[6]Senckenberg Biodiversity and Climate Research Centre (SBiK-F), Senchenberganlage 25, D-60325 Frankfurt am Main, Germany

[7]Géosciences Rennes, UMR CNRS 6118, Univ Rennes, Rennes, France

[8]Institute of Geosciences, Potsdam University, Potsdam, Germany

[9]Departamento de Geología, Facultad de Ciencias Físicas y Matematicas, Universidad de Chile, Chile

[10]Department of Botany and Zoology, Faculty of Science, Masaryk University, Brno, Czech Republic

Corresponding author: Delphine Tardif, delphine.tardif@lsce.ipsl.fr

Corresponding author: Anta-Clarisse Sarr, anta-clarisse.sarr@univ-grenoble-alpes.fr

Abstract

The Asian monsoons are triggered by complex interactions between the atmosphere, Asian and African orography, and the surrounding oceans, resulting in highly seasonal climate and specific regional features. It was thought that the Asian monsoon was established during the Neogene, but recent evidence for monsoon-like precipitation seasonality occurring as early as the Paleogene greenhouse period challenges this paradigm. The possible occurrence of monsoons in a climatic and paleogeographic context very different from the present-day questions our understanding of the drivers underpinning this atmospheric phenomenon, in particular with regard to its dependence on geography. In this study, we first take advantage of the wealth of new studies to tentatively draw an up-to-date picture of Asian tectonic and paleoenvironmental evolution throughout the Cenozoic. We then analyze a set of 20 paleoclimate simulations spanning the late Eocene to latest Miocene ($\sim$ 40-8 Ma) in order to better understand the evolution of the distinct Asian monsoon subsystems. At odds with the traditional view of a monsoonal evolution driven mainly by Himalayan-Tibetan uplift, our work emphasizes the importance of peripheral mountain ranges in driving the evolution of Asian climate. In particular, the uplift of East African and Anatolian-Iranian mountain ranges, as well as the emergence of the Arabian Peninsula, contribute to shaping the modern South Asian summer monsoon. We also suggest that East Asian monsoon establishment and the aridification of inland Asia are driven by a combination of factors including increasing continentality, the orographic evolution of the Tibetan Plateau, Mongolia, Tian Shan and Pamir, and pCO_2 decrease during the Cenozoic.

1 Introduction

The South and East Asian monsoons (SAM and EAM) are highly seasonal climatic phenomena that today support the livelihoods of billions of people. During summer, the Arabian Platform and the Southern Asian continent overheat compared to adjacent Indian and Western Pacific Oceans. These continental masses become the locus of a wide low pressure belt, leading to a regional amplification of the Inter Tropical Convergence Zone (ITCZ) seasonal latitudinal migration, and to the formation of the Somali Jet along the East African coast (Fig. 1). This strong cross-equatorial flow steers low-level moist air from the Indian Ocean to the Asian continent and triggers nutrient-rich upwelling in the western Arabian Sea (Schott & McCreary, 2001; Lévy et al., 2007; Curry et al., 1992). Over the Bay of Bengal, this large scale circulation splits into two branches (SI Fig. 14 f). First, the Indo-Gangetic Low Level Jet (Acosta & Huber, 2017) bifurcates towards northern India and drives important orographic precipitation on the Himalayan foothills during the South Asian summer monsoon (SASM). The second branch continues towards eastern Asia (SI Fig. 14 f) and ascends over northwesterly air masses related to the Jet Stream in the subtropics (Kong et al., 2017; Molnar et al., 2010; Sampe & Xie, 2010), forming the Meiyu-Bayu front, a band of strong convective precipitation stretching from Myanmar to Japan, characterizing the East Asian summer monsoon (EASM) (Ninomiya & Shibagaki, 2007). The front progressively migrates northward during spring and summer, following the Jet Stream's seasonal displacement relative to the Tibetan Plateau (TP): it is located south of the TP in winter and moves to its northern edge in summer (Schiemann et al., 2009). In winter, the temperature and pressure gradients between the Asian continent and the neighboring oceans reverse, as a consequence of the lower troposphere strong radiative cooling over snow-covered Asia (Jeong et al., 2011; Cohen et al., 2001; Jhun & Lee, 2004). The Siberian High, a wide anticyclone, develops over the Mongolian

Plateau (L. Wang & Chen, 2014) (SI Fig. 14 j), flanked by two oceanic low pressure centers, the Aleutian Low (over the Northwestern Pacific Ocean), and the Maritime Continent Low (over the equatorial Western Pacific Ocean). The East Asian winter monsoon (EAWM) results from these pressure patterns, which drive the advection of cold, dry and dust-laden air masses from inland Asia to Eastern and Southern Asia (Fig. 1).

The spectacular extent and intensity of the Asian monsoons, combined with the highly dynamic tectonic context of the region, have triggered a lot of interest within the scientific community, in order to understand potential links between orography, land-sea distribution and Asian climate evolution. The Asian monsoons have long been viewed as an atmospheric phenomenon intimately intertwined with the Himalayan-Tibetan Plateau uplift history (e.g. Molnar et al., 1993; Zhisheng et al., 2001; Tada et al., 2016; X. Liu, Guo, et al., 2015). Records of strong upwelling initiating in the Arabian Sea at $\sim$8 Ma (Kroon et al., 1991) and, later, evidence for important dust deposition on the Chinese Loess Plateau since $\sim$22 Ma (Guo et al., 2002) have rooted the origin of the Asian monsoons in the Neogene. However, a wealth of recent studies challenge this paradigm. Aeolian dust deposits in northeastern Tibet, as well as paleobotanical and isotopic data indicating a seasonal climate in Myanmar and China (Licht et al., 2014; Sorrel et al., 2017; Fang et al., 2021; Zheng et al., 2022; Meng et al., 2018; Y. Xie et al., 2022) have been interpreted as evidence for an active monsoon as early as the late Eocene (see Fig.2 for a summary of available paleoclimate indicators). A potential Paleogene origin for the Asian monsoons questions the traditional view of monsoon development in relation to the Himalayan-Tibetan Plateau uplift history. First, because the Paleogene exhibited a generally warmer and ice-free climate compared to the Neogene (Westerhold et al., 2020). And second, because most modern Asian mountain ranges were in the early stages of their uplift history, and Asian continentality was

lower due to the presence of the Paratethys Sea to the west (Kaya et al., 2019) and higher global sea level (see late Eocene paleogeography in Fig. 3 a).

Climate modeling provides a unique opportunity to individually test the effect of each potential forcing factor on the resulting climate. For instance, model studies have overall tended to highlight that paleogeography out-competes global pCO_2 variations or far-field ice-sheet effects in driving the initiation and intensification of the SAM and EAM over multi-million years time scales (e.g. Farnsworth et al., 2019; J.-Y. Lee et al., 2015; Zoura et al., 2019; Roe et al., 2016; Thomson et al., 2021), independently of the model complexity, resolution, or type of geography (derived from modern or more realistic paleogeography). Sensitivity experiments of increasing complexity and resolution have helped disentangle the effect of the Himalaya-Tibet (and its sub-units) uplift from that of peripheral landforms, such as the Tian Shan ranges, the Anatolian-Iranian orogen, or the Eastern African and Mongolian landforms (H. Tang et al., 2013; Acosta & Huber, 2020; R. Zhang, Jiang, & Zhang, 2017), and from the effect of changes in land-sea distribution (Fluteau et al., 1999; Z. Zhang et al., 2007). While modeling studies provide a mechanistic basis to test potential drivers for monsoons and aridity, robust knowledge of the timing and evolution of paleogeography and paleoclimate remains of paramount importance to understanding the complex Cenozoic history of Asian monsoons. The past decade has been rich in both modeling and field studies, with for example the extension of marine sediment cores back to the Paleogene in the oceans surrounding Asia (see synthesis by Clift et al. (2022)), the increased coverage of well-dated terrestrial paleoclimate indicators from the Asian continent, and new constraints on Cenozoic tectonic and paleoclimate evolution in Asia.

In this contribution, we build upon previous work (Sarr et al., 2022; Tardif et al., 2020; Barbolini et al., 2020) to provide a comprehensive spatial and temporal picture of large-scale wind

circulation, precipitation seasonality, and aridity in continental Asia from the late Eocene to the late Miocene, using up-to-date paleoclimate simulations. In the following sections, we first synthesize Asian monsoon history, as understood from proxy and modeling perspectives, and highlight the remaining outstanding questions (section 2, Fig. 2). Then, we compile a summary of the main paleogeographic events that affected continental Asia and the regions surrounding the Indian Ocean during the Cenozoic (section 3). We further introduce the late Eocene to late Miocene paleogeographic configurations used to run the climate model (Fig.3), as well as the criteria used to track Asian monsoon evolution throughout the different simulations (section 4). Our modeling results are analyzed and discussed in light of current knowledge.

Figure 1. Asian orography (www.geomapapp.org), landforms (black labels), geographical regions (white labels), basins, oceanic drilling sites and seasonal winds, with the following abbreviations: EAWM - East Asian winter monsoon, SASM - South Asian summer monsoon, EASM - East Asian summer monsoon, IGLLJ - Indo-Gangetic Low Level Jet, STP - Southern Tibetan Plateau, NETP - Northeastern Tibetan Plateau, IBR - Indo-Burman Ranges, SBR - Sino-Burman Ranges, CLP - Chinese Loess Plateau. Numbered localities: (1) Huadian B., (2) Qingjiang B., (3) Jianghan B., (4) Xining B., (5) Lanzhou B., (6) Qaidam B., (7) Hoh Xil B., (8) Nangqian B., (9) Markam B., (10) Bayanhot B., (11) Valley of Lakes, (12) Taatsin Gol, (13) Ili B., (14) Issyk Kul B., (15) Tajik B., (16) Zhangpu, (17) Tianshui B., (18) Weihe B., (19) Zaysan B.

2 Evidence for increasingly old Asian monsoons

The classical view of Asian paleoenvironmental evolution during the Cenozoic proposes a transition from a Paleogene “zonal climatic pattern” to a Neogene “monsoonal climatic pattern”

(Guo et al., 2008; X. Sun & Wang, 2005; Jia et al., 2003; F. Wu et al., 2022). The zonal pattern is described as a widespread arid to semi-arid band stretching across China and bracketed in its southern and northern borders by two humid belts, whereas the monsoonal pattern consists of a core of pronounced aridity in the Asian interior, surrounded by monsoonal (seasonally wet) climate on its southern and eastern edges. This view is mostly based on paleoclimate proxy compilations (e.g. Boucot et al. (2013)) used to infer either humid (coal, indicators of forested environments, large mammals, etc.) or semi-arid to arid (evaporites, desert and shrub environments, etc.) conditions. Recent evidence for a highly seasonal climate in India, Myanmar and China as early as the Eocene, at least 20 Ma earlier than previously documented, nevertheless challenges this paradigm. This section comprehensively reviews the broad paleoenvironmental changes inferred from paleoclimate indicators in Asia from the late Eocene to the late Miocene, which are compiled in Figure 2 (upper panel). Localities and basins mentioned throughout the text are detailed in Figure 1.

Figure 2. upper Paleoclimate trends recorded in Asia. Bibliographic references in brackets are listed in SI Table 3 ; **center** Evolution of main landforms, seaways, ice sheets and pCO_2 during the Cenozoic overlain with values used in our reference simulations (elevations expressed in % of modern). White stars indicate parameters that were tested in the sensitivity experiments discussed in the text; **bottom** Overview of the main monsoon indicator evolution computed from simulations presented in this study. We use the following abbreviations: NETP (SETP) - Northeastern (Southeastern) Tibetan Plateau, CLP - Chinese Loess Plateau.

2.1 Eocene to Oligocene paleoenvironmental evolution

2.1.1 A progressive increase in summer monsoon indicators

The oldest evidence for strongly seasonal rainfall in Southern Asia comes from northwestern Indian early Eocene floras (Shukla et al., 2014; Bhatia, Khan, et al., 2021), as well as from mid-late Eocene ($\sim$ 40 Ma) floras and isotopic measurements in freshwater gastropod shells and mammal tooth enamel found in Myanmar (Licht et al., 2014; H. Huang et al., 2021). Both regions were however located between 0-10°N at this time (Shukla et al., 2014; Westerweel et al., 2019), and such precipitation seasonality is therefore mainly interpreted as a pronounced seasonal ITCZ migration rather than a monsoonal climate. Further east, in the Yunnan region (Southwestern China), which is today subject to a mixture of SAM and EAM influence, a shift from arid/semi-arid to humid environments is recorded during the late Eocene and interpreted as the onset of the Asian monsoon (Sorrel et al., 2017; Fang et al., 2021; Zheng et al., 2022). This climate transition is inferred by the presence of coal layers, a transition from xerophytic to mixed forest pollen assemblage, a change in lithology interpreted as lake and swamp expansions, as well as the occurrence of fossils of freshwater fish and large mammals. A seasonally wet monsoonal climate is also inferred from isotopic measurements in gastropods shells (Fang et al., 2021). The exact timing of this paleoenvironmental change is still debated between 41 and 35.5 Ma, but it nevertheless predates the Eocene-Oligocene Transition (EOT, $\sim$34 Ma). The proposed driving mechanisms of this regional climate shift involve either a threshold response to Tibetan Plateau elevation (Zheng et al., 2022), a side effect of the Paratethys Sea retreat in the west (that would have allowed more moisture penetration from the ocean) (Fang et al., 2021), or the global climate cooling initiated in the Middle Eocene and subsequent sea surface temperature changes (Sorrel et al., 2017).

Evidence for the presence of an EASM during the Eocene is also debated. In eastern China,

paleovegetation mostly points to warm, humid and weakly seasonal evergreen forested environments close to the coast (Spicer et al., 2016; X. Ma et al., 2012; Pound & Salzmann, 2017), except for late Eocene floras from Huadian (Meng et al., 2018) and Qingjiang Basins (Y. Xie et al., 2022), situated in northeastern and eastern China respectively, that already indicate highly seasonal rainfall. Further inland, towards the eastern TP, a gradual transition from humid to subhumid and/or seasonally dry paleoenvironments is suggested by botanical evidence (Han et al., 2022; Q. Li et al., 2022) and sedimentary records from various basins displaying an alternation of mudstone and evaporite deposits (D. Wang et al., 2013; Abels et al., 2011). High resolution deposits from the Jianghan Basin spanning the mid-Eocene to early Oligocene ($\sim$40-34 Ma) (C. Huang & Hinnov, 2019) show that the penetration of moisture into eastern China in the late Eocene was likely strongly modulated by orbital forcing. These pieces of evidence suggest that the classical Paleogene wet/dry zonal climatic pattern (Guo et al., 2008; X. Sun & Wang, 2005) was already periodically disturbed in the late Eocene, preceding the more widespread appearance of monsoon-like precipitation seasonality in the Oligocene.

Evidence for increased rainfall seasonality during the Oligocene to early Miocene becomes more common in floras from both China (X. Ma et al., 2012; Herman et al., 2017; Vornlocher et al., 2021; J. Ren et al., 2021; Miao et al., 2013; Ling et al., 2021; S. Li et al., 2018; C. Huang & Hinnov, 2019; H. Tang et al., 2020) and India (Bhatia, Khan, et al., 2021; Spicer et al., 2017; Srivastava et al., 2012). Additionally, paleoceanographic records from the adjacent Bay of Bengal and South China Sea have been used to track the SAM and EAM evolution from the middle Oligocene onwards. Records from the Ying-Qiong Basin (South China Sea) show an increase in terrigenous organic matter influx together with a higher proportion of tropical-subtropical angiosperm pollen at $\sim$25 Ma, interpreted as a sign of increasing EASM intensity (W. Ding et al.,

2021). In the Bay of Bengal (ODP Site 758), the radiogenic isotopic composition of clays indicates relatively constant weathering patterns over the last 27 Ma, and by inference stable SASM activity since at least the late Oligocene (S. Ali et al., 2021).

2.1.2 Late Eocene aridification in response to the Paratethys Sea retreat and global climate cooling

Markers of subhumid to arid climate are widespread in inland Asia in the Eocene, with many basins (e.g. Xining, Hoh Xil, Qaidam and Tarim) recording pollen assemblages characteristic of a steppe-desert environment (Q. Yuan et al., 2020; Miao, Wu, et al., 2016; X. Ma et al., 2012). During the mid-late Eocene ($\sim$40-34 Ma), inland Asia evolves towards even drier conditions, as suggested by increased proportions of xerophytic plants such as *Nitraria* and *Ephedra* in eastern and northeastern Tibet and in the Tarim Basin (Q. Yuan et al., 2020; Barbolini et al., 2020; Hoorn et al., 2012; Miao, Wu, et al., 2016), $\delta^{18}O$ measurements on oyster shells in the Tarim Basin (Bougeois et al., 2018), decreasing saline lakes in the Xining Basin (Abels et al., 2011), reduced chemical weathering observed in the Qaidam and Xining Basins (Fang et al., 2019), $\delta^{2}H$ isotope analyses on sedimentary leaf waxes *n-alkanes* in the Qaidam Basin (M. Wu et al., 2021) and lipid biomarkers and carbon isotopic compositions from bulk sediments in the Nangqian Basin (J. Wei et al., 2022). The presence of detrital material identified as Asian dust in sediments from the central North Pacific (GPC3 and ODP Site 1215) since $\sim$40 Ma also likely indicates the presence of dry conditions on land (Pettke et al., 2002; D. Rea et al., 1985; Ziegler et al., 2007).

This late Eocene aridification episode could result from a reduced westerly moisture input following two successive Paratethys Sea regression phases from the Tarim and the Tajik Basins

between ~41-37 Ma (Carrapa et al., 2015; J. Sun et al., 2020, 2022; Bougeois et al., 2018; Bosboom et al., 2014b; Kaya et al., 2019). High resolution sedimentary records, such as those of the Xining Basin (northeastern Tibet), exhibiting good correlation between wetter saline lake deposits during Paratethys Sea transgressions (Meijer et al., 2019; Bosboom et al., 2014a), confirm the key role played by the westerlies and the Paratethys Sea as a major moisture source for inland Asia in the Eocene. Additionally, the strong obliquity cyclicity imprinted on Xining evaporite/mudflat alternations in the late Eocene (40-34 Ma), coeval with the appearance of loess-like dusts in the alluvial mudflats (Meijer et al., 2021; Licht et al., 2014), hint at a marked influence of high latitude dynamics (incipient polar ice-sheets, variations in the Siberian High intensity) on winter inland Asian climate at that time (Abels et al., 2011; Xiao et al., 2010; Meijer et al., 2021).

2.1.3 Oligocene climate evolution and inception of modern Asian deserts

In the early Oligocene, a few sites situated within the westerly moisture area display increased humidity, recorded by $\delta^{18}O$ isotopic measurements in pedogenic carbonates in the Tarim and western Qaidam Basins (Kent-Corson et al., 2009), together with $\delta^{2}H$ measurements in leaf waxes (M. Wu et al., 2021). Leaf fossil CLAMP analysis (Climate Leaf Analysis Multivariate Program (Feng & Poulsen, 2016; Wolfe, 1993; Jacques, Su, et al., 2011)), further suggest a rather wet (but not monsoonal) rainfall regime in western Qaidam (Song et al., 2020). On the other hand, evidence for a drier climate is reported within the EAM domain by $\delta^{18}O$ isotopic measurements in pedogenic carbonates from eastern Qaidam (Y. Sun et al., 2020; Kent-Corson et al., 2009) and in Lanzhou Basin in the Chinese Loess plateau area (B. Li et al., 2016). CLAMP analysis on fossil leaves in the Lanzhou (Miao et al., 2013) and southeastern Tibetan Markam

Basin (T. Su, Spicer, et al., 2019) advocate for an increased (and monsoon-like) precipitation seasonality due to the TP uplift. Interpretations for this climatic trend in eastern China suggest that it may indicate either decreased EASM rainfall due to global cooling after the EOT (M. Wu et al., 2021) or increased winter aridity due to the Paratethys Sea retreat and/or to global sea level fall after the EOT (B. Li et al., 2016).

In Inner Mongolia (Taatsin Gol region), $\delta^{18}O$ and $\delta^{13}C$ isotopic measurements in pedogenic carbonates indicate aridification since the early Oligocene (Caves Rugenstein et al., 2014) and possible loess occurrence as early as $\sim$34 Ma (J. Sun & Windley, 2015). Proposed mechanisms for this drying involve increased continentality due to Paratethys Sea retreat at 34 Ma (J. Sun & Windley, 2015) and an early Hangay Dome uplift that would have acted as a barrier to moisture advection from Siberia to Mongolia as early as the Oligocene (Caves Rugenstein et al., 2014). However, high resolution records reveal several pulses of aridification at $\sim$34-33, $\sim$31, $\sim$28 and $\sim$23 Ma, coeval with periods of ice-sheet expansion, suggesting that these cooling phases were likely the main drivers of Mongolian hydrological dynamics (Baldermann et al., 2021). Further south, in the Gobi region (Bayanhot Basin), two bursts of aridification inferred from environmental magnetic, mineralogical and geochemical data at $\sim$31 and $\sim$28 Ma further hint at an influence of high latitude ice-sheet fluctuations on Mongolian Oligocene climate (Wasiljeff et al., 2022).

In the mid to late Oligocene, eolian dust deposits are documented in three major sites (see Meijer et al. (2021) for a review), namely the Chinese Loess Plateau, from $\sim$29 Ma onwards (Garzione et al., 2005; Qiang et al., 2011), the Tarim Basin at $\sim$27-22 Ma (Zheng et al., 2015), and the Junggar Basin at $\sim$24 Ma (J. Sun et al., 2010). Aridification is also inferred from $\delta^{18}O$ isotopic measurements in oysters and pedogenic carbonates from the Tarim Basin at $\sim$25 Ma

(Bougeois et al., 2018; Kent-Corson et al., 2009) and from isotopic records in stromatolites from the Junggar Basin, loosely dated to the early Miocene (W. Yang et al., 2019). This second step of aridification is coeval with $\delta^{18}O$ and $\delta^{13}C$ isotopic measurements from pedogenic carbonates suggesting increased orographic precipitation in the Issyk Kul and Ili Basins, both situated on the western side of the Tian Shan ranges (Hellwig et al., 2018; Macaulay et al., 2016). Collectively, these observations are interpreted as an indication of an uplift episode of the Tian Shan-Pamir ranges, which would have started shielding the Tarim and Junggar Basins from westerly moisture input and favored their aridification (Bougeois et al., 2018; W. Yang et al., 2019). This late Oligocene to early Miocene aridification of the Asian interior is also depicted in several oceanic records, where an increase in dust mass accumulation rates is recorded in the Pacific at $\sim$25 Ma (Site GPC3) (D. K. Rea, 1994; Pettke et al., 2002) and at $\sim$22 Ma (ODP Site 1215) (Ziegler et al., 2007).

A reduction in $\Delta\delta^{13}C$ coeval to an increase in bulk sediment Mn/Fe and Mn/Ti and foraminiferal Mn/Ca in the eastern Arabian Sea at $\sim$23 Ma (NGHP01 Site), reflecting an increase in water column mixing and ventilation, are considered as further evidence for the existence of a proto winter monsoon wind system (Beasley et al., 2021).

2.2 Evolution of seasonal and regional monsoons in the Neogene

The better coverage in both continental and marine records in the Neogene allows drawing a more precise picture of monsoon evolution during the Late Cenozoic. This section reviews the many pieces of evidence which now tend to support a scenario of diachronous evolution of regional monsoons, with a decoupling between summer and winter seasons as well as between monsoon-like precipitation seasonality and monsoon-like wind circulation establishment.

2.2.1 Neogene South Asian monsoon variations

The occurrence of monsoon-like rainfall seasonality in the eastern SAM domain is attested to by relatively constant isotopic composition of clays derived from silicate weathering since ~27 Ma in the central Bay of Bengal (ODP Site 758) (S. Ali et al., 2021). Middle Miocene (~13 Ma) plant macrofossils from northeasternmost India (Arunachal Pradesh) also attest to modern-like rainfall seasonality at that time (Khan et al., 2014). In Yunnan, the disappearance from the fossil record of *Metasequoia*, a plant whose modern descendant is intolerant to dry winters, may further attest to a SAM rainfall seasonality intensification after the middle Miocene (L. Wang et al., 2019). On the other hand, plant macrofossils and pollen from the northwestern SAM domain (Nepal, northwestern India and Pakistan) show a progressive vegetation shift from evergreen to deciduous forests from the middle to the latest Miocene, and finally to C4 grasslands (Hoorn et al., 2000; Bhatia et al., 2022; Bhatia, Srivastava, et al., 2021; Srivastava et al., 2018; Tauxe & Feakins, 2020; Vögeli et al., 2017; Sanyal et al., 2004). This vegetation change is also recorded in bulk sediments, leaf waxes, pollen and macrofossils in the Arabian Sea at ~8-7 Ma (ODP Site 722 and IODP Site U1457, (Feakins et al., 2020; Y. Huang et al., 2007; Clift et al., 2022)), and in the Bengal fan at ~7-6 Ma (ODP Sites 717/718, (Polissar et al., 2021)).

Chemical weathering and sediment accumulation rates from both the Indus Fan and the Bay of Bengal suggest that SASM precipitation reached a maximum in the middle Miocene (~16-10 Ma) before declining between ~8-3 Ma (Clift et al., 2008, 2019; Zhou et al., 2021). This has been suggested to reflect an intensification of the SAWM (S. Ali et al., 2021), possibly concomitant with a weakening of the SASM (J. Lee et al., 2020). Wind proxies also point to the presence of a seasonal wind reversal, and corroborate the existence of a winter monsoon since the

middle Miocene. In the Arabian Sea, an increased relative abundance of the foraminifera *Globigerina Bulloides* in the sediments was initially used to infer an intensification (or an onset) of the SASM wind circulation at $\sim$8 Ma (Kroon et al., 1991), based on the assumption that stronger monsoonal winds would translate into stronger upwelling activity. Those records have since been extended back in time (Bialik et al., 2020; Zhuang et al., 2017; Gupta et al., 2015) and combined with the analysis of current-controlled drift sediments and geochemical tracers from the Maldives archipelago (Betzler et al., 2016). These new studies now point to the establishment of a proto SAM wind circulation in the late Oligocene ($\sim$25 Ma), and of its reinforcement in the middle Miocene ($\sim$13-10 Ma) (Betzler et al., 106; Zhuang et al., 2017; Bialik et al., 2020). Strong SAM wind circulation since at least 10 Ma is also supported by export productivity and sediment accumulation patterns from records in the southern Bay of Bengal (IODP Site U1443) (Bolton et al., 2022), together with clay mineralogy in the Andaman Sea (IODP Site 1447) (J. Lee et al., 2020) and isotopic and chemical analyses on sediments in the eastern Arabian Sea (IODP Site 1456) (Tripathi et al., 2017)). An intensification of the SAM in the late Miocene ($\sim$8-7 Ma) has also been inferred based on an increase in percent in *G. Bulloides* and Total Organic Carbon content in sediments from Oman margin (Gupta et al., 2015) but remains debated, as it is not observed in all paleoceanographic records from the Arabian Sea and the Bay of Bengal (Bolton et al., 2022; Tripathi et al., 2017; Betzler et al., 2016; Y. Huang et al., 2007).

2.2.2 East Asian Summer Monsoon evolution in the Neogene

Summer precipitation typical of the EASM likely occurred throughout the Neogene, as shown by records from the South China Sea such as weathering indices (Clift et al., 2008, 2014), $\delta^{13}C$ measurements in black carbon (Jia et al., 2003), pollen, biomarkers, kerogen maceral

composition and clay mineralogy (W. Ding et al., 2021). On land, $\delta^{18}O$ values from paleosol carbonates in the Chinese Loess Plateau (Suarez et al., 2011) and most Chinese paleobotanical and palynological data suggest summer precipitation amounts comparable to modern (Q. Wang et al., 2021; Yao et al., 2011; Xing et al., 2012; Hui et al., 2021; B. Wang et al., 2021; Q.-g. Sun et al., 2002). Many localities nevertheless point to wetter winters due to weaker winter monsoons until the late Miocene (Q. Wang et al., 2021; Liang et al., 2022), except for the mid-Miocene Zhangpu biota flora (southeastern China), whose CLAMP signature shows affinities with EAM and SAM floras, thus suggesting adaption to modern-like rainfall seasonality (B. Wang et al., 2021). A warm and wet period has been identified during the Middle Miocene Climatic Optimum ($\sim$17-14 Ma) in both continental as well as oceanic records and was likely less seasonal than during the rest of the Miocene (Clift et al., 2022). The penetration of EASM moisture would have reached as far as the Qaidam Basin, as suggested by lotus fossils (Luo et al., 2022), increased abundance of *Fupingopollenites*, an extinct palynomorph highly dependent on summer moisture (Miao, Song, et al., 2016), and characterization of iron oxides from the Chinese Loess Plateau (H. Zhao et al., 2020). This warm and wet mid-Miocene climate peak is also inferred from chemical weathering proxies and indicators of stronger physical erosion and fluvial input measured in sediments from the South China Sea at 15-12 Ma (Clift et al., 2014), and from $\delta^{13}C$ in black carbon at 15 Ma (Jia et al., 2003).

The variations in EASM intensity during the late Miocene and Pliocene remain controversial in both continental and marine records, with variations in the suggested timing of changes (Clift et al., 2022). A decline in EASM intensity induced by decreasing pCO_2 after the Mid-Miocene Climate Optimum is suggested by weathering, paleoceanographic indices and pollen from the South China Sea (ODP Site 1146) (Clift et al., 2014; Holbourn et al., 2021, 2018;

Miao et al., 2017; Wei et al., 2006), as well as pollen records from the Liupan Mountains (North China) (Jiang & Ding, 2008). On the other hand, in the South China Sea, late Miocene EASM intensification is inferred from $\delta^{18}O$ and Mg/Ca derived records of surface and sub-surface water characteristics (IODP Site U1501) (C. Yang et al., 2021) and by black carbon $\delta^{13}C$ (Jia et al., 2003). In China, wetter conditions during the latest Miocene are suggested by mineralogical, chemical and magnetic analysis of sedimentary deposits in the Chinese Loess Plateau (Ao et al., 2016, 2021; H. Zhao et al., 2020), pollen records from the Tianshui (Hui et al., 2021) and the Weihe Basins (L. Zhao et al., 2020), and by fossil wood, mammals and fish in the Qaidam Basin (Cheng & Yang, 2016; X. Wang et al., 2007). EASM intensification at this time is usually attributed to global warming (Ao et al., 2021; H. Wang et al., 2019) and/or to Neogene TP uplift phases (Hui et al., 2021; X. Ren et al., 2020; H. Zhao et al., 2020).

2.2.3 Miocene-Pliocene aridification pulses in response to regional uplift

Throughout the Miocene, dust deposition continued in the Chinese Loess Plateau (Guo et al., 2002; Meijer et al., 2021), Tarim-Taklimakan (Kent-Corson et al., 2009; Zheng et al., 2015; Heermance et al., 2018) and Junggar Basins (J. Sun et al., 2010). After a phase of relatively wetter conditions during the Mid Miocene Climate Optimum (see section 2.2.2), a pronounced step-wise aridification was then recorded in most of inland Asia until the Miocene-Pliocene boundary (Lu et al., 2010; Lu & Guo, 2014; Z.-H. Tang & Ding, 2013). The timing of aridification pulses varies depending on the region and is attributed to either northeastern TP uplift (Miao et al., 2012), Altai and Tian Shan mountain uplift (Caves Rugenstein et al., 2014, 2017) and/or to late Miocene cooling (Lu et al., 2010; Lu & Guo, 2014; Peng et al., 2016). In the eastern part of inland Asia, encompassing the Chinese Loess Plateau, central China and northeastern TP, data provide strong

evidence for aridification, including pollen and biomarkers documenting a step-wise transition from a sub-humid to an arid environment starting at $\sim$15 Ma (J. Liu et al., 2016; Miao et al., 2011; Jiang & Ding, 2008; Peng et al., 2016), massive grassland expansions at $\sim$11-7 Ma (Suarez et al., 2011; Barbolini et al., 2020; Y. Ma et al., 2005; L. Zhao et al., 2020; H. Wang et al., 2019), widespread eolian dust deposition at $\sim$8-7 Ma (X. Ma & Jiang, 2015; Guo et al., 2002; Qiang et al., 2011; B. Li et al., 2016; Jiang et al., 2017), increased $\delta^{18}O$ of pedogenic carbonates and terrestrial mammal tooth enamel at $\sim$14-13 and $\sim$7-5 Ma (B. Li et al., 2016; Kent-Corson et al., 2009; M. Wu et al., 2021; W. Liu et al., 2014; Y. Sun et al., 2020; Kaakinen et al., 2006; Y. Wang & Deng, 2005), *n*-alkane analysis from Qaidam sediments since 13 Ma (Z. Liu et al., 2014) and the dominance of cold-aridiphilous mollusks in the Chinese Loess Plateau from 7-5 Ma (F. Li et al., 2008). The Tarim and Junggar Basins also provide multiple evidence for mid to late Miocene aridification, such as increased proportions of xerophytic plants and grass pollen at $\sim$7-5 Ma (J. Sun et al., 2010; J. Sun & Zhang, 2008; J. Sun et al., 2008; Z. Zhang & Sun, 2011; Barbolini et al., 2020), massive aeolian deposition in the western Tarim Basin at $\sim$12-7 Ma (Heermance et al., 2018) and the permanent drying of lakes in the eastern Tarim Basin at $\sim$5 Ma (W. Liu et al., 2014). The pedogenic carbonate $\delta^{18}O$ records of these regions nevertheless offer diverging patterns of evolution, that have tentatively been explained by their locations with respect to the Tian Shan and Altai mountains (Caves Rugenstein et al., 2017). Records from regions today lying upwind of the Tian Shan and Altai mountains, such as the Issyk Kul (Macaulay et al., 2016), Junggar (Charreau et al., 2012) and Zaysan Basins (Caves Rugenstein et al., 2017) exhibit a decline in $\delta^{18}O$ between 10-5 Ma, which has been interpreted as a shift to spring/fall precipitation following the uplift of the Altai and Tian Shan mountains (Caves Rugenstein et al., 2017). Perennial lake formation in the windward Ili Basin (Kazakhstan) at $\sim$10 Ma may further

attest that the Tian Shan ranges acted as an orographic barrier for westerlies moisture input (Frisch et al., 2019). On the other hand, records from the Tarim Basin, situated downwind of the Tian Shan ranges, display $\delta^{18}O$ trends similar to those of the Qaidam Basin (Kent-Corson et al., 2009) with increased values since $\sim$15 Ma peaking at $\sim$7-5 Ma and which are interpreted as indicating aridification at that time.

EAWM intensification is also recorded in the South China Sea at $\sim$15-12, $\sim$8-5 and $\sim$3 Ma, based on increased black carbon accumulation (whose transportation to the sea would be favored by stronger winter winds) (Jia et al., 2003), planktic and benthic $\delta^{18}O$ records and mixed layer temperatures (Holbourn et al., 2021, 2018), and clay mineralogy and grain size analysis (Wan et al., 2007). In the Sea of Japan, clay mineral assemblages and isotopic analyses of the silicate fraction covering the last 15 Ma suggest a stepwise drying of Central Asia at 12, 8 and 3.5 Ma (Shen et al., 2017). A sea surface temperature drop of $\sim$8 °C recorded between 8-6.6 Ma (IODP Site U1425) is further interpreted as a sign for a marked EAWM intensification (Matsuzaki et al., 2020). At approximately the same time (8-4 Ma), an analysis of aluminosilicate end-member contributions shows a shift from a Taklimakan source to a Gobi-Chinese Loess Plateau source in dust exported to the Sea of Japan (Site U1430), suggesting changes in winter wind circulation patterns, or in the extent of these deserts (Anderson et al., 2020). Further east, in the North Pacific, a relative increase in Asian dust is also recorded at $\sim$10 and $\sim$4 Ma (D. Rea et al., 1985; Pettke et al., 2002).

2.3 Assessing monsoon forcing factors through climate models

The major drivers of long-term monsoonal variability are topography, land-sea distribution and global climate variations. Attributing a specific change to one or several of these factors is

nevertheless complicated because they may co-vary, produce non-linear responses with potentially opposite effects, and are sometimes poorly dated or quantified. Modeling experiments, initially utilizing present-day geographies and boundary conditions, have enabled a better understanding of the role played by these different forcing factors in shaping the regional monsoons.

2.3.1 Topographic influences on the South and East Asian monsoon with present-day geography

The TP has long been considered instrumental in driving the Asian monsoonal circulation and precipitation, due to its elevated heated surface in summer acting as a "heat pump" driving the convergence of the surrounding air masses, in particular the ITCZ conveying moisture from the Indian Ocean (Kutzbach et al., 1993; Zou a et al., 2019; Molnar et al., 1993; Wu et al. 2012)). While the presence of the TP would indeed play a key role in the EASM establishment, with the heating of the Plateau inducing a cyclonic circulation anomaly promoting the advection of moist air masses towards Eastern Asia (Z. Zhang et al., 2007; H. Tang et al., 2013; R. Zhang, Jiang, & Zhang, 2017; Wu et al., 2012), several studies suggest that the orographic thermal forcing of the Plateau is not as important as previously thought for the SAM establishment. Instead, the physical barrier created by the topography would insulate the high moist static energy air (warm wet air masses) from the tropics from the low moist static energy air (cold dry air) brought by the westerlies and induces abundant orographic precipitations in northern India, through steering and forced ascension of moist air masses (Boos & Kuang, 2010, 2013; Acosta & Huber, 2020). Although the debate between a thermal versus mechanical role for TP on atmospheric flow is still ongoing, a consensus emerged for the need of having an energetic-based framework to study

monsoon mechanisms at all timescales (Biasutti et al., 2018), and integrate them within the planetary scale circulation dynamics (Rodwell & Hoskins, 1996). The condensation of moisture in these ascending air masses leads to important latent heat release in the high troposphere over northern India, which acts as a positive feedback sustaining summer convection and precipitation in South Asia (He, 2017). On the other hand, the large-scale advection of the ITCZ over Asia in late spring and early summer is essentially driven by surface ocean-continent temperature gradients and resulting pressure patterns (Acosta & Huber, 2020; Merlis et al., 2013). Additionally, numerical simulations show that such enhanced migration of the summer ITCZ is scaled to Asian continental extent, and was likely weaker in the past, when conditions of higher sea level and the presence of the Paratethys Sea prevailed and translated into surface temperature gradients different from today (Z. Zhang et al., 2007).

Smaller orographic features have also been shown to play a critical role in shaping and strengthening both the SAM and EAM. The East African highlands, positioned in the path of the ITCZ flow, impact both African and South Asian climate (Bannon, 1979; Rodwell & Hoskins, 1995; Sepulchre et al., 2006). Recent studies have specifically demonstrated that the East African highlands contribute greatly to the strengthening and concentration of the Somali Jet, but that their absence would result, somewhat counter-intuitively, in higher summer precipitation over the SAM region due to increased advection directly from the ocean to the continent (H.-H. Wei & Bordoni, 2016; Chakraborty et al., 2009). This last aspect hints that strong upwelling in the Arabian Sea, related to a strong Somali Jet, may not always be positively correlated with heavy rainfall on land. The Anatolian-Iranian landforms, by channeling the Somali Jet and insulating it from the subtropical dry westerly flow, greatly contribute to enhancing moisture transport towards India and eastern Asia (Acosta & Huber, 2020; He, 2017; H. Tang et al., 2013). Additionally, the

orographic precipitation observed over smaller Asian landforms, for example the Indian Ghats or the Indo-Burman ranges, have been shown to promote moisture advection and enhanced precipitation in adjacent regions located windward, especially over the Arabian Sea, Bay of Bengal and South China Sea (S.-P. Xie et al., 2006).

The effect of the Pamir, Tian Shan and northeastern TP uplifts on the SAM remains unclear. When these landforms are uplifted together with the Mongolian Plateau, a decrease in precipitation is simulated over India (H. Tang et al., 2013). On the other hand, increased rainfall is simulated in India while testing Pamir, Tian Shan and northeastern TP uplift but maintaining a low Mongolian Plateau (R. Zhang, Jiang, & Zhang, 2017; R. Zhang, Jiang, Zhang, Cheng, & Zhang, 2017), highlighting potential counter effects of those mountains on the Asian climate. The Pamir, Tian Shan and Mongolian landforms are also perfectly situated in the mid-latitudes to interfere both dynamically and thermally with planetary-scale atmospheric circulation. Numerical simulations show that their uplift enhances aridity in inland Asia (modern Gobi and Taklimakan deserts) and reinforces the EAWM circulation patterns (X. Liu & Yin, 2002; X. Liu, Sun, et al., 2015; Baldwin & Vecchi, 2016, Sato, 2009; R. Zhang, Jiang, Zhang, Cheng, & Zhang, 2017). By creating a cold pool and deviating the westerlies towards northern Siberia, the Mongolian orography has been proposed to be responsible for the northward migration of the subtropical Jet Stream in summer (White et al., 2017; Shi et al., 2015; Sha et al., 2020), and for most of the Siberian High location and intensity in winter (Sha et al., 2015; R. Zhang, Jiang, Zhang, Cheng, & Zhang, 2017).

2.3.2 Modeling experiments using paleogeographic reconstructions

Modeling studies based on present-day geographies are limited in the extent to which they

allow us to understand past changes, especially for periods when very different geographies prevailed. Paleoclimate simulations using presumed "realistic" paleo-boundary conditions are however rarer, because they usually entail high computational cost and require important background knowledge of past boundary conditions (paleogeography, CO_2, solar constant, ice-sheet volume). Such modeling experiments confirm that increasing Asian continentality during the Oligocene and the Miocene, either due to the Paratethys Sea retreat and/or global eustatic sea level fall, is a key driver of increased moisture advection towards Asia in summer (Fluteau et al., 199; Ramstein et al., 1997; Z. Zhang et al., 2014; Sarr et al., 2022). Under Oligocene conditions, the uplift of the peripheral Tian Shan, Pamir and northeastern portions of the TP has also been shown to promote inland Asian aridity, in contrast to the sole uplift of the central TP (R. Zhang, Jiang, & Zhang, 2017). Under late Eocene conditions, the latitude at which the proto TP uplifts significantly and non-linearly impacts East Asian climate; an uplift in the tropics ($\sim$11°N) induces precipitation on the TP foothills but aridification in most of China, whereas an uplift at its modern latitude ($\sim$26°N) increases moisture advection to eastern China and aridification in inland Asia (R. Zhang et al., 2018).

Paleoclimate modeling offers a contrasted view regarding Eocene climate, with some studies that simulate the presence of monsoonal climates at that time (Huber & Godner, 2012; Licht et al., 2014; Z. Zhang et al., 2022), and others that do not (Tardif et al., 2020; Z. Zhang et al., 2012; R. Zhang et al., 2018). Discrepancy among simulations can be attributed to many differences in model structure, resolution, parametrization and setting of boundary conditions, among which the choice of paleogeographic reconstruction is a key aspect. Indeed, many features of Eocene paleogeography remain highly controversial, such as the height of the incipient Tibetan topography, the shape of the Indo-Asian collision zone, the height of peripheral landforms, or the

land-sea distribution. Paleoclimate modeling has nevertheless emphasized the importance of geography, rather than pCO_2 variations or far-field ice-sheets effects, as the main driver of both SAM and EAM establishment and intensification on long time scales (Farnsworth et al., 2019; Thomson et al., 2021). Accurate paleogeographic constraints as well as a higher number of sensitivity experiments in a paleo framework are therefore needed, and this is what we intend to contribute with this study.

2.4 Summary: a diachronous establishment of SAM and EAM seasonal features, the influences of geography and topography and remaining uncertainties

The past decade has welcomed a large amount of new data based on fossil material and sedimentary archives, both onshore and offshore. The onset of the SAM, EASM and EAWM and their evolution are now clearly shown to be diachronous and is tightly linked to the evolution of land-sea distribution, topography and global climate over long time scales. Some questions, nevertheless, remain to be answered. First, it is unclear whether Paleogene records of highly seasonal precipitation at low latitudes (< 20°N) describe a monsoon in the strict sense, given that no wind proxies currently exist for this period and that Eocene paleoclimate modeling studies propose widely diverging scenarios. CLAMP paleobotanical analyses provide interesting insights on this point. They generally show that, although strong precipitation seasonality is likely present since the Paleogene in broad parts of Southeastern Asia (Bhatia, Khan, et al., 2021; Spicer et al., 2017; Herman et al., 2017), leaves did not develop the morphological features characteristic of plants growing in present-day SAM or EAM regions until the middle Miocene ($\sim$13 Ma) (Spicer et al., 2017; Bhatia, Srivastava, et al., 2021). Instead, Paleogene Asian floras display a signature

typical of the regions dominated by the ITCZ seasonal migration, also referred to as the Indonesian-Australian monsoon. The reorganization from an ITCZ-dominated to a monsoonal wind circulation pattern may have initiated in the Oligocene ($\sim$28-23 Ma, Fig. 2), according to fossils from northeastern India exhibiting a mixture of SAM and ITCZ leaf signatures (Spicer et al., 2017). These typical monsoonal signatures in floras were likely driven by a combination of both biotic and abiotic factors, although the CLAMP method is unable to disentangle the forcing factors responsible for these specific signatures. They do, however, add to the body of evidence suggesting that precipitation seasonality may have been established prior to typical monsoonal wind circulation.

Second, although modeling studies have started to explore the effects of localized mountain ranges on Asian climate in a paleo context, there is plenty of room for improvement. For example, the climatic impact of these landforms have often been investigated simultaneously in a single climate simulation (e.g. the uplift of the Tian Shan and Mongolian orogens), though the main uplift episodes of these landforms may not be coeval (see section 3.1.2). Various hypotheses remain to be tested, such as identifying the drivers of the Siberian High development, and its impact on inland Asian aridity. Indeed, the presence of loess-like deposits since the Eocene in the Xining Basin were tentatively explained by the presence of an active Siberian High at that time (Meijer et al., 2021; Licht et al., 2014). This questions whether the Tian Shan and/or Mongolian orogens are as important for this wide anticyclone as predicted by modeling experiments, since these landforms are thought to have uplifted later, in the Oligocene to late Miocene (see section 3.1.2). In addition, the notion of elevation thresholds is a key point to tackle, as strongly non-linear responses of atmospheric circulation with respect to this parameter are expected. These considerations highlight the need for an accurate representation of Asian paleogeographic

evolution in order to better understand monsoon history over long time-scales.

3 Cenozoic paleogeographic evolution

Although presenting a full literature review of paleogeographic evolution throughout the Cenozoic for the whole region of interest is outside the scope of this study, this section aims at providing an overview of the main features and persistent uncertainties regarding the paleogeographic evolution during the Cenozoic in our region of interest. This allows us to justify which sensitivity tests were performed on specific geographic units (Fig. 3), further introduced in section 4.2.1.

3.1 Indo-Asia collision and Asian topography evolution

The initiation of the Indo-Asian collision, marking the closure of the Neotethys Ocean, is dated around $\sim$58 Ma based on sedimentological and paleomagnetic evidence (van Hinsbergen et al., 2019; Ingalls et al., 2016). The morphology of the *Greater India* portion (i.e. northern India) before the collision remains unclear. Depending on the collision scenario considered (see Kappand DeCelles (2019); Poblete et al. (2021); J. R. Ali and Aitchison (2005) for reviews), it is represented as fully emerged (Ingalls et al., 2016; C. Wang et al., 2014), partially flooded or divided into two blocks separated by an oceanic basin until the middle-late Eocene (van Hinsbergen et al., 2012, 2019; W. Huang et al., 2015). From the Eocene onwards, the progressive migration of India to the north, its indentation into the Asian continent, and its counterclockwise rotation (Molnar et al., 2010) trigger widespread orographic changes in Asia, which are summarized below. The most important of these events is the TP and Himalayas uplift, and the growth of peripheral mountain

ranges such as the Pamir, Tian Shan and the Mongolian Plateau.

Figure 3. Paleogeographic configurations used in this study for the reference experiments (red box) and alternative configurations used for sensitivity tests. Blue star in (a) highlights the Paratethys Sea location, yellow star in (h) highlights the location of the Tethyan Seaway.

3.1.1 Himalayas-Tibetan Plateau uplift history

The early uplift history of the Tibetan Plateau is highly debated. Oxygen isotope paleoaltimetry studies suggest that the Gangdese (Southern TP, Lhasa terrane) and Qiangtang mountains (Central TP) were already as high as $\sim$4000-5000 m during the early Eocene (Rowley & Currie, 2006; L. Ding et al., 2014; Xu et al., 2013; Xiong et al., 2020; C. Wang et al., 2014). The robustness of this method is however questioned by isotope-enabled climate models, which demonstrate that factors other than elevation affect the $\delta^{18}O$ precipitation signature, including air mass provenance, climate, or water recycling (Poulsen & Jeffery, 2011; Botsyun et al., 2016). A revised TP paleo-elevation of most likely lower than $\sim$3000 m in the Oligocene has therefore been suggested (Botsyun et al., 2019). The presence of frost-intolerant fossil flora assemblages in the central TP in the middle Eocene (T. Su et al., 2020) and late Oligocene (T. Su, Farnsworth, et al., 2019), as well as clumped isotope measurements (Xiong et al., 2022) advocating for a subtropical climate in this region, also seem incompatible with a TP exceeding 4000 m. Therefore, a more complex morphology for this proto TP has been proposed, suggesting the presence of a low-elevation ($\sim$1500 m) valley dividing the almost fully uplifted ($\sim$3000-4000 m) Lhasa and Qiangtang terranes until the late Oligocene (T. Su, Farnsworth, et al., 2019; Xiong et al., 2020; Spicer et al., 2020; Xiong et al., 2022). In the periphery of the proto TP, data collected from

different basins offer contradictory interpretations. In southeastern Tibet, at the extremity of the Qiangtang terrane, paleo-elevation calculated using the CLAMP method suggests that the Markam Basin was already high in the late Eocene ($\sim$3000 m) and could have reached its modern elevation ($\sim$3900 m) by the earliest Oligocene (T. Su, Spicer, et al., 2019). Alternately, paleo-elevation based on oxygen isotopic measurements of the nearby Jianchuan Basin (part of the same terrane) could not have exceeded $\sim$1200 m in the late Eocene (Gourbet et al., 2017). The northern TP is proposed to have remained relatively low (<2000 m) in the Eocene, before uplifting in the Oligocene or the early Miocene, based on isotopic paleoaltimetry from the Hoh Xil Basin (C. Wang et al., 2014). An early uplift of the northeastern TP has been proposed as early as the late Eocene by increased coniferous pollen proportion in the Xining Basin (Hoorn et al., 2012), although global cooling and the Paratethys Sea retreat may also have promoted coniferous trees expansion in this region, without uplift (Barboni et al., 2020).

The history of the TP build-up from the Miocene onwards is less controversial. The Central TP is thought to have reached modern elevation by the early Miocene, while the northern TP uplift was completed by the late Miocene (C. Wang et al., 2014). Stratigraphy and detrital zircon analyses indicate that the western TP (Pamir-Karakoram-Hindu Kush) may have undergone several phases of uplift between the mid-Eocene to latest Miocene (Bershaw et al., 2012; L. Li et al., 2021; Blayney et al., 2016; Carrapa et al., 2015; D. Liu et al., 2017). Finally, the Himalayas start uplifting in the early Miocene ($\sim$20 Ma) and reach their modern elevation by the mid-late Miocene ($\sim$15 Ma) (Gébelin et al., 2013; L. Ding et al., 2017; Xu et al., 2018; C. Wang et al., 2014; Webb et al., 2017).

3.1.2 Inland Asia and Myanmar mountain building

Asian terranes located in the vicinity of the Himalaya-TP complex are impacted by the Indo-Asian collision. In Myanmar, the Indo-Burman ranges built up in a three-step process, in the late Eocene, at the Oligo-Miocene boundary and Pliocene respectively (Najman et al., 2020; Morley, 2018; Maurin & Rangin, 2009; Westerweel et al., 2020; Licht et al., 2018), as a result of the progressive indentation of the Burma block into the eastern Himalayan collision zone. The Sino-Burman Ranges, which inherit old landforms from previous collisions between Indochina and Sibumasu terranes (Metcalfe, 2013), experienced major uplift in the mid-late Miocene ($\sim$ 13-9 Ma) (Cook & Royden, 2008; Clark et al., 2005), as a result of the eastward expansion of the Tibetan Plateau by crustal flow.

North of the TP, the collision propagates through reactivated pre-existing tectonic structures and triggers the uplift of the inland Asian orogenic belt: the Tian Shan and the Mongolian (Altai, Hangay and Sayan) landforms (Jolivet et al., 2010). The southwestern and Central Tian Shan uplift initiation is very loosely constrained, either in the middle to late Miocene ($\sim$15 Ma, (Käßner et al., 2016)) or during the late Oligocene to early Miocene ($\sim$25 Ma) (Bande et al., 2017; Macaulay et al., 2014; D. Liu et al., 2017). The northeastern Tian Shan, together with the Sayan and Altai regions (in western Mongolia), likely remained quiescent until the late Miocene (Bullen et al., 2003; Caves Rugenstein et al., 2017). After a pulse of uplift in the latest Miocene ($\sim$8 Ma) for the whole Tian Shan, Sayan and Altai mountains (W. Yuan et al., 2006; Caves Rugenstein et al., 2017; Charreau et al., 2005), regional landforms probably reached their modern elevation after a final Pliocene uplift phase ($\sim$5-3 Ma, (Bullen et al., 2003; Caves Rugenstein et al., 2014; De Grave et al., 2007, 2009; Jolivet t al., 2007; Vassallo et al., 2007)). The Hangay Dome uplift (in central Mongolia) began in the mid-Oligocene (Caves Rugenstein et al., 2014; Cunningham, 2001), but the date of completion of the uplift remains debated, either in the

mid-Miocene ($\sim$13 Ma, (Smith et al., 2016)), or the Pliocene ($\sim$3 Ma, (Yarmolyuk et al., 2008)).

3.2 Evolution of the Peri-Tethys and Middle East region under the interplay of tectonics and global sea level changes

Throughout the Cenozoic, sea level fluctuations in a context of tectonic convergence have led to a profound paleogeographic reorganization and a general increase in continentality of the regions encompassing the Mediterranean Sea, Middle East and inland Asia.

3.2.1 Retreat of the Paratethys Sea and closure of the Neotethys Ocean

During the Paleocene-Eocene, Eurasia was largely flooded by the proto Paratethys, an epicontinental sea connected to the Arctic Ocean via the Turgai Strait and to the Neotethys Ocean (Meulenkamp & Sissing, 2003; Golonka, 2007). Paleoenvironmental analyses suggest a maximal extension of the proto Paratethys Sea reaching the Tajik and Tarim Basins in inland Asia at the Paleocene-Eocene transition ($\sim$56 Ma), followed by a long-term westward retreat punctuated by marine transgressions of decreasing magnitude (Kaya et al., 2019; Bosboom et al., 2014b, 2017; Carrapa et al., 2015). In Central Asia, the shrinkage of the proto Paratethys Sea during the Eocene is attributed to far-field effects of the Indo-Asia collision and to the early indentation of the Pamir and TP, leading to the progressive infilling of the basins with sediments (Kaya et al., 2019; Carrapa et al., 2015; D. Liu et al., 2017). The onset of the Antarctic ice-sheet at the EOT ($\sim$33.5 Ma) resulted in a sea-level drop of $\sim$70 m (Miller et al., 2020)), which drastically reduced the extent of the Paratethys and favored its isolation (Kaya et al., 2019; Bosboom et al., 2014b, 2017). Water exchanges between the Paratethys and neighboring oceans were progressively restricted, as indicated by the increasing divergence between the $\delta^{18}O$ and $\delta^{13}C$ signatures of Paratethys

foraminifera shells and the other oceanic signals at that time (Ozsvárt et al., 2016). The Tethyan Seaway, connecting the Indian and Atlantic Oceans, remained fully open before the Miocene (Straume et al., 2020). εNd isotope data from foraminifers suggest that it became strongly restricted around $\sim$22 Ma (Bialik et al., 2019), with intermittent periods of closure, as indicated by evidence of mammal exchanges between Eurasia and Africa across a land bridge (Rögl, 1999; Harzhauser & Piller, 2007). The Tethyan Seaway permanently closed at $\sim$14 Ma, due to the combined effect of Arabian-Eurasian plate collision and glacio-eustatic sea level fall associated with cooling following the Mid-Miocene Climatic Optimum (Bialik et al., 2019). Until the late Miocene, the Paratethys Sea experienced phases of transgression, extending as far as $\sim$60° E, and regression that may have reduced its surface by up to 70% (Palcu et al., 2021), thus highly modulating Eurasian continentality.

3.2.2 Middle-East: Anatolian-Iranian Plateau, Zagros and Alborz Mountains uplift

During the Cenozoic, the Middle-East experienced multiple changes in land-sea distribution and topography, forced by the collision of the Arabian plate with Eurasia that drove the uplift of the Zagros Mountains and of the Iranian Plateau. The exact timing of the Arabia-Eurasia collision in eastern Anatolia remains highly debated, with estimated dates ranging from the Eocene-Oligocene (Karaoğlan et al., 2016; Darin et al., 2018; McQuarrie & Hinsbergen, 2013; Pirouz et al., 2017), the early Miocene (Okay et al., 2010; Gülyüz et al., 2020), to the late Miocene (H. Su & Zhou, 2020; Z. Zhang et al., 2017). Most studies however propose an early Miocene age ($\sim$20 Ma) for the hard collision related to the arrival of thick Arabian crust along the Bitilis suture zone (Okay et al., 2010; Cavazza et al., 2018; Gülyüz et al., 2020) and a Miocene age for the uplift of most landforms (Zagros and Alborz mountains, Anatolian-Iranian Plateau). After

the collision, the Zagros orogen builds up during three successive pulses occurring within the last $\sim$ 20 Ma (Agard et al., 2011; Mouthereau, 2011). Field geology, stable isotopes and thermochronology suggest that the Alborz mountains uplift (north of the Zagros) occured during the middle Miocene ($\sim$17.5-13 Ma) (Ballato et al., 2010, 2015) and may have continued until the latest Miocene (Mouthereau et al., 2012). A Miocene age for the initiation of the eastern Anatolian-Iranian Plateau growth is also suggested, based on its youngest marine unit ($\sim$17 Ma) (Gülyüz et al., 2020) and apatite fission-track data (18-13 Ma) (Okay et al., 2010; Karaoğlan et al., 2016). Stratigraphic evidence suggests an uplift phase of the eastern Anatolian-Iranian Plateau between 15 and 12 Ma due to crustal shortening and thickening (Mouthereau et al., 2012). In contrast, numerical simulations suggest that the final building of the Plateau is only reached during the late Miocene ($\sim$7-10 Ma), likely sustained by slab break-off, mantle flow disruption and associated changes in dynamic topography and followed by isostatic adjustment (François et al., 2014).

3.3 East Africa and Arabian Peninsula evolution

While much attention has been paid to the Eastern African topography evolution in the Neogene due to its implication for early hominins development, its history fits into a broader paleogeographic context rooted in the Paleogene (see Couvreur et al. (2021); Guillocheau et al. (2018) for a synthesis). Landforms in East Africa (Kenyan and Ethiopian plateaus) developed during the late Cenozoic, triggered by a combination of tectonics, basaltic flooding, and large wave-length deformation related to the African superswell activity (Moucha & Forte, 2011; Faccenna et al., 2019; Roberts et al., 2012). Uplift in the Ethiopian region began during the Eocene, with a doming event sustained by dynamic topography (Roberts et al., 2012; Faccenna et

al., 2019) that then propagated to Kenya during the middle Miocene. In the early Oligocene, basaltic flooding in Ethiopia is thought to have contributed to the formation of these large-scale elevated features (Sembroni et al., 2016). Rifting initiated during the middle Miocene with the main uplift of rift shoulders (Wichura et al., 2015). Overall, past elevations during the Cenozoic are poorly constrained in East Africa, but modern elevations were most likely reached by the late Miocene to early Pliocene (Couvreur et al., 2021).

The Arabian Peninsula records successive marine and freshwater environments from the early Oligocene to the late Miocene, as indicated by paleo-ichthyofaunas (Otero & Gayet, 2001). Before the Neogene, the Arabian plate is assumed to have been flat and at low elevation (Daradich et al., 2003) and thus particularly sensitive to sea-level changes. It was therefore largely submerged during the Eocene, and its southwestern part became partially emerged after the sea-level fall at the EOT (Barrier et al., 2018). During the Miocene, the Arabian plate was tilted when transiting over the East-Africa mantle plume (Vicente de Gouveia et al., 2018), leading to the uplift of the Red Sea margin and the flooding of its northeastern corner, due to mantle convective drawdown (Daradich et al., 2003; Moucha & Forte, 2011). This mechanism promoted temporary transgression phases in the subdued northeastern region in early Miocene times (Barrier et al., 2018), until its full emergence in the late Miocene, possibly favored by global sea-level fall after the mid-Miocene Climate Transition (Golonka, 2009; Harzhauser & Piller, 2007; Miller et al., 2020).

4 Materials and Methods

4.1 IPSL-CM5A2 model

We perform simulations with the IPSL-CM5A2 Earth System Model (Sepulchre et al.,

2020), an updated version of the IPSL-CM5A model (Dufresne et al., 2013) designed for deep-time paleoclimate simulations. It is composed of the atmospheric model LMDz5A (Hourdin et al., 2013), the land surface and vegetation model ORCHIDEE (Krinner et al., 2005) and the oceanic model NEMO (v3.6) (Madec, 2016) that also includes the LIM2 sea-ice model (Fichefet & Maqueda, 1997). The OASIS coupler ensures synchronization between the different model components (Valcke et al., 2006). The atmospheric model has a nominal horizontal resolution of 96x95 grid points (3.75° in longitude by 1.9° in latitude) with 39 irregularly distributed vertical levels from the surface to 40 km high. The ORCHIDEE model is coupled with LMDZ5a and redirects runoff water towards the ocean. The vegetation cover is represented through 11 Plant Functional Types, including one describing bare soil. NEMO solves ocean dynamics and thermodynamics equations on a tripolar grid, with two poles located below continental masses in the Northern Hemisphere, thereby avoiding North Pole singularity in the ocean (Madec & Imbard, 1996). It has a nominal resolution of 2° by 2° refined up to 0.5° in the equatorial region, with 31 vertical levels, the thickness of which ranges from 10 meters near the surface to 500 meters in the deep ocean. Full description of IPSL-CM5A2 can be found in Sepulchre et al. (2020); Dufresne et al. (2013). IPSL-CM5A2 has been previously used for paleoclimatic simulations of the Miocene (Burls et al., 2021; Sarr et al., 2022; Pillot et al., 2022) and the Eocene (Tardif et al., 2020, 2021; Toumoulin et al., 2022, 2020; Barbolini et al., 2020). The ability of the model to simulate the modern Asian climate has previously been described (Sepulchre et al., 2020; Tardif et al., 2020) and compared to observations (SI Fig. 14). While general atmospheric circulation patterns are well reproduced, IPSL-CM5A2 overall underestimates precipitation amounts and delays inland monsoonal precipitation onset by about a month, which are characteristics shared with the earlier IPSL-CM5A version of the model (Sepulchre et al., 2020).

4.2 Numerical simulations design

Simulations presented in this study are performed with paleogeographic configurations used in previous work, presented in Figure 3 and Table 1 and detailed below. The reference experiments have been run for 3000 years and the deep ocean has reached quasi-equilibrium after $\sim$2000 years of integration. Sensitivity experiments are restarted from their reference experiment and run for 300 to 500 years until upper ocean equilibrium. Model outputs are averaged over the last 50 years of each simulation.

Table 1. List of reference simulations (bold) and sensitivity experiments used in this study. Abbreviations stand for East Antarctic Ice Sheet (EAIS), Antarctic Ice Sheet (AIS) and Greenland + Antarctic Ice Sheet (G+AIS). The last column details the paleogeographic configurations, highlighting the pairs of simulations that can be compared. For example, the effect of pCO_2 halving in the Eocene is obtained with the "LEo1_REF - LEo1_2X" anomaly.

Simulation	pCO_2	Ice sheets	Paleogeography
LEo1_REF	**1120**	-	from (Tardif et al., 2020)
LEo2_TP	1120	-	from (Poblete et al., 2021)
LEo2_TPlow	1120	-	from LEo2_TP, TP lowered to 800 m
LEo2_TPhigh	1120	-	from LEo2_TP, TP raised to 4500 m
LEo2_TPsouth	1120	-	from LEo2_TP, TP shifted to the South (Poblete et al., 2021)

LEo2_BengalSea	1120	-	from LEo2_TP, with a Bengal Sea (Poblete et al., 2021)
LEo1_2X	560	-	from LEo1_REF, pCO_2 halved to 560 ppm
EOli_REF	**560**	**AIS**	from LEo1_REF, 70 m sea level drop (Barbolini et al., 2020)
EMio_REF	**560**	**EAIS**	from (Poblete et al., 2021)
EMio_TetSw	560	EAIS	from EMio_REF, open Tethyan Seaway (120 m depth)
EMio_EAfr	560	EAIS	from EMio_REF, modern East African landforms
MMio_REF	**560**	**AIS**	from (Sarr et al., 2022)
LMio_smallT	560	AIS	from MMio_REF, reduced Paratethys
LMio_noAr	560	AIS	from LMio_smallT, immersed Arabia
LMio_noM	560	AIS	from LMio_smallT, Mongolia lowered to 800 m
LMio_noTS	560	AIS	from LMio_smallT, Tian Shan lowered to 800 m
LMio_noTSM	560	AIS	from LMio_smallT, Tian Shan+Mongolia lowered to 800 m
LMio_noTSP	560	AIS	from LMio_smallT, Tian Shan+Pamir lowered to 800 m
LMio_REF	**560**	**G+AIS**	from (Sarr et al., 2022)
LMio_1.5X	420	G+AIS	from LMio_REF, pCO_2 lowered to 420 ppm

4.2.1 Paleogeographic reconstructions and sensitivity tests

Our late Eocene reference paleogeography (**LEo1_REF**, $\sim$40 Ma, Fig. 3 a), previously introduced in Tardif et al. (2020), displays a fully emerged *Greater India* and a $\sim$3000 m elevation TP. The proto Paratethys Sea fills the Tarim Basin, the Turgai Strait is closed and East African topography is low. Considering the ongoing debate surrounding the extension of India and TP morphology at that time, other configurations are tested: **LEo2_TP** (Fig. 3 b) is an alternative

late Eocene paleogeography, with a slightly different TP shape obtained with the "double collision model" (Poblete et al., 2021), from which sensitivity tests with a lower ($\sim$800 m, **LEo2_TPlow**, Fig. 3 c) and a higher TP ($\sim$4500 m, **LEo2_TPhigh**, Fig. 3 d) are derived. Two additional tests are performed. The first exhibits a TP located more to the South (**LEo2_TPsouth**, Fig. 3 f) and is obtained with the collision model from Jagoutz et al. (2015). The second features the presence of a remaining inlet between India and continental Asia (**LEo2_BengalSea**, Fig. 3 g), according to van Hinsbergen et al. (2012, 2019). The early Oligocene simulation (**EOl_REF**, $\sim$33 Ma, previously introduced in Barbolini et al. (2020)) is designed to represent the Asian paleogeography right after the Eocene-Oligocene Transition (Fig. 3 e). The late Eocene paleogeography of LEo1_REF is used as a base, on which the sea level is eustatically lowered by 70 m (Miller et al., 2020), to account for a modern-sized ice sheet over Antarctica, as an end-member scenario. This leads to the emergence of continental portions in Arabia and North Africa and the drying of the Tarim Basin and lowlands north of the Turgai Strait, which all act to significantly increase Asian continentality. The former shallow connection between the Paratethys and the Tethys ceases in the Pamir-Zagros region at that time.

The early Miocene paleogeography (**EMio_REF**, $\sim$20 Ma, Fig. 3 h), is from Poblete et al. (2021) and was previously introduced in Sarr et al. (2022) and Burls et al. (2021). It displays an Indian subcontinent translated 5° further north compared to the Eocene and an uplifted Central TP close to its modern elevation ($\sim$5000 m), whereas western and northeastern TP portions are lower (2000-3000 m). The Tethyan Seaway that previously connected the Mediterranean Sea and the Indian Ocean is closed, but a shallow sea persists at the location of the Arabian Peninsula. The alternative configuration **EMio_TetSw**, with a 120 m deep Tethyan seaway, is tested (Fig. 3 i). Considering the large uncertainties related to East African elevation, we also test the impact of a

full uplift of this region as early as the early Miocene with the **EMio_EAfr** experiment (Fig. 3 j).

The mid and late Miocene paleogeographies are based on the PRISM4 reconstruction (Dowsett et al., 2016) used in PlioMIP2 (Haywood et al., 2020) with manual modifications including the Australian continent shifted southward compared to present day and an emerged Sunda Shelf (Torsvik et al., 2008; Hall et al., 2012) (see Sarr et al. (2022) for details). In the middle (**MMio_REF**, $\sim$12 Ma, Fig. 3 k) and late Miocene (**LMio_REF**, $\sim$8 Ma, Fig. 3 o) reference paleogeographic configurations, the Himalayas, Tibetan Plateau, Myanmar, inland Asia and East African landforms have reached their present-day configuration (Fig. 3). In the mid-Miocene, the elevation of the Anatolian-Iranian orogen is half ($\sim$1000 m) that of present-day and the Paratethys Sea extends up to 60°E (**MMio_REF**), while by the late Miocene (**LMio_REF**), the Paratethys is strongly reduced and the Anatolian-Iranian landforms have reached their modern elevation. An intermediate mid-late Miocene reconstruction is tested, in which the impact of a Paratethys retreat is investigated (**LMio_smallT**, Fig. 3 i). Sensitivity tests are also performed on inland Asian landforms, by lowering to $\sim$800 m the Mongolian Plateau (**LMio_noM**, Fig. 3 p), Tian Shan (**LMio_noTS**, Fig. 3 q), Mongolia and Tian Shan (**LMio_noTSM**, Fig. 3 n), and finally, Tian Shan and Pamir (**LMio_noTSP**, Fig. 3 r). Additionally, **LMio_noAr** (Fig. 3 m), displaying an almost fully flooded Arabian Peninsula, is designed to account for the high sensitivity of this region to sea level fluctuations during that period. Note that LMio_smallT is the paleogeography to which all other late and middle Miocene simulations can be compared to.

4.2.2 pCO_2, ice-sheets, solar constant and vegetation

CO_2 concentrations vary from 1120 ppm in the late Eocene to 560 ppm in the late Miocene (Table 1) (Foster et al., 2017; Rae et al., 2021) and other greenhouse gases are maintained at

pre-industrial values. Acknowledging uncertainties regarding precise pCO_2 concentrations during the Cenozoic, we perform two additional sensitivity tests on this parameter by prescribing 560 ppm in a late Eocene simulation (**LEo1_2X**) and 420 ppm in a late Miocene simulation (**LMio_1.5X**). Late Eocene experiments are considered ice-free, as pCO_2 is above the threshold for permanent Antarctic glaciation (Ladant et al., 2014; DeConto & Pollard, 2003). Unipolar glaciation over the Antarctic continent is used for the Oligocene, early and mid-Miocene, and both Greenland and Antarctic ice-sheets are present in late Miocene configurations (Bierman et al., 2016). The solar constant is adjusted (Gough, 1981) and set to $1360.19\ W.m^{-2}$ for late Eocene and early Oligocene simulations, $1362.92\ W.m^{-2}$ for early Miocene simulations and $1364.30\ W.m^{-2}$ for late and middle Miocene simulations. Although orbital variations are known to impact monsoonal circulation (Zhisheng et al., 2015; P. Wang et al., 2005; Tardif et al., 2021), we prescribe a modern-like orbital configuration in all simulations because this study focuses on the impact of paleogeography. In the absence of congruent global vegetation reconstructions over the Cenozoic, all the experiments are forced with prescribed latitudinal bands of idealized vegetation cover based on modern distribution, as done in previous studies (Tardif et al., 2020; Laugié et al., 2020).

4.3 Monsoon metrics

The evolution of Asian monsoons over time is assessed through specific markers that are characteristic of the present-day SAM and EAM, such as precipitation amounts, seasonality, and wind direction and strength. The evolution of precipitation seasonality using the Monsoon Precipitation Index (MPI) (B. Wang & Ding, 2008) is expressed as follows:

$$\text{MPI} = \frac{\text{Seasonal range of precipitation}}{\text{Mean annual precipitation}}$$

where the seasonal range of precipitation is the difference between May to September minus November to March precipitations. Monsoon-like seasonality is considered to occur if the seasonal range is superior to 300 mm and more than half of the precipitation falls during the extended summer season (MPI > 0.5). This metric has the benefit of proposing a discrete metric for seasonality amplitude (from 0 to 1, instead of "with or without" monsoon). It also imposes that the wet season occur in summer, unlike other existing precipitation metrics (such as the ratio of the 3 wettest month over the 3 driest month precipitation, commonly used in paleobotany studies).

The wind patterns, described via their shape and strength, are the second fundamental characteristic that we focus on. First, we track the latitudinal migration of the Somali Jet over the Arabian Sea (Fluteau et al., 1999) as a proxy for SASM intensity. Second, we use the Webster-Yang Index (Webster et al., 1998), calculated as the difference between the zonal component of 850 and 200 hPa winds ($U_{850} - U_{200}$) in the region 0°:20°N to 40°E:110°E, to evaluate the wind shear between the low and high troposphere over India, which describes the vigor of the SASM zonal circulation. Third, we use the positive thermal anomaly observed at 300 hPa over northern India in summer as a marker of the deep convection characterizing the modern SASM (Boos & Kuang, 2010; Acosta & Huber 2020). This anomaly is due to the important latent heat release in the high troposphere provoked by the condensation of moisture in convecting air masses ascending the southern flank of the Himalayas (see Fig. 14 d).

In addition to the precipitation seasonality, we explore the EASM evolution through the latitudinal displacement of the Jet Stream with respect to Tibetan and inland Asian landforms and with surface wind patterns. The EAWM is tracked principally with the evolution of temperature and pressure gradients, leading to the Siberian High formation in winter, and of its associated wind

patterns. We also use the EAWM index (L. Wang & Chen, 2014), that accounts for both the North-South (Siberia-Maritime continent) and West-East (Siberia-North Pacific) pressure gradients and is expressed as follows:

$$I_{EAWM} = (2xSLP_S - SLP_{NP} - SLP_{MC})/2$$

where SLP_S, SLP_{NP} and SLP_{MC} is the area-averaged Sea Level Pressure (SLP) over Siberia (40°:60°N, 70°:120°E), North Pacific (30°:50°N, 140°E:170°W) and the Maritime continent (20°S:10°N, 110°:160°E), respectively.

5 Results

For each regional monsoon, we first present the results obtained for the five reference numerical simulations (red box in Fig. 3). The underlying forcing factors are then explored, taking advantage of the sensitivity tests summarized in Table 1. The main outcomes in terms of seasonal winds and precipitations are qualitatively summed up in Table 2.

Table 2. Overview of each tested forcing factor on seasonal precipitation and wind circulation simulated in each region. Abbreviations stand for Transition Area (TA), cardinal directions (E, W, S, N), basins mentioned in Figure 1 (e.g. Tajik Basin, Tjk)

5.1 The South Asian monsoon, controlled by the orography surrounding the Indian Ocean

5.1.1 Evolution of spatial and seasonal precipitation patterns

In the late Eocene, a wide arid region (< 500 mm/year) spreads from northern India to north

of proto Tibet (Fig. 4 a). The extent of this simulated arid region is most likely overestimated, which is further discussed in section 6.1. High mean annual precipitation amounts (> 3000 mm/yr) are simulated over equatorial regions in southern India and southeastern Asia. There is no monsoon-like seasonality according to the MPI index in India, because the rainy season in this region occurs in winter (as previously described in Tardif et al. (2020)). The precipitation pattern evolves from the early Oligocene onwards, as the arid region progressively shifts to Arabia and northern Africa (Fig. 4 e, i, m, q). This allows the penetration of rainfall in summer into southeastern Asia and the onset of a monsoon-like seasonality in this region, as well as a reinforcement of monsoon-like seasonality in Eastern Asia. Over the course of the Miocene, as India drifts northwards, its southern tip receives less precipitation ($\sim$1500 mm/yr in the late Miocene, Fig. 4 q) and the intensity and extent of highly seasonal precipitation increases greatly over southern and eastern Asia (red dotted regions in Fig. 4 e, i, m, q). Orographic precipitation over the southern flank of the Himalayas initiates in the mid-Miocene simulation ($\sim$900 mm/yr, Fig. 4 m) and further increases in the late Miocene simulation ($\sim$1200-1500 mm/yr, Fig. 4 q). These changes in precipitation patterns in both space and time are triggered by a profound reorganization of surface pressure patterns and winds throughout the set of Cenozoic simulations.

Figure 4. Evolution of summer monsoon diagnostics since the Eocene. **First column:** Mean Annual Precipitation (shading, mm/yr) overlain with regions where the Monsoon Precipitation Index is over 0.5 (thin red dots) and 0.75 (thick red dots); **Second column:** June-August (JJA) normalized Sea Level Pressure (SLP) anomaly defined as the difference between summer SLP and mean annual SLP (shading, hPa) and 850 hPa winds over 4 m/s (vectors); **Third column:** August Jet Stream speed (magenta contour, maximal zonal wind velocity in the mid to high troposphere, in

m/s), August monthly precipitation amounts (shading, mm/month) and 850 hPa winds over 4 m/s (vectors) ; **Fourth column:** JJA mean temperature at 2 m (shading, Celsius) and 300 hPa atmospheric temperature (white contour, Kelvin). On all figure pannels, topography is overlain as gray contours, at 1000 m intervals.

5.1.2 Summer pressure and wind pattern reorganization

The summer (June to August, JJA) sea level pressure patterns in Eurasia in the late Eocene experiment (Fig. 4 b) contrast strongly with the modern ones (SI Fig. 14 f). A low-pressure center forms, driven by extreme summer temperature over southeastern Asia (up to 50 °C over *Greater India*, Fig. 4 d) whereas the Paratethys Sea and Neotethys Ocean are the locus of a wide high pressure cell (Fig. 4 b). This pressure pattern induces low tropospheric anticyclonic winds that counteract potential moisture advection from the Indian Ocean towards South Asian regions. From the early Oligocene onwards, the shrinkage of the Paratethys Sea and Neotethys Ocean increases Eurasian continentality and the surface of emerged land, such as Anatolia and Arabia. They become the locus of high summer temperatures (35-45 °C, Fig. 4 l, p, t), leading to the progressive widening of the South Asian low-pressure belt, while the Neotethyan anticyclone gradually regresses westward (Fig. 4 f, j, n, r). This low pressure cell reaches its modern-like extent in the mid-Miocene simulation (Fig. 4 n) but a modern-like magnitude ($\sim$-14 hPa over Arabia and northern India) occurs only in the late Miocene simulation (Fig. 4 r, SI Fig. 14).

Mirroring this progressive strengthening and widening of the summer low-pressure belt over south Asia and Arabia, an increasing amount of moisture-loaded air masses are gradually advected from the Indian Ocean towards the continent over the Cenozoic. A weak cross equatorial flow (<4 m/s, Fig. 4, against $\sim$25 m/s today, SI Fig. 14), confined to low latitudes (<10°N, Fig. 5

a, simulations LEo1_REF and EOli_REF), is simulated over the Arabian Sea in the late Eocene and early Oligocene experiments (Fig. 4 b, f). A mostly zonal proto-Somali Jet, also confined to low latitudes (<11°N), is simulated in the early Miocene simulation (Fig. 5 b, simulation EMio_REF). From the mid-Miocene onwards, and following the reinforcement of the Asian low-pressure belt, the now fully-formed Somali Jet increases in strength and migrates further north over the Arabian Sea ($\sim$18-24°N) (Fig. 4 n, r, Fig. 5 b, simulations MMio_REF and LMio_REF). The simulated tropospheric circulation above southern Asia is drastically rearranged from the late Eocene to the Miocene simulation, as indicated by the Webster-Yang Index. This index doubles between the late Eocene and the early Oligocene (from $\sim$5 to 11 m/s, Fig. 5 c, reference simulations LEo1_REF and EOli_REF) and keeps increasing in the Miocene (from $\sim$16 to 21 m/s, Fig. 5 d, simulations EMio_REF, MMio_REF and LMio_REF). Finally, while a heating of the high troposphere ($\sim$300 hPa) due to deep convection is observed in most experiments (Fig. 4 d, h, l, p, t), this heat anomaly relocates over northern India only in the mid-Miocene experiment, following the increase in summer convective precipitation in this region driven by orographic uplift.

Figure 5. Estimation of the evolution of South Asian monsoon strength in all the simulations via: (**a, b**) the calculation of the summer (JJA) cross-equatorial flow latitude over the Arabian Sea, after Fluteau et al. (1999) and (**c, d**) the calculation of the Webster-Yang Index (WYI, 850 hPa minus 200 hPa zonal wind velocity, in the region 0:20°N ; 40:110°E, after Webster and Yang (1992)). For better readability, the experiments are split into Eocene-Oligocene (a, c) and Miocene (b, d) simulations. Reference simulations are highlighted in bold characters and continuous lines, while sensitivity tests are in dotted lines.

5.1.3 Limited effect of pCO_2 decrease and alternative Eocene Tibetan Plateau configurations on South Asian summer monsoon evolution

The non-linearity in the response of the Somali Jet through time calls for an individual analysis of the different forcing factors between each of these simulations. Our sensitivity experiments reveal the weak sensitivity of the SASM to pCO_2 changes in comparison to paleogeographic forcing. This is true for the late Eocene experiments, in which a change from 1120 ppm to 560 ppm (difference between experiments LEo1_2X and LEo1_REF) only induces minimal variations in the Webster-Yang Index, summer northward ITCZ migration (Fig. 5 a, c), or monsoon-like seasonality extension (Fig. 7 f). This is also the case for the late Miocene experiments when the pCO_2 is changed from 560 ppm to 420 ppm (difference between experiments LMio_1.5X and LMio_REF in Fig. 5 b, d). The paleogeography of *Greater India* and Tibetan regions have been repeatedly proposed as a driver of monsoon onset or intensification (R. Zhang et al., 2012; Yu et al., 2018; Molnar et al., 1993). While alternative TP configurations lead to slightly different results, their impact on the simulated SASM large-scale wind circulation remains limited (Fig. 5 a, c, Fig. 6). In the late Eocene, increasing TP elevation strengthens the zonal wind shear over India (3000 m, Webster-Yang Index = $\sim$6 m/s, for experiment LEo2_TP, Fig. 5 c) with respect to the Eocene experiment with low TP topography elevation (Webster-Yang Index = 1 m/s, LEo2_TPlow). Additionally, the magnitude of the Webster-Yang Index gradually increases with TP latitude, with values of 3 m/s for a southern edge at $\sim$20°N (LEo2_TPsouth), 4 m/s at $\sim$25°N (LEo2_TP), and 6 m/s at $\sim$30°N (LEo1_REF). The presence of a sea inlet flooding *Greater India* in the late Eocene configuration limits the northward migration of the ITCZ in summer (from $\sim$7 to 3°N between experiments LEo2_BengalSea and LEo2_TP, Fig. 5

c). It also produces a decrease in year-round precipitation, especially in south and inland Asia (Fig. 6 m, n, o).

5.1.4 Continentality increase and East African and Iranian uplifts as major drivers of the South Asian monsoon

The changes induced by the TP uplift or by its latitudinal location on South Asian climate are by far out-competed by the effects of land-sea distribution changes, or by the uplift of peripheral mountain ranges (Fig. 5). Indeed, the increase in continentality driven by the Eocene-Oligocene sea level fall induces colder and drier winters (Fig. 7 g), as well as warmer and wetter summers (Fig. 7 h). This results in a monsoon-like seasonality signal expanding over southeastern Asia (Fig. 7 i). It also translates into a doubling of the Webster-Yang Index (from 6 to 11 m/s between experiments EOli_REF and LEo1_REF, Fig. 5 c) and an important reorganization of the summer Jet Stream behavior (see section 5.2.2). Likewise, increasing continentality during the Miocene appears to be key for inducing a more pronounced migration of the ITCZ over the Arabian Sea (from 18 to 21°N in the more continental case, Fig. 5 b), as well as a slight increase of the Webster-Yang Index (Fig. 5 d). This is achieved either with the emergence of the Arabian Platform (Fig. 8 h), or with the shrinkage of the Paratethys Sea (Fig. 8 e). In both cases, the amplification of the summer low pressure belt increases moisture advection from the Arabian Sea, leading to enhanced summer rainfall in the SAM domain. The increase in precipitation seasonality in the SAM domain is, however, more widespread with a Paratethys Sea retreat than with an emerged Arabian platform (Fig. 8 f, i), due to the contrasted effect of these paleogeographic changes on winter precipitation (Fig. 8 d, g). Both events are also shown to strongly impact central Asian aridity and the climate of the EAM domain.

Additionally, the buildup of both East African (difference between experiments EMio_EAfr-EMio_REF) and Anatolian-Iranian landforms (difference between experiments LMio_REF-LMio_smallT) is critical for the amplification of the ITCZ migration and strengthening of the SAM. Each uplift triggers a $\sim$4-5° northward migration of the ITCZ over the Arabian Sea in summer, as well as a slight increase in the Webster-Yang Index in July (Fig. 5 b, d and SI Fig. 16). The uplift of East African landforms under Early Miocene conditions reinforces the Somali Jet and brings moisture to Iran and the SAM domain in summer (Fig. 9 e), which results in an intensification of monsoon-like seasonality in the Himalayan foothills and in southeastern Asia (mainly Myanmar, Fig. 9 f). Anatolian-Iranian landforms' final uplift under late Miocene conditions promotes winter aridity and summer precipitation in the SAM domain through a large strengthening of the Somali Jet, resulting in reinforced monsoon-like seasonality (Fig. 9 j, k, l). By preventing the advection of drier westerly mid-latitudes winds to lower latitudes, the Anatolian-Iranian Plateau channels humidity towards inland Asia in summer, reducing the aridity of the region. On the other hand, the sole effect of the Tethyan Seaway closure, without strong modification of land extension in the Arabian Peninsula region, remains limited in our experiments (+1 m/s for the Webster-Yang Index between experiments EMio_REF and EMio_TetSw in Fig. 5 d), in contrast to the hypothesis that the closure of the Tethyan Seaway may contribute to altering the intensity of the monsoon during the Miocene (Bialik et al., 2019, 2020; Rögl, 1997; J. Sun et al., 2021),

Figure 6. Sensitivity to the Tibetan configurations on Eocene climate: (**a, d, g, j, m**) winter precipitation (shading), 850 hPa winds (vectors), jet stream speed (contour) ; (**b, e, h, k, n**) on summer precipitation (shading), 850 hPa winds (vectors), jet stream speed (contour); (**c, f, i, l, o**)

mean annual precipitation (shading) and monsoon-like seasonality according to the MPI index (red dots). Sensitivity tests are compared to the LEo2_TP simulation (**a, b, c**) and anomalies (**d to o**) are expressed as "test - LEo2_TP", except for the "lowered TP effect" which is "LEo2_TP - LEo2_TPflat"). Precipitation anomalies (shading) are expressed in % and normalized by the averaged precipitation of both simulations (therefore, a change from or to zero mm/year accounts for +/- 200%). In (**f, i, l, o**): four types of seasonality change induced by uplift are displayed (e.g., regions showing a decrease of monsoon-like seasonality after lowering the TP are in small black dots) ; white and black topographic contours indicate the LEo2_TP and tested topography.

Figure 7. Influence of pCO_2 decrease and sea level fall at the EOT on: (**a, d, g**) winter precipitation (shading), 850 hPa winds (vectors), Sea Level Pressure (contour) ; (**b, e, h**) on summer precipitation (shading), 850 hPa wind (vectors), jet stream speed (contour); (**c, f, i**) mean annual precipitation (shading) and monsoon-like seasonality according to the MPI index (red dots). Sensitivity tests are compared to the LEo1_REF simulation (**a, b, c**) and anomalies (**d to i**) are expressed in order to highlight the impact of the test (i.e. test-LEo1_REF). We refer the reader to Figure 6 for an extended description of the pannels.

Figure 8. Influence of continentality increase in a mid-late Miocene context on: (**a, d, g**) winter precipitation (shading), 850 hPa winds (vectors), Sea Level Pressure (contour) ; (**b, e, h**) on summer precipitation (shading), 850 hPa winds (vectors), jet stream speed (contour); (**c, f, i**) and on mean annual precipitation (shading) and monsoon-like seasonality according to the MPI index (red dots). Sensitivity tests are compared to the LMio_smallT simulation (**a, b, c**) and anomalies (**d to i**) are expressed in order to highlight the impact of the continentality increase (i.e.

LMio_smallT-test). We refer the reader to Fig. 6 for an extended description of the pannels.

Figure 9. Influence of East African uplift in the early Miocene (a to f) and of Anatolian-Iranian uplift in the late Miocene (g to l) on: (**a, d, g, j**) winter precipitation (shading), 850 hPa winds (vectors), Sea Level Pressure (contour) ; (**b, e, h, k**) on summer precipitation (shading), 850 hPa winds (vectors), jet stream speed (contour); (**c, f, i, l**) and mean annual precipitation (shading) and monsoon-like seasonality according to the MPI index (red dots). East African (Anatolian-Iranian) uplift is compared to the EMio_REF simulation (LMio_SmallT) (**a, b, c** and **g, h, i**) and anomalies (**d, e, f** and **j, k, l**) are expressed in order to highlight the impact of uplift (i.e. EMio_EAfr-EMio_REF and LMio_REF-LMio_smallT respectively). We refer the reader to Figure 6 for an extended description of the pannels

5.2 The East Asian monsoon under the combined influence of Asian orography, continentality and pCO_2

5.2.1 East Asian summer monsoon: precipitation patterns and summer Jet Stream position evolution

As opposed to the South Asian region, monsoon-like precipitation seasonality is simulated in eastern Asia in all reference experiments, although it remains initially confined to northeastern China in the Eocene (Fig. 4 a). As this region of monsoon-like precipitation expands to southeastern and inland China throughout the Cenozoic and reaches a modern-like extent in the mid-Miocene experiment, the Paleogene broad zonal arid band retreats from China (Fig. 4 m). Today, precipitation in eastern China is triggered by the penetration of the Meiyu-Bayu front as it follows the migration of the Jet Stream north of the TP during summer (Kong et al., 2017). In our

simulations, the summer Jet Stream (approximated by the location of maximum zonal wind velocity in the troposphere in August) circulates above the proto TP and eastern China in a strong zonal flux in the Eocene and Oligocene experiments (up to 30-35 m/s centered at $\sim$30°N Fig. 4 c, g). It then weakens (10-20 m/s) and progressively migrates north of the TP in the Miocene experiments (Fig. 4 k, o, s). The Jet configuration evolves from purely zonal (east-west) to more SW-NE. This relocation of the Jet Stream is accompanied by increased precipitation in eastern China, southeastern Siberia and Japan, reaching 200-300 mm in August (Fig. 4 k, o, s), which locally accounts for up to 25% of the annual precipitation. These results suggest that the evolution of the Jet Stream seasonal displacement indeed amplifies the EASM rainy season, although seasonal precipitation is simulated prior to the Jet acquiring its modern position in summer.

5.2.2 Summer Jet Stream migration driven by pCO_2 decrease at the EOT and Tian Shan uplift in the Miocene

Our sensitivity experiments allow us to identify the drivers responsible for the establishment of modern-like Jet Stream seasonal migrations over Asia. All 1120 ppm Eocene simulations display a behavior of the Jet opposite to its modern counterpart, with a northward migration in winter and a southward migration in summer independent of the TP configuration (Fig. 10 a, Fig. 6 e, h, k, n). Halving pCO_2 at the EOT reverses this tendency (LEo1_2X and EOli_REF, compared to LEo1_REF), inducing a migration north of the TP in late summer to early fall (Fig. 10 a, Fig. 7 e, h) and an important decrease in winter zonal velocity ($\sim$50 m/s against $\sim$ 70 m/s in other Eocene simulations, Fig. 10 a). This northward migration is however restricted to the TP region and the Jet Stream remains at low latitude over eastern Asia ($\sim$35°N, Fig. 10 b, SI Fig. 18), with low summer rainfall amounts (100-150 mm/month). All subsequent Miocene

simulations display an important latitudinal migration of the Jet over the year, both in the TP region (Fig. 10 c, e) and over eastern Asia (Fig. 10 d, f). The northward migration of the Jet is comparable between early Oligocene and early Miocene experiments (up to $\sim$38-40°N in September), despite a higher (from 3000 to 4000 m) and wider TP, due to the incipient uplift of northeastern and northwestern TP portions in the early Miocene simulation (the Tian Shan is $\sim$ 1000 m and the NE Tibet $\sim$2000 m high). We therefore suggest that the Jet Stream latitudinal migration is primarily driven by pCO_2 decrease and resulting changes in tropospheric temperature gradients, and that a significant threshold in the behavior of the Jet Stream may be crossed at the greenhouse-icehouse transition (EOT, $\sim$34 Ma). In contrast, variations in the Jet Stream latitudinal migration during the Miocene appear to be driven by topographic changes. Indeed, sensitivity experiments show that the Tian Shan, and to a lesser extent Mongolian and Pamir topographies, are critical to deviate the Jet northward in summer, both in the TP region and in eastern Asia (from 39-41°N in LMio_noTS, LMio_noTSP, LMio_noTSM and LMio_noM to 43°N in MMio_REF and LMio_REF, Fig. 10 e, Fig. 11 h, k, n). Northward migration of the Jet Stream in summer induces orographic precipitation on the uplifted landforms, aridification in the windward regions (-20 to -60% of summer precipitation in eastern Kazakhstan and Uzbekistan) and increased summer rainfall in eastern Asia (Fig. 11 e, h, k, n). Monsoon-like seasonality in eastern Asia (magenta dots in Fig. 11 f, i, l, o) also greatly increases, due to the important effect of uplift of these mountains on wintertime climate as well (see section 5.2.4). On the other hand, changes in the configuration of the Tethyan Seaway in the early Miocene (comparing EMio_REF and EMio_TetSw), the Anatolian-Iranian Plateau uplift (comparing LMio_SmallT and LMio_REF), or a pCO_2 decrease (comparing LMio_REF and LMio_1.5X) in the late Miocene, do not yield important variations in the Jet Stream migration (Fig. 10 c to f).

Figure 10. Jet Stream behavior throughout the year over the Tibetan Plateau and eastern China for all sensitivity experiments, divided into (**up**) late Eocene, (**mid**) early Miocene and (**bottom**) mid to late Miocene. (**left**) Jet Stream latitudinal migration and speed (shading) evolution along the year in the Tibetan region (averaged over 80:90°E). Mean latitudes of the northern and southern bounds of the Himalaya-Tibet and Mongolian landforms are indicated. (**right**) Jet Stream latitudinal position and precipitation amounts (shading) throughout the year in east Asia (averaged over 100:120°E).

Figure 11. Influence of Mongolia, Tian Shan and Pamir regional uplifts on (**left column**) winter precipitation (shading), 850 hPa winds (vectors), Sea Level Pressure (contour) ; (**middle column**) on summer precipitation (shading), 850 hPa wind (vectors), jet stream speed (contour); (**right column**) mean annual precipitation (shading) and monsoon-like seasonality according to the MPI index (red dots). Sensitivity tests are compared to the LMio_smallT simulation (**a, b, c**) and anomalies (**d to o**) are expressed in order to highlight the impact of the uplift (i.e. LMio_smallT-test). We refer the reader to Figure 6 for an extended description of the pannels.

5.2.3 East Asian winter monsoon: the Siberian High genesis

Our results suggest that pressure and wind patterns characterizing the modern EAWM established progressively, following an important reorganization of surface temperature gradients (Fig. 12, Fig. 13). In our Eocene experiment, a high-pressure band centered around 30°N is simulated but remains mainly zonal, following the large-scale winter descending branch of the Hadley cell driven by latitudinal surface temperature gradients (Fig. 12 b). The temperature

difference between the Tibetan region (~10 °C, located below the high pressure cell) and neighboring North Pacific Ocean (~30 °C) remains relatively low (~20 °C, Fig. 12 a) compared to modern winter temperature difference (~40 °C, Fig. 14 h). As a result, no significant pressure difference is simulated between the Asian continent and the North Pacific in the Eocene and the calculated EAWM index is low (< 5, Fig. 13), reflecting only the North-South pressure gradient between Asia and the Maritime Continent. The extent of the Asian high pressure zone increases gradually in the early Oligocene and early Miocene experiments (Fig. 12 d, f), but a modern-like Siberian High is only simulated in the mid and late Miocene experiments, when the anticyclone relocates over Siberia (~40-60°N, Fig. 12 h, j). Additionally, the (North Pacific) Aleutian low relocates 10° to the south from the early Oligocene onwards and steadily weakens until the late Miocene (from over ~14 to 10 hPa anomaly). These changes concur to progressively increase both North-South and East-West pressure gradients, and therefore the EAWM index, which reaches maximal values in the mid and late Miocene experiments (~15, Fig. 13). Following this simulated pressure pattern reorganization, low tropospheric winds circulating over China display a progressive change in orientation: while remaining primarily zonal in the Paleogene and early Miocene experiments (Fig. 12 b, d), they increasingly tilt in the meridional direction under the development of the Siberian High in the mid and late Miocene experiments (Fig. 12 h, j). This profound reorganization of atmospheric circulation is driven by temperature gradient changes and mainly due to the progressive cooling of the Tibetan, Mongolian and Siberian regions, as illustrated by the ~22° southward shift of the 0 °C isotherm between the late Eocene and the late Miocene simulations (Fig. 12 a, i).

Figure 12. Evolution of the winter monsoon diagnostics throughout the Cenozoic. **Left column:**

December-February (DJF) mean temperature at 2 m (shading, Celsius), and 0 °C isotherm (white contour); **Right column:** DJF normalized Sea Level Pressure anomaly (shading, hPa) and 850 hPa winds above 4 m/s (vectors). In all captions, topography is overlain in gray contour each 1000 m. Yellow boxes indicate the regions over which the sea level pressure gradients are calculated for the East Asian Winter Monsoon Index, presented in section 4.3

Figure 13. Upper panel: December-February (DJF) Sea Level Pressure (hPa) evolution over Siberia, North Pacific and the Maritime Continent ; **lower panel:** Evolution of the East Asian Winter Monsoon index (purple) and of the East-West and North-South regional indexes throughout the different reference and sensitivity experiments, after (L. Wang & Chen, 2014).

5.2.4 Siberian High inception driven mainly by Mongolian uplift in the Miocene and its impact on precipitation seasonality

Our sensitivity experiments reveal the very strong impact of the Mongolian landform uplift (alone or together with the Tian Shan) in the mid-late Miocene on Asian winter pressure patterns. Indeed, their growth induces a strengthening of both the Siberian High (up to $\sim$6 hPa, Fig. 11 d, g) and the Aleutian Low, resulting in a reinforcement of the East-West and North-South pressure gradients and ultimately of the EAWM index (from $\sim$8 to $\sim$15, Fig. 13). Mongolian (and/or Tian Shan and/or Pamir) uplift also results in localized precipitation intercepted by the landforms (Fig. 11 d to o), despite the overall dryness of the inland Asian region (SI Fig. 15). As Mongolian uplift deviates the winter westerlies flux northward, Eastern China is swept by colder and drier winds coming from Siberia, which translates into a marked decrease in winter precipitation (up to 80% decrease, Fig. 11 d). These changes in the wintertime climate lead to an important expansion

of regions displaying monsoon-like precipitation seasonality in eastern Asia (Fig. 11 f, i). The uplift of Tian Shan landforms, alone or together with the Pamir, has a lower impact on the winter pressure patterns compared to Mongolia uplift (Fig. 13) but nonetheless generates an almost complete drying on their eastern flanks (modern Gobi and Taklimakan deserts) because they act as an orographic barrier to westerly moisture flux (Fig. 11 g, j, m). Considering other sensitivity experiments, Asian winter climate exhibits only a weak response to changing Tibetan orography or pCO_2 values for Eocene conditions (SI Fig. 17 a to g, Fig. 13). Likewise, the Miocene winter pressure patterns in Asia are only mildly impacted by the Anatolian-Iranian landform uplift, the closure of the Tethyan Seaway, the Paratethys extent, or a pCO_2 drop from 560 to 420 ppm, when compared to the effect triggered by the Mongolian Plateau uplift (Fig. 13, SI Fig. 17 i to n and s, t).

6 Discussion

A long-standing debate pits the effect of continentality against that of orography as the main driver of Asian climate evolution (Prell & Kutzbach, 1992; Kutzbach et al., 1993; Ramstein et al., 1997; Fluteau et al., 1999; Z. Zhang et al., 2007; Roe et al., 2016; Zoura et al., 2019; R. Zhang et al., 2021). Our results (summarized in Table 2) suggest that these two features impacted different climatic characteristics of the Asian monsoons and all contributed to the emergence of current Asian climate. In the following sections, we put our main findings in perspective with available paleoclimatic indicators and previous modeling work, and tackle specific questions raised in section 2.4.

6.1 Summer monsoons in the Eocene: driven by pCO_2, Tibetan paleogeography or continentality ?

Although the LEo1_REF experiment simulates the seasonally wet climate indicated by eastern Chinese floras well (Meng et al., 2018; Y. Xie et al., 2022), it fails to identify the subhumid to humid climate inferred from fossil paleoflora and paleofauna in northern India (Saxena & Trivedi, 2009) and Tibet (T. Su et al., 2020; Sorrel et al., 2017). In a previous study, this south Asian aridity bias in our experiment was interpreted as resulting from the hot surface temperatures simulated in India, together with strong mid-tropospheric subsidence that inhibits deep convection and condensation, especially over northern India (Tardif et al., 2020). However, a previous study using the same model and paleogeography was able to simulate monsoon-like climate in both the EAM and SAM domains, providing that orbital configurations induced summer solar maxima (Tardif et al., 2021). This orbitally-paced wet/dry climate dichotomy is, at least qualitatively, in agreement with stratigraphic and paleobotanic evidence from southern and eastern China (C. Huang & Hinnov, 2019; Licht et al., 2014) and hints at a strong sensitivity of the South Asian region to surface temperature gradients in the Eocene. Such sensitivity seems further confirmed by the fact that, in the present study, South Asian Eocene climate appears especially sensitive to experiments affecting land-sea distribution and global temperature (LEo1_2X and LEo2_BengalSea, SI Fig. 15 f, g).

The East Asian monsoon domain, on the other hand, displays sensitivity to topographic changes in the Tibetan region. We simulate that an uplift of a proto-TP (LEo2_TP - LEo2_TPLow) would result in an onset or increase in EAM monsoon-like precipitation seasonality due to increased summer precipitation (up to 50%, Fig. 6 e, SI Fig. 15 b, c, d), in agreement with previous modeling work (R. Zhang et al., 2018; R. Zhang, Jiang, & Zhang, 2017; R. Zhang et al., 2021; Z.

Zhang et al., 2007; X. Liu & Yin, 2002; X. Li et al., 2017; Farnsworth et al., 2019; Thomson et al., 2021). Likewise, the decreased EAM intensity and increased inland Asian aridity when the souther adge of the TP is situated at 30°N is coherent with a previous study testing the impact of the latitudinal position of the incipient TP (R. Zhang et al., 2018). Therefore, the inception or reinforcement of the East Asian summer monsoon in the Eocene seems intertwined with the TP evolution history, as well as with existing topography before the TP uplift (e.g. the Lhasa terrane), although their paleoelevation and extent is not well constrained. Furthermore, we show that monsoon-like rainfall seasonality may have occurred prior to the establishment of modern-like East Asian winter monsoon circulation and Jet Stream summer migration, which were likely established during the late Paleogene or the Neogene.

6.2 Forcing factors of wintertime climate variability

The observation of loess deposits in northeastern Tibet as early as 40 Ma was interpreted as resulting from the periodic inception (or reinforcement) of the Siberian High in winter due to enhanced continentality after the Paratethys Sea retreat (Meijer et al., 2021). Other loess deposits reported during the Oligocene in the Chinese Loess Plateau and Mongolia, apparently coeval with periods of cooling and ice-sheet expansion (J. Sun & Windley, 2015; Wasiljeff et al., 2022), further suggest the presence of a Siberian High and corresponding dust transport in the late Paleogene. The potential forcing factors driving the establishment of this winter pressure pattern have, however, been significantly less studied than summer monsoons dynamics, with studies mostly focusing on the impact of orography rather than continentality (White et al., 2017; Sha et al., 2015; Baldwin & Vecchi, 2016). Our results suggest that both increased continentality and regional uplift contributed together to the progressive inception of the modern Siberian High,

while pCO_2 decrease alone had a lesser impact (Fig. 13). A modern-like Siberian High with typical EAWM wind patterns is however not simulated until our middle and late Miocene simulations, when the Tian Shan, but especially the Mongolian landforms, are set to their present-day elevation in the model.

Previous modeling work based on present-day geography that tested the effect of Mongolian landform uplift (Sha et al., 2015; Shi et al., 2015; Yu et al., 2018; R. Zhang, Jiang, Zhang, Cheng, & Zhang, 2017) reproduced the same tendencies that we present here, namely a strong increase of the winter sea level pressure over Siberia and typical deviation of the westerlies towards northern latitudes resulting in a pronounced drying of eastern Asia and EAWM amplification (Fig. 11 d). Other studies focusing more on the summer monsoon simulate increased EASM precipitation and wind circulation, although they incorporate Tian Shan uplift together with Mongolia (Yu et al., 2018; R. Zhang et al., 2012; H. Tang et al., 2013; Zhisheng et al., 2001), which remains coherent with our findings testing the uplift of both features (Fig. 11 h). Although the effect of Mongolian landforms has not been explicitly tested in paleoclimate modeling studies using realistic paleogeographic reconstructions, we can generally observe that when a modern-like Mongolian orography is prescribed, the simulated winds and precipitation are close to the modern-like EAWM (Licht et al., 2014; X. Li et al., 2017), while this is not the case with a reduced Mongolia elevation (Huber & Goldner, 2012). Given the large uncertainties related to the Hangay Dome uplift history, performing additional experiments testing the impact of an early uplift in an Oligocene configuration could enable one to evaluate the potential presence of a Siberian High at that time, and therefore help interpret early loess-like deposits observed at that time in the Chinese Loess Plateau and Mongolia (J. Sun & Windley, 2015; Wasiljeff et al., 2022). Loess-like deposition in the Xining Basin at ~ 40 Ma, however, seems too old to be attributed to the

development of the modern Siberian High, given that Mongolia was probably at low elevation and that continentality alone does not seem sufficient to trigger a modern-like Siberian anticyclone. This suggests that alternative mechanisms for dust transport should be explored for this period, although testing this hypothesis would require new data such as daily to hourly wind speed model outputs (Aoki et al., 2005).

6.3 The critical role of peripheral landforms in the establishment of monsoon seasonal features in the Miocene

In agreement with previous studies (R. Zhang, Jiang, & Zhang, 2017; Acosta & Huber, 2020; H. Tang et al., 2013), our results highlight the key role played by the Anatolian-Iranian Plateau uplift in modern-like SAM establishment, as it reinforces both summer rainfall and winter aridity (Fig. 9 j, k). The effect of the Tian Shan uplift on Asian climate is less conspicuous, likely owing to the proximity of these mountains to other important landforms (e.g. Pamir-Karakoram, Anatolian-Iranian Plateau, Mongolia), which may result in competing effects on the regional climate. While a rigorous comparison between our results and previous studies is hampered by many diverging boundary conditions, all tend to indicate that the Tian Shan uplift would have: i) increased yearly orographic precipitation on the ranges, ii) decreased precipitation in inland Asian mid-latitudes and iii) reinforced the EAM through increased summer precipitation (Fig. 11 m, n, o) (Baldwin & Vecchi, 2016; H. Tang et al., 2013; Yu et al., 2018; R. Zhang, Jiang, & Zhang, 2017; R. Zhang, Jiang, Zhang, Cheng, & Zhang, 2017). The key role played by the Tian Shan ranges (together with the Pamir and Mongolian landforms) in triggering the Jet Stream northward migration in summer (SI Fig. 18 e, f, Fig. 9 e, h, k, n), as suggested by previous modeling work derived from present-day geography (Sha et al., 2020; Shi et al., 2015), likely contributes to this

EASM intensification. Substantial differences are nevertheless noted with other modeling studies, especially regarding the impact of Tian Shan uplift on inland Asian and northeastern Indian climate, likely due to these regions' key location on the westerlies path. Westerlies may indeed be deviated either to the North or the South, depending on the respective degree of elevation of the Iranian-Anatolian Plateau and the Tian Shan. While we simulate a weakening of SAM rainfall seasonality due to increased winter precipitation after the Tian Shan uplift, the opposite trend is simulated in studies where the Anatolian-Iranian Plateau is already fully uplifted at the time of the Tian Shan uplift, thus preventing the westerlies from bringing moisture to India (Baldwin & Vecchi, 2016; H. Tang et al., 2013; Yu et al., 2018; R. Zhang, Jiang, & Zhang, 2017; X. Wang et al., 2020).

Our set of simulations also highlights that East African topography can strongly impact the Neogene evolution of the SASM as it greatly contributes to the establishment of modern-like atmospheric circulation, as discussed by Sarr et al. (2022). The presence of intermediate to high elevation topography in East Africa in the early Miocene is for example crucial for the "early" bending of the Somali Jet, before the closure of the West Tethys Seaway and establishment of Anatolian-Iranian topography with modern-like elevation (Fig. 9 e). Increasing elevation in Eastern Africa is also responsible, in our simulations, for increasing SASM precipitation. This contrasts with previous studies that simulate reduced SASM precipitation, due to African topography blocking the advection of moisture from equatorial Africa towards India (H.-H. Wei & Bordoni, 2016; Chakraborty et al., 2009). We hypothesize that this difference may come from these studies using present-day paleogeography, and/or unchanged fixed sea surface temperatures for all the experiments, thereby neglecting the potential effect of the East African uplift on Indian Ocean surface temperature gradients. It is also very likely that the impact of East African

highlands uplift on South Asian rainfall regime may be modulated by the degree of uplift in the Iranian-Anatolian region. Better constraints on the relative degree of uplift of these different mountain ranges in the past, although seldom taken into account, is therefore critical to interpreting paleoenvironmental indicators.

6.4 Continentality increase in the Miocene and acts as an amplifier of SAM, EAM and inland aridity

The northward motion of the ITCZ over the Arabian Sea and the stronger SASM precipitation in response to continentality increase in the Miocene is a feature clearly simulated in our experiments, and which is obtained with either the Paratethys Sea retreat or an emerging Arabian Peninsula (Fig. 8 e, h). The role of the Paratethys Sea retreat as a vector of amplified summer low pressure and resulting moisture advection via a strengthened Somali Jet is well established by modeling experiments (Ramstein et al., 1997; Fluteau et al., 1999; R. Zhang et al., 2021; Z. Zhang et al., 2007). The Paratethys Sea retreat also drastically dries the winter-time "westerly corridor" (centered around 40°N, Fig. 8 h), resulting in increased inland Asian aridity (Fig. 8 i), here again mostly in coherence with previous modeling studies (R. Zhang et al., 2021; Z. Zhang et al., 2007), and field evidence (Palcu et al., 2021). On the other hand, the effect of increased land exposure in the Arabian Peninsula region on Asian climate has been, to our knowledge, significantly less explored by modeling studies and is rarely mentioned as a potential forcing factor in proxy data studies. We tentatively attribute this to the lack of constraints and data in this region. Given the shallow depth and extension of the Arabian Peninsula (roughly comparable to India's area), it is very likely that the episodes of partial or complete flooding that occurred throughout the Oligocene to late Miocene (Barrier et al., 2018; Otero & Gayet, 2001)

may have had great consequences on atmospheric circulation patterns. Following Sarr et al. (2022), our results show that increased peninsula exposure reinforces the Somali Jet in summer and enhances summer precipitation in SAM and EAM domains (Fig. 8 e). Additionally, it drives the onset of upwelling in the Arabian Sea (see Sarr et al. (2022)), which is traditionally used as a proxy for the establishment of a monsoon wind regime in South Asia. Our simulations suggest that a proto Somali Jet and intense summer precipitation were most likely established in the middle Miocene, before the Arabian Peninsula emergence, and therefore before any strong upwelling activity initiated in the Arabian Sea. In addition, the onset of upwelling in the Arabian Sea was likely uncorrelated to potential Miocene uplift events in the Himalaya-Tibet region (Sarr et al., 2022).

6.5 Persistent uncertainties and directions for future work

Our study demonstrates the key role played by land-sea distribution and by all topographic features surrounding the Indian Ocean in shaping the modern SAM, EAM and inland Asia aridity. Nevertheless, additional work is required both from modeling and in the field to help refine our understanding of the mechanisms at play throughout the Cenozoic in Asia. By showing the influence of several geographical units on Asian climate during different geological periods, our results highlight the conceptual limitations of performing tests based on present-day geographies or assuming homogeneous Asian orographic uplift throughout geological history to evaluate past monsoon evolution. In that respect, it is not surprising that most of those type of studies simulate modern-like summer and winter monsoons features when maintaining high-elevation African, Mongolian and Anatolian-Iranian landforms, as well as an emerged Arabian platform (Roe et al., 2016; Zoura et al., 2019; Acosta & Huber, 2020). Our results also suggest that some

paleogeographic events considered roughly coeval may have had opposite influences on the Asian climate's seasonal features, for example the Tian Shan and Anatolian-Iranian Plateau uplift discussed in section 6.2. Refining the relative chronology of these various uplift phases is therefore paramount to better interpret the variations in monsoon intensity recorded by proxy data. Additionally, paleoelevation thresholds are likely to be critical for constraining Asian climate evolution, due to interactions of the topography with either low level (e.g. the summer monsoon winds) or mid tropospheric (e.g. the Jet Stream) air masses (X. Liu & Yin, 2002; X. Wang et al., 2020; Zhisheng et al., 2001; Prell & Kutzbach, 1992).

We also aknowledge that a better understanding of the seasonal monsoon mechanisms simulated here would benefit from additional simulations performed with increased spatial and temporal resolution. Previous work have for example demonstrated the importance of high spatial resolution in the full depiction of the SASM circulation (Acosta & Huber, 2017) or the study of the interplay between the summer Jet Stream behavior and the formation of the Meiyu-Bayu front in Eastern Asia (Kong et al., 2017; Sampe & Xie, 2010). Additional diagnostics at planetary-scale, may also provide interesting comparison with previous studies on the impact of monsoon dynamics on large scale circulation patterns and long-distance teleconnections (Rodwell & Hoskins, 1996; Merlis et al., 2013; Biasutti et al., 2018).

A more precise view of land-sea distribution and regional seaway evolution is also paramount. Indeed, these factors influence SST gradients, thereby controlling sea level pressure patterns, low tropospheric circulation, and oceanic circulation. Although our results point to a minimal effect of the mechanical closure of the Tethyan Seaway on regional climate, other features need to be tested. For example, a better understanding of the Indonesian Gateway and Indonesian throughflow evolution would be of great interest, as these control in part Indo-Pacific

Warm Pool SST distribution (Cane & Molnar, 2001; Tan et al., 2022) and may thus have influenced Asian climate (Q. Su et al., 2019). While the final step of the Indonesian Gateway constriction likely occurred during the Pliocene (Auer et a., 2019), its paleobathymetry and complex geometric configuration remain largely undocumented between 17-3.5 Ma (Kuhnt et al., 2004). While no major tectonic deformation is thought to have occurred during this period, the shallow depth of the gateway likely made it sensitive to middle Miocene sea level fluctuations (Sosdian & Lear, 2020), with possible impact on the Eastern Indian and Western Pacific Oceans surface temperatures and therefore on SST gradients. Although more distant from Asia, studies have also pointed to a possible influence of the Central American Seaway (Prabhat et al., 2022) or Drake (Toumoulin et al., 2020) and Tasman (Scher et al., 2015) Gateway openings on oceanic circulation, which may have in turn impacted sea surface temperature gradients and monsoon activity.

7 Conclusions

In this study, we took advantage of recent work that extended the Asian paleo-monsoonal record back to the Paleogene and of the improved understanding of the physical concepts underpinning the monsoons derived from climate model sensitivity experiments. Overall, we simulate an intensification of monsoonal metrics throughout the Cenozoic, in response to evolving paleogeography and global climate trends. Our results suggest that modern-like monsoons likely existed since at least the mid-late Miocene when considering together patterns of atmospheric circulation as well as seasonality and precipitation amounts, in agreement with paleoclimate indicators. However, we also show that high rainfall seasonality already existed since the Paleogene in both SAM and EAM domains, before the establishment of modern atmospheric

circulation patterns. In accord with previous studies, our results highlight the limited effect of pCO_2 on monsoon dynamics, when compared to the effect of paleogeographic changes. A notable exception is the strong impact of a pCO_2 drawdown at the EOT on the northward migration of the subtropical Jet Stream during summer, which increases precipitation in the EAM region.

Our results also strongly suggest that any variations in the land-sea distribution, whether due to tectonic activity or sea level fluctuations, would have strongly impacted Asian climate, despite the fact that the exact shape and extent of coastal shallow-water environments remain poorly constrained. Many episodes of increased continentality are documented over the course of the Cenozoic, including regional regressions of the Paratethys epicontinental Sea and periodic exposure of the Arabian Platform due to sea level fluctuations since the Eocene-Oligocene Transition. All of these events likely favored the enhancement of summer moisture penetration into Asia, by promoting the extension of the wide subtropical low pressure belt, thereby amplifying the seasonal latitudinal migration of the ITCZ on land.

In addition, while the evolution of the Himalayan-TP complex is recurrently put forward as the leading phenomenon driving Asian climate evolution, our results rather point towards a combined effect of all landforms surrounding the modern Indian Ocean. We also emphasize that all paleogeographic features do not bear the same importance on the SASM, EASM or EAWM, respectively. Our simulations suggest that the Tibetan Plateau uplift likely favored the onset of monsoon-like precipitation seasonality in eastern Asia in the Eocene, by promoting the advection of moist air masses in summer and partially shielding the region from westerly moisture input during winter. Alongside that, we show that the uplift of Eastern African and Anatolian-Iranian landforms was critical to intensify and redirect the Somali Jet towards the Indian subcontinent,

thereby contributing to the development of a modern-like South Asian monsoon summer circulation and amplifying moisture advection towards Asia in summer. In addition, in our simulations, the uplift of the Anatolian-Iranian orogen contributed to enhancing winter aridity in most of southeastern Asia by blocking moisture advection from the westerlies to lower latitudes.

Our simulations further show that uplift of the Tian Shan and the Mongolian mountains was key for the establishment of the winter Siberian High, and resulting aridification of inland and eastern Asia during winter. The summer Jet Stream migration north of the Tibetan Plateau was likely amplified in the mid-late Miocene, as the Pamir and Tian Shan landforms approached their modern elevations and contributed to channeling the jet towards higher latitudes. This relocation of the Jet Stream amplifies the penetration of moist air masses over eastern China, which contributes to increasing EAM precipitation seasonality. Overall, our results do suggest a fundamentally polygenetic history of monsoonal evolution, in agreement with available paleoclimate indicators and previous modeling studies. This suggests that the very concept of a "monsoon onset" is inappropriate. We also stress the need for more accurate constraints on the evolution of paleo-shorelines, the relative timing of peripheral mountain belts uplift, as well as on the paleo-evelation of landforms in order to better understand the evolution of Asian climate in the past.

Acronyms

ITCZ Inter Tropical Convergence Zone

SASM South Asian Summer Monsoon

EASM East Asian Summer Monsoon

EAWM East Asian Winter Monsoon

TP Tibetan Plateau

EOT Eocene Oligocene Transition

CLAMP Climate Leaf Analysis Multivariate Program

Acknowledgments

D.T., G.L.H., F.F., A.T., Y.D., P.S., J-B.L. and A-C.S. were granted access to the HPC resources of TGCC under the allocations 2018-A0050107601, 2018-A0050102212, 2019-A0070107601, 2019-A0050102212 and 2020-A0090107601 made by GENCI. D.T. has received funding from the European Research Council (ERC) under the European Union's Horizon 2020 research and innovation programme (grant agreement No 865787). Y.D. acknowledges support from ANR AMOR (ANR-16-CE31-0020). Most of the Figures were done using NOAA pyferret within Jupyter notebooks, thanks to the ferretmagic add-on developed at LSCE by Patrick Brockmann. Ferret is a product of NOAA's Pacific Marine Environmental Laboratory. Information is available at http://ferret.pmel.noaa.gov/Ferret (last access: 1 Jan 2022; NOAA's Pacific Marine Environmental Laboratory, 2020), distributed under the Open Source Definition. The Jupyter notebook is an open-source web application. The paleogeographic configurations from F.P. were produced using the paleoenvironment online application (https://map.paleoenvironment.eu/). Other reconstructions were obtained with NetCDF editor online tools developed by the Paleoclimate modelling group at CEREGE laboratory (https://paleoclim-cnrs.github.io/documentation-processing/IPSL_Boundary_Conditions/). The scientific color maps (https://www.fabiocrameri.ch/colourmaps/) (Crameri, 2021) used in most of the Figures prevent visual distortion of the data and exclusion of readers with color vision deficiencies (Crameri et al., 2020).

References

Abbott, A. N., Haley, B. A., Tripati, A. K., & Frank, M. (2016, April). Constraints on ocean circulation at the Paleocene–Eocene Thermal Maximum from neodymium isotopes. *Climate of the Past*, *12*(4), 837–847. Retrieved 2017-10-09, from http://www.clim-past.net/12/837/2016/ doi: 10.5194/cp-12-837-2016

Abels, H. A., Dupont-Nivet, G., Xiao, G., Bosboom, R., & Krijgsman, W. (2011, January). Step-wise change of Asian interior climate preceding the Eocene–Oligocene Transition (EOT). *Palaeogeography, Palaeoclimatology, Palaeoecology*, *299*(3-4), 399–412. Retrieved 2017-10-09, from http://linkinghub.elsevier.com/retrieve/pii/S0031018210007042 doi: 10.1016/j.palaeo.2010.11.028

Acosta, R. P., & Huber, M. (2017). The neglected Indo-Gangetic Plains low-level jet and its importance for moisture transport and precipitation during the peak summer monsoon. *Geophysical Research Letters*, *44*(16), 8601–8610. Retrieved 2021-03-08, from https://agupubs.onlinelibrary.wiley.com/doi/abs/10.1002/2017GL074440 (eprint: https://agupubs.onlinelibrary.wiley.com/doi/pdf/10.1002/2017GL074440) doi: https://doi.org/10.1002/2017GL074440

Acosta, R. P., & Huber, M. (2020, February). Competing Topographic Mechanisms for the Summer Indo-Asian Monsoon. *Geophysical Research Letters*, *47*(3). Retrieved 2020-06-19, from

https://onlinelibrary.wiley.com/doi/abs/10.1029/2019GL085112 doi: 10.1029/2019GL085112

Agard, P., Omrani, J., Jolivet, L., Whitechurch, H., Vrielynck, B., Spakman, W., . . . Wortel, R. (2011, November). Zagros orogeny: a subduction-dominated process. *Geological Magazine*, *148*(5-6), 692–725. Retrieved 2017-10-09, from http://www.journals.cambridge.org/abstract S001675681100046X doi: 10.1017/S001675681100046X

Ali, J. R., & Aitchison, J. C. (2005, October). Greater India. *Earth Science Reviews*, *72*(3-4), 169–188. Retrieved 2022-09-13, from https://linkinghub.elsevier.com/retrieve/pii/S0012825205001042 doi: 10.1016/j.earscirev.2005.07.005

Ali, S., Hathorne, E. C., & Frank, M. (2021). Persistent Provenance of South Asian Monsoon-Induced Silicate Weathering Over the Past 27 Million Years. *Paleoceanography and Paleoclimatology*, *36*(3), e2020PA003909. Retrieved 2022-05-02, from https://onlinelibrary.wiley.com/doi/abs/10.1029/2020PA003909 eprint: https://onlinelibrary.wiley.com/doi/pdf/10.1029/2020PA003909) doi: 10.1029/2020PA003909

Anderson, C., Murray, R., Dunlea, A., Giosan, L., Kinsley, C., McGee, D., & Tada, R. (2020, May). Aeolian delivery to Ulleung Basin, Korea (Japan Sea), during development of the East Asian Monsoon through the last 12 Ma. *Geological Magazine*, *157*(5), 806–817. Retrieved 2022-11-14, from https://www.cambridge.org/core/product/identifier/S001675681900013X/type/journal article doi: 10.1017/S001675681900013X

Ao, H., Roberts, A. P., Dekkers, M. J., Liu, X., Rohling, E. J., Shi, Z., . . . Zhao, X. (2016, June). Late Miocene–Pliocene Asian monsoon intensification linked to Antarctic icesheet growth. *Earth and Planetary Science Letters*, *444*, 75–87. Retrieved 2022-05-03, from https://linkinghub.elsevier.com/retrieve/pii/S0012821X16301157 doi: 10.1016/j.epsl.2016.03.028

Ao, H., Rohling, E. J., Zhang, R., Roberts, A. P., Holbourn, A. E., Ladant, J.-B., . . . An, Z. (2021, November). Global warming-induced Asian hydrological climate transition across the Miocene–Pliocene boundary. *Nature Communications*, *12*(1), 6935. Retrieved 2022-05-03, from http://www.nature.com/articles/s41467-021-27054-5 (Number: 1 Publisher: Nature Publishing Group) doi: 10.1038/s41467-021-27054-5

Aoki, I., Kurosaki, Y., Osada, R., Sato, T., & Kimura, F. (2005). Dust storms generated by mesoscale cold fronts in the Tarim Basin, Northwest China. *Geophysical Research Letters*, *32*(6). Retrieved 2022-02-21, from http://onlinelibrary.wiley.com/doi/abs/10.1029/2004GL021776 (eprint:https://agupubs.onlinelibrary.wiley.com/doi/pdf/10.1029/2004GL021776) doi: 10.1029/2004GL021776

Auer, G., Vleeschouwer, D. D., Smith, R. A., Bogus, K., Groeneveld, J., Grunert, P., . . . Henderiks, J. (2019). Timing and Pacing of Indonesian Throughow Restriction and Its Connection to Late Pliocene Climate Shifts. *Paleoceanography and Paleoclimatology*, *34*(4), 635–657. Retrieved 2021-09-02, from http://agupubs.onlinelibrary.wiley.com/doi/abs/10.1029/2018

PA003512 (eprint:https://onlinelibrary.wiley.com/doi/pdf/10.1029/2018PA003512) doi: 10.1029/2018PA003512

Averyanova, A., Tarasevich, V., Popova, S., Utescher, T., Li, S.-F., Mosbrugger, V., & Xing, Y. (2021, February). Rupelian Kazakhstan oras in the context of early Oligocene climate and vegetation in Central Asia. *Terra Nova*, *33*. doi: 10.1111/ter.12523

Baldermann, A., Wasser, O., Abdullayev, E., Bernasconi, S., Löhr, S., Wemmer, K., . . . Richoz, S. (2021, September). Palaeo-environmental evolution of Central Asia during the Cenozoic: new insights from the continental sedimentary archive of the Valley of Lakes (Mongolia). *Climate of the Past*, *17*(5), 1955–1972. Retrieved 2022-03-09, from https://cp.copernicus.org/articles/17/1955/2021/ doi: 10.5194/cp-17-1955-2021

Baldwin, J., & Vecchi, G. (2016, August). Influence of the Tian Shan on Arid Extratropical Asia. *Journal of Climate*, *29*(16), 5741–5762. Retrieved 2021-09-23, from https://journals.ametsoc.org/view/journals/clim/29/16/jcli-d-15-0490.1.xml (Publisher: American Meteorological Society Section: Journal of Climate) doi: 10.1175/JCLI-D-15-0490.1

Ballato, P., Landgraf, A., Schildgen, T. F., Stockli, D. F., Fox, M., Ghassemi, M. R., . . . Strecker, M. R. (2015, September). The growth of a mountain belt forced by base-level fall: Tectonics and surface processes during the evolution of the Alborz Mountains, N Iran. *Earth and Planetary Science Letters*, *425*, 204–218. Retrieved 2021-03-10, from https://www.sciencedirect.com/science/article/pii/S0012821X15003490 doi: 10.1016/j.epsl.2015.05.051

Ballato, P., Mulch, A., Landgraf, A., Strecker, M. R., Dalconi, M. C., Friedrich, A., & Tabatabaei, S. H. (2010, November). Middle to late Miocene Middle Eastern climate from stable oxygen and carbon isotope data, southern Alborz mountains, N Iran. *Earth and Planetary Science Letters*, *300*(1), 125–138. Retrieved 2021-04-07, from https://www.sciencedirect.com/science/article/pii/S0012821X10006308 doi: 10.1016/j.epsl.2010.09.043

Bande, A., Sobel, E. R., Mikolaichuk, A., Schmidt, A., & Stockli, D. F. (2017). Exhumation history of the western Kyrgyz Tien Shan: Implications for intramontane basin formation. *Tectonics*, *36*(1), 163–180. Retrieved 2021-03-26, from http://agupubs.onlinelibrary.wiley.com/doi/abs/10.1002/2016TC004284 (eprint: https://onlinelibrary.wiley.com/doi/pdf/10.1002/2016TC004284) doi: https://doi.org/10.1002/2016TC004284

Bannon, P. R. (1979, November). On the Dynamics of the East African Jet. I: Simulation of Mean Conditions for July. *Journal of the Atmospheric Sciences*, *36*(11), 2139–2152. Retrieved 2019-07-05, from http://journals.ametsoc.org/doi/abs/10.1175/1520-0469%281979%29036%3C2139%3AOTDOTE%3E2.0.CO%3B2 doi: 10.1175/1520-0469(1979)036h2139:OTDOTEi2.0.CO;2

Barbolini, N., Woutersen, A., Dupont-Nivet, G., Silvestro, D., Tardif, D., Coster, P. M. C., . . . Hoorn, C. (2020). Cenozoic evolution of the steppe-desert biome in Central Asia. *Science Advances*, *6*(41), eabb8227. Retrieved 2022-05-03, from https://www.science.org/doi/10.1126/sciadv.abb8227 (Publisher: American Association for the Advancement of Science) doi: 10.1126/sciadv.abb8227

Barrier, , Vrielynck, B., & Brunet-Lourdin, M.-F. (2018). *Paleotectonic Reconstruction of the Central Tethyan Realm: Tectonono-Sedimentary-Palinspastic Maps from Late Permian to Pliocene: Atlas of 20 Maps*.

Beasley, C., Kender, S., Giosan, L., Bolton, C. T., Anand, P., Leng, M. J., . . . Littler, K. (2021). Evidence of a South Asian Proto-Monsoon During the Oligocene-Miocene Transition. *Paleoceanography and Paleoclimatology*, *36*(9), e2021PA004278. Retrieved 2022-05-03, from https://onlinelibrary.wiley.com/doi/abs/10.1029/2021PA004278 (eprint:https://onlinelibrary.wiley.com/doi/pdf/10.1029/2021PA004278) doi: 10.1029/2021PA004278

Bershaw, J., Garzione, C. N., Schoenbohm, L., Gehrels, G., & Tao, L. (2012, January). Cenozoic evolution of the Pamir plateau based on stratigraphy, zircon provenance, and stable isotopes of foreland basin sediments at Oytag (Wuyitake) in the Tarim Basin (west China). *Journal of Asian Earth Sciences*, *54*, 136–148. Retrieved 2017-10-09, from http://linkinghub.elsevier.com/retrieve/pii/S1367912011001878 doi: 10.1016/j.jseaes.2011.04.020

Betzler, C., Eberli, G. P., Kroon, D., Wright, J. D., Swart, P. K., Nath, B. N., . . . Young, J. R. (2016, July). The abrupt onset of the modern South Asian Monsoon winds. *Scientific Reports*, *6*(1), 29838. Retrieved 2022-05-03, from http://www.nature.com/articles/srep29838 (Number: 1 Publisher: Nature Publishing Group) doi: 10.1038/srep29838

Betzler, C., Eberli, G. P., Lüdmann, T., Reolid, J., Kroon, D., Reijmer, J. J. G., . . . Yao, Z. (2018, January). Refinement of Miocene sea level and monsoon events from the sedimentary

archive of the Maldives (Indian Ocean). *Progress in Earth and Planetary Science*, *5*(1), 5. Retrieved 2021-03-17, from https://doi.org/10.1186/s40645-018-0165-x doi: 10.1186/s40645-018-0165-x

Bhatia, H., Khan, M. A., Srivastava, G., Hazra, T., Spicer, R., Hazra, M., . . . Roy, K. (2021, May). Late Cretaceous–Paleogene Indian monsoon climate vis-à-vis movement of the Indian plate, and the birth of the South Asian Monsoon. *Gondwana Research*, *93*, 89–100. Retrieved 2022-05-03, from https://linkinghub.elsevier.com/retrieve/pii/S1342937X21000289 doi: 10.1016/j.gr.2021.01.010

Bhatia, H., Srivastava, G., Adhikari, P., Tao, S., Utescher, T., Paudayal, K. N., & Mehrotra, R. C. (2022, April). Asian monsoon and vegetation shift: evidence from the Siwalik succession of India. *Geological Magazine*, 1–18. Retrieved 2022-05-02, from http://www.cambridge.org/core/journals/geological-magazine/article/asian-monsoon-and-vegetation-shift-evidence-from-the-siwalik-succession-of-india/C11DD05BB2C70B0BA4ED7930A80219D2 (Publisher: Cambridge University Press) doi: 10.1017/S0016756822000243

Bhatia, H., Srivastava, G., Spicer, R., Farnsworth, A., Spicer, T., Mehrotra, R., . . . Valdes, P. (2021, January). Leaf physiognomy records the Miocene intensification of the South Asia Monsoon. *Global and Planetary Change*, *196*, 103365. Retrieved 2022-05-03, from https://linkinghub.elsevier.com/retrieve/pii/S0921818120302563 doi:10.1016/j.gloplacha.2020.103365

Bialik, O. M., Auer, G., Ogawa, N. O., Kroon, D., Waldmann, N. D., & Ohkouchi, N. (2020). Monsoons, Upwelling, and the Deoxygenation of the Northwestern Indian Ocean in

Response to Middle to Late Miocene Global Climatic Shifts. *Paleoceanography and Paleoclimatology*, *35*(2), e2019PA003762. Retrieved 2021-03-17, from http://agupubs.onlinelibrary.wiley.com/doi/abs/10.1029/2019PA003762 (eprint: https://onlinelibrary.wiley.com/doi/pdf/10.1029/2019PA003762) doi: https://doi.org/10.1029/2019PA003762

Bialik, O. M., Frank, M., Betzler, C., Zammit, R., & Waldmann, N. D. (2019, June). Two-step closure of the Miocene Indian Ocean Gateway to the Mediterranean. *Scientific Reports*, *9*(1), 8842. Retrieved 2021-03-09, from https://www.nature.com/articles/s41598-019-45308-7 (Number: 1 Publisher: Nature Publishing Group) doi: 10.1038/s41598-019-45308-7

Biasutti, M., Voigt, A., Boos, W. R., Braconnot, P., Hargreaves, J. C., Harrison, S. P., . . . Xie, S.-P. (2018, June). Global energetics and local physics as drivers of past, present and future monsoons. *Nature Geoscience*, *11*(6), 392–400. Retrieved 2019-01-22, from http://www.nature.com/articles/s41561-018-0137-1 doi: 10.1038/s41561-018-0137-1

Bierman, P. R., Shakun, J. D., Corbett, L. B., Zimmerman, S. R., & Rood, D. H. (2016, December). A persistent and dynamic East Greenland Ice Sheet over the past 7.5 million years. *Nature*, *540*(7632), 256–260. Retrieved 2021-06-21, from http://www.nature.com/articles/nature20147 (Bandiera abtest: a Cg type: Nature Research Journals Number: 7632 Primary atype: Research Publisher: Nature Publishing Group Subject term: Cryospheric science;Nuclear chemistry;Palaeoclimate Subject term id: cryospheric-science;nuclear-chemistry;palaeoclimate) doi: 10.1038/nature20147

Blayney, T., Najman, Y., Dupont-Nivet, G., Carter, A., Millar, I., Garzanti, E., . . . Vezzoli, G. (2016, October). Indentation of the Pamirs with respect to the northern margin of Tibet: Constraints from the Tarim basin sedimentary record: INDENTATION OF THE PAMIRS. *Tectonics*, *35*(10), 2345–2369. Retrieved 2017-10-09, from http://doi.wiley.com/10.1002/2016TC004222 doi: 10.1002/2016TC004222

Bolton, C. T., Gray, E., Kuhnt, W., Holbourn, A. E., Lübbers, J., Grant, K., . . . Andersen, N. (2022, April). Secular and orbital-scale variability of equatorial Indian Ocean summer monsoon winds during the late Miocene. *Climate of the Past*, *18*(4), 713–738. Retrieved 2022-06-02, from https://cp.copernicus.org/articles/18/713/2022/ doi: 10.5194/cp-18-713-2022

Boos, W. R., & Kuang, Z. (2010, January). Dominant control of the South Asian monsoon by orographic insulation versus plateau heating. *Nature*, *463*(7278), 218–222. Retrieved 2017-10-09, from http://www.nature.com/doifinder/10.1038/nature08707 doi: 10.1038/nature08707

Boos, W. R., & Kuang, Z. (2013, February). Sensitivity of the South Asian monsoon to elevated and non-elevated heating. *Scientific Reports*, *3*(1), 1192. Retrieved 2023-03-31, from https://www.nature.com/articles/srep01192 (Number: 1 Publisher: Nature Publishing Group) doi: 10.1038/srep01192

Bosboom, R., Dupont-Nivet, G., Grothe, A., Brinkhuis, H., Villa, G., Mandic, O., . . . Krijgsman, W. (2014a, October). Linking Tarim Basin sea retreat (west China) and Asian aridification

in the late Eocene. *Basin Research*, *26*(5), 621–640. Retrieved 2017-10-09, from http://doi.wiley.com/10.1111/bre.12054 doi: 10.1111/bre.12054

Bosboom, R., Dupont-Nivet, G., Grothe, A., Brinkhuis, H., Villa, G., Mandic, O., . . . Guo, Z. (2014b, June). Timing, cause and impact of the late Eocene stepwise sea retreat from the Tarim Basin (west China). *Palaeogeography, Palaeoclimatology, Palaeoecology*, *403*, 101–118. Retrieved 2017-10-09, from http://linkinghub.elsevier.com/retrieve/pii/S0031018214001709 doi: 10.1016/j.palaeo.2014.03.035

Bosboom, R., Mandic, O., Dupont-Nivet, G., Proust, J.-N., Ormukov, C., & Aminov, J. (2017). Late Eocene palaeogeography of the proto-Paratethys Sea in Central Asia (NW China, southern Kyrgyzstan and SW Tajikistan). *Geological Society, London, Special Publications*, *427*(1), 565–588. Retrieved 2019-11-22, from http://sp.lyellcollection.org/lookup/doi/10.1144/SP427.11 doi: 10.1144/SP427.11

Botsyun, S., Sepulchre, P., Donnadieu, Y., Risi, C., Licht, A., & Caves Rugenstein, J. K. (2019, March). Revised paleoaltimetry data show low Tibetan Plateau elevation during the Eocene. *Science*, *363*(6430), eaaq1436. Retrieved 2019-07-23, from http://www.sciencemag.org/lookup/doi/10.1126/science.aaq1436 doi:10.1126/science.aaq1436

Botsyun, S., Sepulchre, P., Risi, C., & Donnadieu, Y. (2016, June). Impacts of Tibetan Plateau uplift on atmospheric dynamics and associated precipitation ^{18}O. *Climate of the Past*, *12*(6), 1401–1420. Retrieved 2017-10-09, from http://www.clim-past.net/12/1401/2016/ doi: 10.5194/cp-12-1401-2016

Boucot, A. J., Xu, C., Scotese, C. R., & Morley, R. J. (2013). *Phanerozoic Paleoclimate: An Atlas of Lithologic Indicators of Climate*. Tulsa, Oklahoma, U.S.A.: SEPM (Society for Sedimentary Geology). Retrieved 2019-11-04, from https://pubs.geoscienceworld.org/books/book/1966/ doi: 10.2110/sepmcsp.11

Bougeois, L., Dupont-Nivet, G., de Rafélis, M., Tindall, J. C., Proust, J.-N., Reichart, G.-J., . . . Ormukov, C. (2018, March). Asian monsoons and aridification response to Paleogene sea retreat and Neogene westerly shielding indicated by seasonality in Paratethys oysters. *Earth and Planetary Science Letters*, *485*, 99–110. Retrieved 2018-04-03, from http://linkinghub.elsevier.com/retrieve/pii/S0012821X17307483 doi: 10.1016/j.epsl.2017.12.036

Bullen, M., Burbank, D., & Garver, J. (2003, March). Building the Northern Tien Shan: Integrated Thermal, Structural, and Topographic Constraints. *The Journal of Geology*, *111*(2), 149–165. Retrieved 2021-03-26, from https://www.journals.uchicago.edu/doi/10.1086/345840 doi: 10.1086/345840

Burls, N. J., Bradshaw, C. D., Boer, A. M. D., Herold, N., Huber, M., Pound, M., . . . Zhang, Z. (2021). Simulating Miocene Warmth: Insights From an Opportunistic Multi-Model Ensemble (MioMIP1). *Paleoceanography and Paleoclimatology*, *36*(5), e2020PA004054. Retrieved 2021-06-21, from http://agupubs.onlinelibrary.wiley.com/doi/abs/10.1029/2020PA004054 (eprint: https://onlinelibrary.wiley.com/doi/pdf/10.1029/2020PA004054) doi: 10.1029/2020PA004054

Cane, M. A., & Molnar, P. (2001, May). Closing of the Indonesian seaway as a precursor to east African aridification around 3–4 million years ago. *Nature*, *411*(6834), 157–162. Retrieved 2021-09-09, from http://www.nature.com/articles/35075500 (Bandiera abtest: a Cg type: Nature Research Journals Number: 6834 Primary atype: Research Publisher: Nature Publishing Group) doi: 10.1038/35075500

Carrapa, B., DeCelles, P. G., Wang, X., Clementz, M. T., Mancin, N., Stoica, M., . . . Chen, F. (2015, August). Tectono-climatic implications of Eocene Paratethys regression in the Tajik basin of central Asia. *Earth and Planetary Science Letters*, *424*, 168–178. Retrieved 2022-03-21, from https://www.sciencedirect.com/science/article/pii/S0012821X15003325 doi: 10.1016/j.epsl.2015.05.034

Cavazza, W., Cattò, S., Zattin, M., Okay, A. I., & Reiners, P. (2018, August). Thermochronology of the Miocene Arabia-Eurasia collision zone of southeastern Turkey. *Geosphere*, *14*(5), 2277–2293. Retrieved 2022-03-24, from https://doi.org/10.1130/GES01637.1 doi: 10.1130/GES01637.1

Caves Rugenstein, J., Bayshashov, B., Zhamangara, A., Ritch, A., Ibarra, D., Mix, H., . . . Chamberlain, C. (2017, February). Late Miocene Uplift of the Tian Shan and Altai and Reorganization of Central Asia Climate. *GSA Today*, *27*. doi: 10.1130/GSATG305A.1

Caves Rugenstein, J., Sjostrom, D., Mix, H., Winnick, M., & Chamberlain, C. (2014, September). Aridification of Central Asia and Uplift of the Altai and Hangay Mountains, Mongolia: Stable Isotope Evidence. *American Journal of Science*, *314*, 1171–1201. doi: 10.2475/08.2014.01]

Chakraborty, A., Nanjundiah, R. S., & Srinivasan, J. (2009). Impact of African orography and the Indian summer monsoon on the low-level Somali jet. *International Journal of Climatology*, *29*(7), 983–992. Retrieved 2022-06-28, from http://onlinelibrary.wiley.com/doi/abs/10.1002/joc.1720 (eprint:https://rmets.onlinelibrary.wiley.com/doi/pdf/10.1002/joc.1720) doi: 10.1002/joc.1720

Charreau, J., Chen, Y., Gilder, S., Dominguez, S., Avouac, J.-P., Sen, S., . . . Wang, W.-M. (2005, January). Magnetostratigraphy and rock magnetism of the Neogene Kuitun He section (northwest China): implications for Late Cenozoic uplift of the Tianshan mountains. *Earth and Planetary Science Letters*, *230*(1), 177–192. Retrieved 2021-03-29, from https://www.sciencedirect.com/science/article/pii/S0012821X04006739 doi: 10.1016/j.epsl.2004.11.002

Charreau, J., Kent-Corson, M. L., Barrier, L., Augier, R., Ritts, B. D., Chen, Y., . . . Guil1 mette, C. (2012, August). A high-resolution stable isotopic record from the Junggar Basin (NW China): Implications for the paleotopographic evolution of the Tianshan Mountains. *Earth and Planetary Science Letters*, *341-344*, 158–169. Retrieved 2017-10-09, from http://linkinghub.elsevier.com/retrieve/pii/S0012821X12002622 doi: 10.1016/j.epsl.2012.05.033

Cheng, Y.-M., & Yang, X.-N. (2016, February). Miocene woods from the Qaidam Basin on northern Qinghai-Tibet Plateau with implications for paleoenvironmental change. *Journal of Asian Earth Sciences*, *116*, 198–207. Retrieved 2023-01-03, from https://linkinghub.elsevier.com/retrieve/pii/S1367912015301516 doi: 10.1016/j.jseaes.2015.11.022

Clark, M., House, M., Royden, L., Whipple, K., Burchfiel, B., Zhang, X., & Tang, W. (2005, June). Late Cenozoic uplift of southeastern Tibet. *Geology*, *33*(6), 525–528. Retrieved 2022-03-03, from https://doi.org/10.1130/G21265.1 doi: 10.1130/G21265.1

Clift, P. D. (2020, June). Asian monsoon dynamics and sediment transport in SE Asia. *Journal of Asian Earth Sciences*, *195*, 104352. Retrieved 2022-05-02, from https://linkinghub.elsevier.com/retrieve/pii/S1367912020301334 doi: 10.1016/j.jseaes.2020.104352

Clift, P. D., Betzler, C., Christensen, B., Clemens, S., Eberli, G., France-Lanord, C., . . . Wan, S. (2022, July). A synthesis of monsoon exploration in the Asian marginal seas. *Scientific Drilling*, *10*, 1–29. doi: 10.5194/sd-10-1-2022

Clift, P. D., Hodges, K., Heslop, Hannigan, R., Hoang, L., & Calves, G. (2008, November). Correlation of Himalayan exhumation rates and Asia monsoon intensity. *Nature Geoscience*, *1*, doi:10.1038/ngeo351. doi: 10.1038/ngeo351

Clift, P. D., Kulhanek, D. K., Zhou, P., Bowen, M. G., Vincent, S. M., Lyle, M., & Hahn, A. (2019, June). Chemical weathering and erosion responses to changing monsoon climate in the Late Miocene of Southwest Asia. *Geological Magazine*, *157*(6), 939–955. Retrieved 2021-05-27, from https://doi.org/10.1017/S0016756819000608 doi:10.1017/S0016756819000608

Clift, P. D., Wan, S., & Blusztajn, J. (2014, March). Reconstructing chemical weathering, physical erosion and monsoon intensity since 25Ma in the northern South China Sea: A review of competing proxies. *Earth-Science Reviews*, *130*, 86–102. Retrieved 2022-09-13, from https://www.sciencedirect.com/science/article/pii/S0012825214000051 doi: 10.1016/j.earscirev.2014.01.002

Cohen, J., Saito, K., & Entekhabi, D. (2001, January). The role of the Siberian high in northern hemisphere climate variability. *Geophysical Research Letters*, *28*(2), 299–302. Retrieved 2020-06-20, from http://doi.wiley.com/10.1029/2000GL011927 doi: 10.1029/2000GL011927

Cook, K. L., & Royden, L. H. (2008). The role of crustal strength variations in shaping orogenic plateaus, with application to Tibet. *Journal of Geophysical Research: Solid Earth*, *113*(B8). Retrieved 2021-03-29, from http://agupubs.onlinelibrary.wiley.com/doi/abs/10.1029/2007JB005457 (eprint: https://onlinelibrary.wiley.com/doi/pdf/10.1029/2007JB005457) doi: https://doi.org/10.1029/2007JB005457

Couvreur, T. L. P., Dauby, G., Blach-Overgaard, A., Deblauwe, V., Dessein, S., Droissart, V., . . . Sepulchre, P. (2021). Tectonics, climate and the diversification of the tropical African terrestrial ora and fauna. *Biological Reviews*, *96*(1), 16–51. Retrieved 2021-03-09, from https://onlinelibrary.wiley.com/doi/abs/10.1111/brv.12644 (eprint: https://onlinelibrary.wiley.com/doi/pdf/10.1111/brv.12644) doi: https://doi.org/10.1111/brv.12644

Crameri, F. (2021, February). *Scientific colour maps*. Zenodo. Retrieved 2021-04-15, from https://zenodo.org/record/4491293 (Language: eng) doi: 10.5281/zenodo.4491293

Crameri, F., Shephard, G. E., & Heron, P. J. (2020, October). The misuse of colour in science communication. *Nature Communications*, *11*(1), 5444. Retrieved 2021-04-15, from http://www.nature.com/articles/s41467-020-19160-7 (Number: 1 Publisher: Nature Publishing Group) doi: 10.1038/s41467-020-19160-7

Cunningham, W. D. (2001, February). Cenozoic normal faulting and regional doming in the southern Hangay region, Central Mongolia: implications for the origin of the Baikarift province. *Tectonophysics*, *331*(4), 389–411. Retrieved 2021-03-26, from https://www.sciencedirect.com/science/article/pii/S0040195100002286 doi: 10.1016/S0040-1951(00)00228-6

Curry, W. B., Ostermann, D. R., Guptha, M. V. S., & Ittekkot, V. (1992, January). Foraminiferal production and monsoonal upwelling in the Arabian Sea: evidence from sediment traps. *Geological Society, London, Special Publications*, *64*(1), 93–106. Retrieved 2023-03-30, from https://www.lyellcollection.org/doi/10.1144/GSL.SP.1992.064.01.06 doi: 10.1144/GSL.SP.1992.064.01.06

Daradich, A., Mitrovica, J. X., Pysklywec, R. N., Willett, S. D., & Forte, A. M. (2003). Mantle ow, dynamic topography, and rift-flank uplift of Arabia. *Geology*, *31*(10), 901–904.

Darin, M. H., Umhoefer, P. J., & Thomson, S. N. (2018). Rapid Late Eocene Exhumation of the Sivas Basin (Central Anatolia) Driven by Initial Arabia-Eurasia Collision. *Tectonics*, *37*(10), 3805–3833. Retrieved 2022-03-04, from http://onlinelibrary.wiley.com/doi/abs/10.1029/2017TC004954 (eprint: https://agupubs.onlinelibrary.wiley.com/doi/pdf/10.1029/2017TC004954) doi: 10.1029/2017TC004954

DeConto, R. M., & Pollard, D. (2003, September). A coupled climate–ice sheet modeling approach to the Early Cenozoic history of the Antarctic ice sheet. Palaeogeography, Palaeoclimatology, *Palaeoecology*, *198*(1-2), 39–52. Retrieved 2018-01-08, from

http://linkinghub.elsevier.com/retrieve/pii/S0031018203003936 doi:10.1016/S0031-0182(03)00393-6

De Grave, J., Buslov, M. M., & Van den haute, P. (2007, February). Distant effects of India–Eurasia convergence and Mesozoic intracontinental deformation in Central Asia: Constraints from apatite fission-track thermochronology. *Journal of Asian Earth Sciences*, *29*(2), 188–204. Retrieved 2021-03-26, from https://www.sciencedirect.com/science/article/pii/S136791200600071X doi: 10.1016/j.jseaes.2006.03.001

De Grave, J., Buslov, M. M., Van Den Haute, P., Metcalf, J., Dehandschutter, B., & McWilliams, M. O. (2009). Multi-method chronometry of the Teletskoye graben and its basement, Siberian Altai Mountains: new insights on its thermo-tectonic evolution. *Geological Society, London, Special Publications*, *324*(1), 237–259. Retrieved 2021-04-20, from http://sp.lyellcollection.org/lookup/doi/10.1144/SP324.17 doi: 10.1144/SP324.17

Ding, L., Spicer, R., Yang, J., Xu, Q., Cai, F., Li, S., . . . Mehrotra, R. (2017, March). Quantifying the rise of the Himalaya orogen and implications for the South Asian monsoon. *Geology*, *45*(3), 215–218. Retrieved 2017-10-09, from https://pubs.geoscienceworld.org/geology/article/45/3/215-218/195254 doi: 10.1130/G38583.1

Ding, L., Xu, Q., Yue, Y., Wang, H., Cai, F., & Li, S. (2014, April). The Andeantype Gangdese Mountains: Paleoelevation record from the Paleocene–Eocene Linzhou Basin. *Earth and Planetary Science Letters*, *392*, 250–264. Retrieved 2017-10-09, from

http://linkinghub.elsevier.com/retrieve/pii/S0012821X14000612 doi: 10.1016/j.epsl.2014.01.045

Ding, W., Hou, D., Gan, J., Wu, P., Zhang, M., & George, S. C. (2021, April). Palaeovegetation variation in response to the late Oligocene-early Miocene East Asian summer monsoon in the Ying-Qiong Basin, South China Sea. *Palaeogeography, Palaeoclimatology, Palaeoecology, 567*, 110205. Retrieved 2022-05-03, from https://linkinghub.elsevier.com/retrieve/pii/S0031018220306532 doi: 10.1016/j.palaeo.2020.110205

Ding, Z., Huang, G., Liu, F., Wu, R., & Wang, P. (2021, June). Responses of global monsoon and seasonal cycle of precipitation to precession and obliquity forcing. *Climate Dynamics*, *56*. doi: 10.1007/s00382-021-05663-6

Dowsett, H., Dolan, A., Rowley, D., Moucha, R., Forte, A. M., Mitrovica, J. X., . . . Haywood, A. (2016, July). The PRISM4 (mid-Piacenzian) paleoenvironmental reconstruction. *Climate of the Past*, *12*(7), 1519–1538. Retrieved 2022-04-15, from https://cp.copernicus.org/articles/12/1519/2016/ doi: 10.5194/cp-12-1519-2016

Dufresne, J.-L., Foujols, M.-A., Denvil, S., Caubel, A., Marti, O., Aumont, O., . . . Vuichard, N. (2013, May). Climate change projections using the IPSL-CM5 Earth System Model: from CMIP3 to CMIP5. *Climate Dynamics*, *40*(9-10), 2123–2165. Retrieved 2019-11-22, from http://link.springer.com/10.1007/s00382-012-1636-1 doi: 10.1007/s00382-012-1636-1

Faccenna, C., Glišović, P., Forte, A., Becker, T. W., Garzanti, E., Sembroni, A., & Gvirtzman, Z. (2019, December). Role of dynamic topography in sustaining the Nile River over 30

million years. *Nature Geoscience*, *12*(12), 1012–1017. Retrieved 2021-03-10, from http://www.nature.com/articles/s41561-019-0472-x (Number: 12 Publisher: Nature Publishing Group) doi: 10.1038/s41561-019-0472-x

Fang, X., Galy, A., Yang, Y., Zhang, W., Ye, C., & Song, C. (2019, October). Paleogene global cooling–induced temperature feedback on chemical weathering, as recorded in the northern Tibetan Plateau. *Geology*, *47*(10), 992–996. Retrieved 2022-10-03, from https://pubs.geoscienceworld.org/gsa/geology/article/47/10/992/573474/Paleogene-global-coolingiinduced-temperature doi: 10.1130/G46422.1

Fang, X., Yan, M., Zhang, W., Nie, J., Han, W., Wu, F., . . . Yang, Y. (2021, November). Paleogeography control of Indian monsoon intensification and expansion at 41 Ma. *Science Bulletin*, *66*(22), 2320–2328. Retrieved 2022-05-02, from https://linkinghub.elsevier.com/retrieve/pii/S2095927321005041 doi: 10.1016/j.scib.2021.07.023

Farnsworth, A., Lunt, D. J., Robinson, S. A., Valdes, P. J., Roberts, W. H. G., Clift, P. D., . . . Pancost, R. D. (2019, October). Past East Asian monsoon evolution controlled by paleogeography, not CO_2. *Science Advances*, *5*(10), eaax1697. doi: 10.1126/sciadv.aax1697

Feakins, S. J., Liddy, H. M., Tauxe, L., Galy, V., Feng, X., Tierney, J. E., . . . Warny, S. (2020). Miocene C4 Grassland Expansion as Recorded by the Indus Fan. *Paleoceanography and Paleoclimatology*, *35*(6), e2020PA003856. Retrieved 2022-06-07, from http://onlinelibrary.wiley.com/doi/abs/10.1029/2020PA003856

(eprint: https://agupubs.onlinelibrary.wiley.com/doi/pdf/10.1029/2020PA003856) doi: 10.1029/2020PA003856

Feng, R., & Poulsen, C. J. (2016, February). Refinement of Eocene lapse rates, fossil-leaf altimetry, and North American Cordilleran surface elevation estimates. *Earth and Planetary Science Letters*, *436*, 130–141. Retrieved 2020-03-23, from https://linkinghub.elsevier.com/retrieve/pii/S0012821X15007852 doi: 10.1016/j.epsl.2015.12.022

Fichefet, T., & Maqueda, M. A. M. (1997). Sensitivity of a global sea ice model to the treatment of ice thermodynamics and dynamics. *Journal of Geophysical Research: Oceans*, *102*(C6), 12609–12646.

Fluteau, F., Ramstein, G., & Besse, J. (1999, May). Simulating the evolution of the Asian and African monsoons during the past 30 Myr using an atmospheric general circulation model. *Journal of Geophysical Research: Atmospheres*, *104*(D10), 11995–12018. Retrieved 2019-05-10, from http://doi.wiley.com/10.1029/1999JD900048 doi: 10.1029/1999JD900048

Foster, G. L., Royer, D. L., & Lunt, D. J. (2017, April). Future climate forcing potentially without precedent in the last 420 million years. *Nature Communications*, *8*(1). Retrieved 2020-05-28, from http://www.nature.com/articles/ncomms14845 doi:10.1038/ncomms14845

François, T., Burov, E., Agard, P., & Meyer, B. (2014). Buildup of a dynamically supported orogenic plateau: Numerical modeling of the Zagros/Central Iran case study. *Geochemistry, Geophysics, Geosystems*, *15*(6), 2632–2654. Retrieved 2021-03-09, from https://agupubs.onlinelibrary.wiley.com/doi/abs/10.1002/201

3GC005223 (eprint: https://agupubs.onlinelibrary.wiley.com/doi/pdf/10.1002/2013GC005223) doi: https://doi.org/10.1002/2013GC005223

Frisch, K., Voigt, S., Verestek, V., Appel, E., Albert, R., Gerdes, A., . . . Batenburg, S. (2019, November). Long-Period Astronomical Forcing of Westerlies' Strength in Central Asia During Miocene Climate Cooling. *Paleoceanography and Paleoclimatology, 34*. doi: 10.1029/2019PA003642

Garzione, C. N., Ikari, M. J., & Basu, A. R. (2005, September). Source of Oligocene to Pliocene sedimentary rocks in the Linxia basin in northeastern Tibet from Nd isotopes: Implications for tectonic forcing of climate. *GSA Bulletin, 117*(9-10), 1156–1166. Retrieved 2021-09-07, from https://doi.org/10.1130/B25743.1 doi: 10.1130/B25743.1

Golonka, J. (2009). Phanerozoic paleoenvironment and paleolithofacies maps : Cenozoic. *Geologia / Akademia Górniczo-Hutnicza im. Stanisl awa Staszica w Krakowie, T. 35, z. 4*, 507–587. Retrieved 2021-04-06, from http://yadda.icm.edu.pl/yadda/element/bwmeta1.element.baztech-article-AGHM-0011-0001

Gough, D. O. (1981). Solar Interior Structure and Luminosity Variations. In V. Domingo (Ed.), *Physics of Solar Variations* (pp. 21–34). Dordrecht: Springer Netherlands. Retrieved 2019-10-03, from http://link.springer.com/10.1007/978-94-010-9633-1_4 doi: 10.1007/978-94-010-9633-1_4

Gourbet, L., Leloup, P. H., Paquette, J.-L., Sorrel, P., Maheo, G., Wang, G., . . . Shen, T. (2017, March). Reappraisal of the Jianchuan Cenozoic basin stratigraphy and its implications on

the SE Tibetan plateau evolution. *Tectonophysics*, *700-701*, 162–179. Retrieved 2021-03-29, from https://www.sciencedirect.com/science/article/pii/S0040195117300537 doi: 10.1016/j.tecto.2017.02.007

Guillocheau, F., Simon, B., Baby, G., Bessin, P., Robin, C., & Dauteuil, O. (2018, January). Planation surfaces as a record of mantle dynamics: The case example of Africa. *Gondwana Research*, *53*, 82–98. Retrieved 2021-04-07, from https://www.sciencedirect.com/science/article/pii/S1342937X17302496 doi: 10.1016/j.gr.2017.05.015

Guo, Z. T., Ruddiman, W. F., Hao, Q. Z., Wu, H. B., Qiao, Y. S., Zhu, R. X., . . . Liu, T. S. (2002, March). Onset of Asian desertification by 22 Myr ago inferred from loess deposits in China. *Nature*, *416*(6877), 159–163. Retrieved 2020-04-24, from http://www.nature.com/articles/416159a doi: 10.1038/416159a

Guo, Z. T., Sun, B., Zhang, Z. S., Peng, S. Z., Xiao, G. Q., Ge, J. Y., . . . Liu, J. F. (2008). A major reorganization of Asian climate by the early Miocene. *Climate of the Past*, *4*(3), 153–174.

Gupta, A. K., Yuvaraja, A., Prakasam, M., Clemens, S. C., & Velu, A. (2015, November). Evolution of the South Asian monsoon wind system since the late Middle Miocene. *Palaeogeography, Palaeoclimatology, Palaeoecology*, *438*, 160–167. Retrieved 2021-09-07, from https://www.sciencedirect.com/science/article/pii/S0031018215004332 doi: 10.1016/j.palaeo.2015.08.006

Gébelin, A., Mulch, A., Teyssier, C., Jessup, M. J., Law, R. D., & Brunel, M. (2013, July). The Miocene elevation of Mount Everest. *Geology*, *41*(7), 799–802. Retrieved 2017-10-09,

from http://pubs.geoscienceworld.org/geology/article/41/7/799/131318/The-Miocene-elevation-of-Mount-Everest doi: 10.1130/G34331.1

Gülyüz, E., Durak, H., Özkaptan, M., & Krijgsman, W. (2020, January). Paleomagnetic constraints on the early Miocene closure of the southern Neo-Tethys (Van region; East Anatolia): Inferences for the timing of Eurasia-Arabia collision. *Global and Planetary Change*, *185*, 103089. Retrieved 2022-03-04, from https://www.sciencedirect.com/science/article/pii/S0921818119305740 doi: 10.1016/j.gloplacha.2019.103089

Hall, R., Gower, D., Johnson, K., Richardson, J., Rosen, B., Rüber, L., & Williams, S. (2012). Sundaland and Wallacea: geology, plate tectonics and palaeogeography. *Biotic evolution and environmental change in Southeast Asia*, *82*, 32. (Publisher: Cambridge University Press Cambridge)

Han, Z., Jia, H., Meng, X., Ferguson, D., Luo, M., Liu, P., . . . Quan, C. (2022, October). A New Clue for the Late Eocene Freshwater Ecosystem of Central China Evidenced by New Fossils of Trapa L. and Hemitrapa Miki (Lythraceae). *Biology*, *11*, 1442. doi: 10.3390/biology11101442

Harzhauser, M., & Piller, W. E. (2007, September). Benchmark data of a changing sea | Palaeogeography, Palaeobiogeography and events in the Central Paratethys during the Miocene. *Palaeogeography, Palaeoclimatology, Palaeoecology*, *253*(1), 8–31. Retrieved 2021-04-01, from https://www.sciencedirect.com/science/article/pii/S0031018207001927 doi: 10.1016/j.palaeo.2007.03.031

Haywood, A. M., Tindall, J. C., Dowsett, H. J., Dolan, A. M., Foley, K. M., Hunter, S. J., . . . Lunt, D. J. (2020, November). The Pliocene Model Intercomparison Project Phase 2: large-scale climate features and climate sensitivity. *Climate of the Past*, *16*(6), 2095–2123. Retrieved 2021-03-09, from https://cp.copernicus.org/articles/16/2095/2020/ (Publisher: Copernicus GmbH) doi: https://doi.org/10.5194/cp-16-2095-2020

He, B. (2017, May). Influences of elevated heating effect by the Himalaya on the changes in Asian summer monsoon. *Theoretical and Applied Climatology*, *128*(3-4), 905–917. Retrieved 2017-10-09, from http://link.springer.com/10.1007/s00704-016-1746-5 doi: 10.1007/s00704-016-1746-5

Heermance, R., Pearson, J., Moe, A., Langhao, L., Jianhong, X., Chen, J., . . . Bogue, S. (2018, September). Erg deposition and development of the ancestral Taklimakan Desert (western China) between 12.2 and 7.6 Ma. *Geology*, *46*. doi: 10.1130/G45085.1

Hellwig, A., Voigt, S., Mulch, A., Frisch, K., Bartenstein, A., Pross, J., . . . Voigt, T. (2018). Late Oligocene to early Miocene humidity change recorded in terrestrial sequences in the Ili Basin (south-eastern Kazakhstan, Central Asia). *Sedimentology*, *65*(2), 517–539. Retrieved 2022-03-22, from http://onlinelibrary.wiley.com/doi/abs/10.1111/sed.12390 (eprint:https://onlinelibrary.wiley.com/doi/pdf/10.1111/sed.12390) doi: 10.1111/sed.12390

Herman, A. B., Spicer, R. A., Aleksandrova, G. N., Yang, J., Kodrul, T. M., Maslova, N. P., . . . Jin, J.-H. (2017, August). Eocene–early Oligocene climate and vegetation change in

southern China: Evidence from the Maoming Basin. *Palaeogeography, Palaeoclimatology, Palaeoecology*, *479*, 126–137. Retrieved 2017-10-09, from http://linkinghub.elsevier.com/retrieve/pii/S0031018217300664 doi: 10.1016/j.palaeo.2017.04.023

Holbourn, A., Kuhnt, W., Clemens, S. C., & Heslop, D. (2021). A 12 Myr Miocene Record of East Asian Monsoon Variability From the South China Sea. *Paleoceanography and Paleoclimatology*, *36*(7), e2021PA004267. Retrieved 2021-09-08, from http://agupubs.onlinelibrary.wiley.com/doi/abs/10.1029/2021PA004267 (eprint: https://onlinelibrary.wiley.com/doi/pdf/10.1029/2021PA004267) doi: 10.1029/2021PA004267

Holbourn, A., Kuhnt, W., Clemens, S. C., Kochhann, K. G. D., Jöhnck, J., Lübbers, J., & Andersen, N. (2018, December). Late Miocene climate cooling and intensification of southeast Asian winter monsoon. *Nature Communications*, *9*(1). Retrieved 2020-10-09, from http://www.nature.com/articles/s41467-018-03950-1 doi: 10.1038/s41467-018-03950-1

Hoorn, C., Ohja, T., & Quade, J. (2000, November). Palynological evidence for vegetation development and climatic change in the Sub-Himalayan Zone (Neogene, Central Nepal). *Palaeogeography, Palaeoclimatology, Palaeoecology*, *163*(3-4), 133–161. Retrieved 2022-06-07, from https://linkinghub.elsevier.com/retrieve/pii/S0031018200001498 doi: 10.1016/S0031-0182(00)00149-8

Hoorn, C., Straathof, J., Abels, H. A., Xu, Y., Utescher, T., & Dupont-Nivet, G. (2012, August). A late Eocene palynological record of climate change and Tibetan Plateau uplift (Xining

Basin, China). *Palaeogeography, Palaeoclimatology, Palaeoecology*, *344-345*, 16–38. Retrieved 2017-10-09, from http://linkinghub.elsevier.com/retrieve/pii/S0031018212002775 doi: 10.1016/j.palaeo.2012.05.011

Hourdin, F., Foujols, M.-A., Codron, F., Guemas, V., Dufresne, J.-L., Bony, S., . . . Bopp, L. (2013, May). Impact of the LMDZ atmospheric grid configuration on the climate and sensitivity of the IPSL-CM5A coupled model. *Climate Dynamics*, *40*(9-10), 2167–2192. Retrieved 2018-06-05, from http://link.springer.com/10.1007/s00382-012-1411-3 doi: 10.1007/s00382-012-1411-3

Huang, C., & Hinnov, L. (2019, December). Astronomically forced climate evolution in a saline lake record of the middle Eocene to Oligocene, Jianghan Basin, China. *Earth and Planetary Science Letters*, *528*, 115846. Retrieved 2020-09-07, from https://linkinghub.elsevier.com/retrieve/pii/S0012821X19305382 doi: 10.1016/j.epsl.2019.115846

Huang, H., Pérez-Pinedo, D., Morley, R. J., Dupont-Nivet, G., Philip, A., Win, Z., . . . Hoorn, C. (2021, April). At a crossroads: The late Eocene flora of central Myanmar owes its composition to plate collision and tropical climate. *Review of Palaeobotany and Palynology*, 104441. Retrieved 2021-05-06, from https://www.sciencedirect.com/science/article/pii/S0034666721000658 doi: 10.1016/j.revpalbo.2021.104441

Huang, W., Dupont-Nivet, G., Lippert, P. C., van Hinsbergen, D. J. J., Dekkers, M. J., Waldrip, R., . . . Kapp, P. (2015, March). What was the Paleogene latitude of the Lhasa terrane? A

reassessment of the geochronology and paleomagnetism of Linzizong volcanic rocks (Linzhou basin, Tibet). *Tectonics*, *34*(3), 594–622. Retrieved 2017-10-09, from http://doi.wiley.com/10.1002/2014TC003787 doi: 10.1002/2014TC003787

Huang, Y., Clemens, S., Liu, W., Wang, Y., & Prell, W. (2007, June). Large-scale hydrological change drove the late Miocene C4 plant expansion in the Himalayan foreland and Arabian Peninsula. *Geology*, *35*. doi: 10.1130/G23666A.1

Huber, M., & Goldner, A. (2012, January). Eocene monsoons. *Journal of Asian Earth Sciences*, *44*, 3–23. Retrieved 2017-10-09, from http://linkinghub.elsevier.com/retrieve/pii/S1367912011003725 doi: 10.1016/j.jseaes.2011.09.014

Hui, Z., Zhou, X., Chevalier, M., Wei, X., Yan, Y., & Chen, Y. (2021, August). Miocene East Asia summer monsoon precipitation variability and its possible driving forces. *Palaeogeography, Palaeoclimatology, Palaeoecology*, 110609. Retrieved 2021-09-22, from https://www.sciencedirect.com/science/article/pii/S0031018221003941 doi: 10.1016/j.palaeo.2021.110609

Ingalls, M., Rowley, D. B., Currie, B., & Colman, A. S. (2016, November). Large-scale subduction of continental crust implied by India–Asia mass-balance calculation. *Nature Geoscience*, *9*(11), 848–853. Retrieved 2020-10-16, from http://www.nature.com/articles/ngeo2806 (Number: 11 Publisher: Nature Publishing Group) doi: 10.1038/ngeo2806

Jacques, F. M., Guo, S.-X., Su, T., Xing, Y.-W., Huang, Y.-J., Liu, Y.-S. C., . . . Zhou, Z.-K. (2011, May). Quantitative reconstruction of the Late Miocene monsoon climates of southwest China: A case study of the Lincang ora from Yunnan Province. *Palaeogeography, Palaeoclimatology, Palaeoecology*, *304*(3-4), 318–327. Retrieved 2022-05-03, from https://linkinghub.elsevier.com/retrieve/pii/S0031018210002233 doi: 10.1016/j.palaeo.2010.04.014

Jacques, F. M., Su, T., Spicer, R. A., Xing, Y., Huang, Y., Wang, W., & Zhou, Z. (2011, March). Leaf physiognomy and climate: Are monsoon systems different? *Global and Planetary Change*, *76*(1-2), 56–62. Retrieved 2022-05-06, from https://linkinghub.elsevier.com/retrieve/pii/S0921818110002560 doi: 10.1016/j.gloplacha.2010.11.009

Jagoutz, O., Royden, L., Holt, A. F., & Becker, T. W. (2015, June). Anomalously fast convergence of India and Eurasia caused by double subduction. *Nature Geoscience*, *8*(6), 475–478. Retrieved 2019-11-22, from http://www.nature.com/articles/ngeo2418 doi: 10.1038/ngeo2418

Jeong, J.-H., Ou, T., Linderholm, H. W., Kim, B.-M., Kim, S.-J., Kug, J.-S., & Chen, D. (2011, December). Recent recovery of the Siberian High intensity: RECOVERY OF THE SIBERIAN HIGH INTENSITY. *Journal of Geophysical Research: Atmospheres*, *116*(D23), n/a–n/a. Retrieved 2020-06-20, from http://doi.wiley.com/10.1029/2011JD015904 doi: 10.1029/2011JD015904

Jhun, J.-G., & Lee, E.-J. (2004, February). A New East Asian Winter Monsoon Index and Associated Characteristics of the Winter Monsoon. *Journal of Climate*, *17*(4), 711–726. Retrieved 2021-11-10, from https://journals.ametsoc.org/view/journals/clim/17/4/1520-0442_2004_017_0711_aneawm_2.0.co_2.xml (Publisher: American Meteorological Society Section: Journal of Climate) doi: 10.1175/1520-0442(2004)017h0711:ANEAWMi2.0.CO;2

Jia, G., Peng, P., Zhao, Q., & Jian, Z. (2003, December). Changes in terrestrial ecosystem since 30 Ma in East Asia: Stable isotope evidence from black carbon in the South China Sea. *Geology*, *31*(12), 1093–1096. Retrieved 2022-05-03, from https://doi.org/10.1130/G19992.1 doi: 10.1130/G19992.1

Jiang, H., & Ding, Z. (2008, July). A 20 Ma pollen record of East-Asian summer monsoon evolution from Guyuan, Ningxia, China. *Palaeogeography, Palaeoclimatology, Palaeoecology*, *265*(1-2), 30–38. Retrieved 2022-06-14, from https://linkinghub.elsevier.com/retrieve/pii/S0031018208002629 doi: 10.1016/j.palaeo.2008.04.016

Jiang, H., Wan, S., Ma, X., Zhong, N., & Zhao, D. (2017, October). End-member modeling of the grain-size record of Sikouzi fine sediments in Ningxia (China) and implications for temperature control of Neogene evolution of East Asian winter monsoon. *PLOS ONE*, *12*(10), e0186153. Retrieved 2022-06-14, from https://dx.plos.org/10.1371/journal.pone.0186153 doi: 10.1371/journal.pone.0186153

Jolivet, M., Dominguez, S., Charreau, J., Chen, Y., Li, Y., &Wang, Q. (2010). Mesozoic and Cenozoic tectonic history of the central Chinese Tian Shan: Reactivated tectonic structures and active deformation. *Tectonics*, *29*(6). Retrieved 2021-03-29, from http://agupubs.onlinelibrary.wiley.com/doi/abs/10.1029/2010TC002712 (eprint: https://onlinelibrary.wiley.com/doi/pdf/10.1029/2010TC002712) doi: https://doi.org/10.1029/2010TC002712

Jolivet, M., Ritz, J.-F., Vassallo, R., Larroque, C., Braucher, R., Todbileg, M., . . . Arzhanikov, S. (2007, October). Mongolian summits: An uplifted, at, old but still preserved erosion surface. *Geology*, *35*(10), 871–874. Retrieved 2021-03-29, from http://pubs.geoscienceworld.org/gsa/geology/article/35/10/871/129664/Mongolian-summits-An-uplifted-flat-old-but-still (Publisher: Geo-ScienceWorld) doi: 10.1130/G23758A.1

Kaakinen, A., Sonninen, E., & Lunkka, J. P. (2006, August). Stable isotope record in paleosol carbonates from the Chinese Loess Plateau: Implications for late Neogene paleoclimate and paleovegetation. *Palaeogeography, Palaeoclimatology, Palaeoecology*, *237*(2-4), 359–369. Retrieved 2022-06-16, from https://linkinghub.elsevier.com/retrieve/pii/S0031018205007315 doi: 10.1016/j.palaeo.2005.12.011

Kapp, P., & DeCelles, P. G. (2019, March). Mesozoic–Cenozoic geological evolution of the Himalayan-Tibetan orogen and working tectonic hypotheses. *American Journal of Science*, *319*(3), 159–254. Retrieved 2019-11-15, from http://www.ajsonline.org/lookup/doi/10.2475/03.2019.01 doi: 10.2475/03.2019.01

Karaoğlan, F., Parlak, O., Hejl, E., Neubauer, F., & Klötzli, U. (2016, May). The temporal evolution of the active margin along the Southeast Anatolian Orogenic Belt (SE Turkey): Evidence from U–Pb, Ar–Ar and fission track chronology. *Gondwana Research*, *33*, 190–208. Retrieved 2022-03-04, from https://www.sciencedirect.com/science/article/pii/S1342937X16000599 doi: 10.1016/j.gr.2015.12.011

Kaya, M. Y., Dupont-Nivet, G., Proust, J., Roperch, P., Bougeois, L., Meijer, N., . . . Zhaojie, G. (2019, June). Paleogene evolution and demise of the proto-Paratethys Sea in Central Asia (Tarim and Tajik basins): Role of intensified tectonic activity at ca. 41 Ma. *Basin Research*, *31*(3), 461–486. Retrieved 2019-11-22, from https://onlinelibrary.wiley.com/doi/abs/10.1111/bre.12330 doi: 10.1111/bre.12330

Kent-Corson, M. L., Ritts, B. D., Zhuang, G., Bovet, P. M., Graham, S. A., & Page Chamberlain, C. (2009, May). Stable isotopic constraints on the tectonic, topographic, and climatic evolution of the northern margin of the Tibetan Plateau. *Earth and Planetary Science Letters*, *282*(1-4), 158–166. Retrieved 2017-10-09, from http://linkinghub.elsevier.com/retrieve/pii/S0012821X0900154X doi: 10.1016/j.epsl.2009.03.011

Khan, M. A., Spicer, R. A., Bera, S., Ghosh, R., Yang, J., Spicer, T. E. V., . . . Grote, P. J. (2014, February). Miocene to Pleistocene floras and climate of the Eastern Himalayan Siwaliks, and new palaeoelevation estimates for the Namling–Oiyug Basin, Tibet. *Global and Planetary Change*, *113*, 1–10. Retrieved 2022-05-02, from

https://www.sciencedirect.com/science/article/pii/S0921818113002749 doi: 10.1016/j.gloplacha.2013.12.003

Kong, W., Swenson, L. M., & Chiang, J. C. H. (2017, May). Seasonal Transitions and the Westerly Jet in the Holocene East Asian Summer Monsoon. *Journal of Climate*, *30*(9), 3343–3365. Retrieved 2020-03-04, from http://journals.ametsoc.org/doi/10.1175/JCLI-D-16-0087.1 doi: 10.1175/JCLI-D-16-0087.1

Krinner, G., Viovy, N., de Noblet-Ducoudré, N., Ogée, J., Polcher, J., Friedlingstein, P., . . . Prentice, I. C. (2005, March). A dynamic global vegetation model for studies of the coupled atmosphere-biosphere system: DVGM FOR COUPLED CLIMATE STUDIES. *Global Biogeochemical Cycles*, *19*(1). Retrieved 2018-10-22, from http://doi.wiley.com/10.1029/2003GB002199 doi: 10.1029/2003GB002199

Kroon, D., Steens, T., & Troelstra, S. R. (1991). Onset of monsoonal related upwelling in the western Arabian sea as revealed by planktonic foraminifers. In *Proceedings of the ocean drilling program, scientific results* (Vol. 11).

Kuhnt, W., Holbourn, A., Hall, R., Zuvela, M., & Käse, R. (2004). Neogene history of the Indonesian Throughow. In P. Clift, W. Kuhnt, P.Wang, & D. Hayes (Eds.), *Geophysical Monograph Series* (Vol. 149, pp. 299–320). Washington, D. C.: American Geophysical Union. Retrieved 2021-09-02, from https://onlinelibrary.wiley.com/doi/10.1029/149GM16 doi: 10.1029/149GM16

Kutzbach, J. E., Prell, W. L., & Ruddiman, W. F. (1993, March). Sensitivity of Eurasian Climate to Surface Uplift of the Tibetan Plateau. *The Journal of Geology*, *101*(2), 177–190. Retrieved 2020-05-11, from https://www.journals.uchicago.edu/doi/10.1086/648215 doi: 10.1086/648215

Käßner, A., Ratschbacher, L., Jonckheere, R., Enkelmann, E., Khan, J., Sonntag, B.-L., . . . Oimahmadov, I. (2016). Cenozoic intracontinental deformation and exhumation at the northwestern tip of the India-Asia collision|southwestern Tian Shan, Tajikistan, and Kyrgyzstan. *Tectonics*, *35*(9), 2171–2194. Retrieved 2021-03-26, from http://agupubs.onlinelibrary.wiley.com/doi/abs/10.1002/2015TC003897 (eprint: https://onlinelibrary.wiley.com/doi/pdf/10.1002/2015TC003897) doi: https://doi.org/10.1002/2015TC003897

Ladant, J.-B., Donnadieu, Y., Lefebvre, V., & Dumas, C. (2014, August). The respective role of atmospheric carbon dioxide and orbital parameters on ice sheet evolution at the Eocene-Oligocene transition: Ice sheet evolution at the EOT. *Paleoceanography*, *29*(8), 810–823. Retrieved 2018-05-10, from http://doi.wiley.com/10.1002/2013PA002593 doi: 10.1002/2013PA002593

Laugié, M., Donnadieu, Y., Ladant, J.-B., Green, J. A. M., Bopp, L., & Raisson, F. (2020, June). Stripping back the modern to reveal the Cenomanian–Turonian climate and temperature gradient underneath. *Climate of the Past*, *16*(3), 953–971. Retrieved 2021-03-09, from https://cp.copernicus.org/articles/16/953/2020/ (Publisher: Copernicus GmbH) doi: https://doi.org/10.5194/cp-16-953-2020

Lee, J., Kim, S., Lee, J. I., Cho, H. G., Phillips, S. C., & Khim, B.-K. (2020, January). Monsoon-influenced variation of clay mineral compositions and detrital Nd-Sr isotopes in the western Andaman Sea (IODP Site U1447) since the late Miocene. *Palaeogeography, Palaeoclimatology, Palaeoecology*, *538*, 109339. Retrieved 2022-06-02, from https://linkinghub.elsevier.com/retrieve/pii/S0031018219303773 doi: 10.1016/j.palaeo.2019.109339

Lee, J.-Y., Wang, B., Seo, K.-H., Ha, K.-J., Kitoh, A., & Liu, J. (2015, August). Effects of mountain uplift on global monsoon precipitation. *Asia-Pacific Journal of Atmospheric Sciences*, *51*(3), 275–290. Retrieved 2017-10-09, from http://link.springer.com/10.1007/s13143-015-0077-2 doi: 10.1007/s13143-015-0077-2

Li, B., Sun, D., Wang, X., Zhang, Y., Hu, W., Wang, F., . . . Liang, B. (2016, August). 18O and 13C records from a Cenozoic sedimentary sequence in the Lanzhou Basin, Northwestern China: Implications for palaeoenvironmental and palaeoecological changes. *Journal of Asian Earth Sciences*, *125*, 22–36. Retrieved 2022-05-12, from https://linkinghub.elsevier.com/retrieve/pii/S1367912016301249 doi: 10.1016/j.jseaes.2016.05.010

Li, F., Rousseau, D.-D., Wu, N., Hao, Q., & Pei, Y. (2008, October). Late Neogene evolution of the East Asian monsoon revealed by terrestrial mollusk record in Western Chinese Loess Plateau: From winter to summer dominated sub-regime. *Earth and Planetary Science Letters*, *274*(3-4), 439–447. Retrieved 2022-06-16, from https://linkinghub.elsevier.com/retrieve/pii/S0012821X08004986 doi: 10.1016/j.epsl.2008.07.038

Li, L., Dupont-Nivet, G., Najman, Y., Kaya, M., Meijer, N., Poujol, M., & Aminov, J. (2021). Middle to late Miocene growth of the North Pamir. *Basin Research, n/a*(n/a). Retrieved 2021-11-09, from http://onlinelibrary.wiley.com/doi/abs/10.1111/bre.12629 (eprint: https://onlinelibrary.wiley.com/doi/pdf/10.1111/bre.12629) doi: 10.1111/bre.12629

Li, Q., Utescher, T., Liu, Y. C., Ferguson, D., Jia, H., & Quan, C. (2022, September). Monsoonal climate of East Asia in Eocene times inferred from an analysis of plant functional types. *Palaeogeography, Palaeoclimatology, Palaeoecology*, *601*, 111138. Retrieved 2022-10-24, from https://linkinghub.elsevier.com/retrieve/pii/S003101822200308X doi: 10.1016/j.palaeo.2022.111138

Li, S., Xing, Y., Valdes, P. J., Huang, Y., Su, T., Farnsworth, A., . . . Zhou, Z. (2018, September). Oligocene climate signals and forcings in Eurasia revealed by plant macrofossil and modelling results. *Gondwana Research*, *61*, 115–127. Retrieved 2019-10-18, from https://linkinghub.elsevier.com/retrieve/pii/S1342937X18301473 doi: 10.1016/j.gr.2018.04.015

Li, X., Zhang, R., Zhang, Z., & Yan, Q. (2017, October). What enhanced the aridity in Eocene Asian inland: Global cooling or early Tibetan Plateau uplift? *Palaeogeography, Palaeoclimatology, Palaeoecology*. Retrieved 2018-01-16, from http://linkinghub.elsevier.com/retrieve/pii/S0031018217306922 doi: 10.1016/j.palaeo.2017.10.029

Liang, J.-q., Leng, Q., Xiao, L., Höfig, D. F., Royer, D. L., Zhang, Y. G., & Yang, H. (2022, October). Early Miocene redwood fossils from Inner Mongolia: CO2 reconstructions and paleoclimate effects of a low Mongolian plateau. *Review of Palaeobotany and Palynology*, *305*, 104743. Retrieved 2022-08-21, from https://linkinghub.elsevier.com/retrieve/pii/S0034666722001415 doi: 10.1016/j.revpalbo.2022.104743

Licht, A., Dupont-Nivet, G., Win, Z., Swe, H. H., Kaythi, M., Roperch, P., . . . Sein, K. (2018, November). Paleogene evolution of the Burmese forearc basin and implications for the history of India-Asia convergence. *GSA Bulletin*, *131*(5-6), 730–748. Retrieved 2021-03-29, from https://doi.org/10.1130/B35002.1 doi: 10.1130/B35002.1

Licht, A., van Cappelle, M., Abels, H. A., Ladant, J.-B., Trabucho-Alexandre, J., France-Lanord, C., . . . Jaeger, J.-J. (2014, September). Asian monsoons in a late Eocene greenhouse world. *Nature*, *513*(7519), 501–506. Retrieved 2017-10-09, from http://www.nature.com/doifinder/10.1038/nature13704 doi: 10.1038/nature13704

Ling, C.-C., Ma, F.-J., Deng, J. L., Zhou, G.-H., Wang, Q.-J., & Sun, B.-N. (2021, October). A mid-altitude area in southwestern China experienced a humid subtropical climate with subtle monsoon signatures during the early Oligocene: Evidence from the Ningming flora of Guangxi. *Palaeogeography, Palaeoclimatology, Palaeoecology*, *579*, 110601. Retrieved 2022-05-03, from https://linkinghub.elsevier.com/retrieve/pii/S0031018221003862 doi: 10.1016/j.palaeo.2021.110601

Liu, D., Li, H., Sun, Z., Cao, Y., Wang, L., Pan, J., . . . Ye, X. (2017, August). Cenozoic episodic uplift and kinematic evolution between the Pamir and Southwestern Tien Shan. *Tectonophysics*, *712-713*, 438–454. Retrieved 2021-03-26, from https://www.sciencedirect.com/science/article/pii/S00401951 1730255X doi: 10.1016/j.tecto.2017.06.009

Liu, J., Li, J., Song, C., Yu, H., Peng, T., Hui, Z., & Ye, X. (2016, July). Palynological evidence for late Miocene stepwise aridification on the northeastern Tibetan Plateau. *Climate of the Past*, *12*, 1473–1484. doi: 10.5194/cp-12-1473-2016

Liu, W., Liu, Z., An, Z., Sun, J., Chang, H., Wang, N., . . . Wang, H. (2014, November). Late Miocene episodic lakes in the arid Tarim Basin, western China. *Proceedings of the National Academy of Sciences*, *111*(46), 16292–16296. Retrieved 2022-06-17, from https://www.pnas.org/doi/full/10.1073/pnas.1410890111 (Publisher: Proceedings of the National Academy of Sciences) doi: 10.1073/pnas.1410890111

Liu, X., Guo, Q., Guo, Z., Yin, J., Dong, B., & Smith, R. (2015, October). Where were the monsoon regions and arid zones in Asia prior to the Tibetan Plateau uplift? *National Science Review*, 2, nwv068. doi: 10.1093/nsr/nwv068

Liu, X., Sun, H., Miao, Y., Dong, B., & Yin, Z.-Y. (2015, May). Impacts of uplift of northern Tibetan Plateau and formation of Asian inland deserts on regional climate and environment. *Quaternary Science Reviews*, *116*, 1–14. Retrieved 2022-06-22, from https://www.sciencedirect.com/science/article/pii/S02773791 15001171 doi: 10.1016/j.quascirev.2015.03.010

Liu, X., & Yin, Z.-Y. (2002, July). Sensitivity of East Asian monsoon climate to the uplift of the Tibetan Plateau. *Palaeogeography, Palaeoclimatology, Palaeoecology*, *183*(3), 223–245. Retrieved 2021-04-14, from https://www.sciencedirect.com/science/article/pii/S0031018201004886 doi: 10.1016/S0031-0182(01)00488-6

Liu, Z., Zhang, K., Sun, Y., Liu, W., Liu, Y. C., & Quan, C. (2014). Cenozoic Environmental Changes in the Northern Qaidam Basin Inferred from n-alkane Records. *Acta Geologica Sinica - English Edition*, *88*(5), 1547–1555. Retrieved 2022-06-17, from http://onlinelibrary.wiley.com/doi/abs/10.1111/1755-6724.12317 (eprint: https://onlinelibrary.wiley.com/doi/pdf/10.1111/1755-6724.12317) doi: 10.1111/1755-6724.12317

Lu, H., & Guo, Z. (2014, January). Evolution of the monsoon and dry climate in East Asia during late Cenozoic: A review. *Science China Earth Sciences*, *57*(1), 70–79. Retrieved 2017-10-09, from http://link.springer.com/10.1007/s11430-013-4790-3 doi: 10.1007/s11430-013-4790-3

Lu, H., Wang, X., & li, l. (2010, August). Aeolian sediment evidence that global cooling has driven late Cenozoic stepwise aridification in Central Asia. *Geological Society London Special Publications*, *342*, 29–44. doi: 10.1144/SP342.4

Luo, M., Jia, H., Li, Q., Meng, X., Ferguson, D., Liu, P., . . . Quan, C. (2022, August). Middle Miocene lotus (Nelumbonaceae, Nelumbo) from the Qaidam Basin, Northern Tibet Plateau. *Biology*, *11*, 1261. doi: 10.3390/biology11091261

Lévy, M., Shankar, D., André, J.-M., Shenoi, S. S. C., Durand, F., & de Boyer Montégut, C. (2007, December). Basin-wide seasonal evolution of the Indian Ocean's phytoplankton blooms. *Journal of Geophysical Research*, *112*(C12). Retrieved 2020-07-30, from http://doi.wiley.com/10.1029/2007JC004090 doi: 10.1029/2007JC004090

Ma, X., & Jiang, H. (2015, June). Combined tectonics and climate forcing for the widespread aeolian dust accumulation in the Chinese Loess Plateau since the early late Miocene. *International Geology Review*, *57*, 1861–1876. doi: 10.1080/00206814.2015.1027305

Ma, X., Jiang, H., Cheng, J., & Xu, H. (2012, September). Spatiotemporal evolution of Paleogene palynoora in China and its implication for development of the extensional basins in East China. *Review of Palaeobotany and Palynology*, *184*, 24–35. Retrieved 2019-02-10, from https://linkinghub.elsevier.com/retrieve/pii/S0034666712001935 doi: 10.1016/j.revpalbo.2012.07.013

Ma, Y., Fang, X., Li, J., Wu, F., & Zhang, J. (2005, May). The vegetation and climate change during Neocene and Early Quaternary in Jiuxi Basin, China. *Science in China Series D: Earth Sciences*, *48*(5), 676. Retrieved 2022-06-16, from http://link.springer.com/10.1360/03yd0110 doi: 10.1360/03yd0110

Macaulay, E. A., Sobel, E. R., Mikolaichuk, A., Kohn, B., & Stuart, F. M. (2014). Cenozoic deformation and exhumation history of the Central Kyrgyz Tien Shan. *Tectonics*, *33*(2), 135–165. Retrieved 2022-03-22, from http://onlinelibrary.wiley.com/doi/abs/10.1002/2013TC003376 (eprint: https://agupubs.onlinelibrary.wiley.com/doi/pdf/10.1002/2013TC003376) doi: 10.1002/2013TC003376

Macaulay, E. A., Sobel, E. R., Mikolaichuk, A., Wack, M., Gilder, S. A., Mulch, A., . . . Apayarov, F. (2016). The sedimentary record of the Issyk Kul basin, Kyrgyzstan: climatic and tectonic inferences. *Basin Research*, *28*(1), 57–80. Retrieved 2022-03-22, from http://onlinelibrary.wiley.com/doi/abs/10.1111/bre.12098 (eprint: https://onlinelibrary.wiley.com/doi/pdf/10.1111/bre.12098) doi: 10.1111/bre.12098

Madec, G. (2016). NEMO ocean engine. *Note du Pnôle de modélisation de l'Institut Pierre-Simon Laplace*(27), 396.

Madec, G., & Imbard, M. (1996, May). A global ocean mesh to overcome the North Pole singularity. *Climate Dynamics*, *12*(6), 381–388. Retrieved 2021-03-09, from https://doi.org/10.1007/BF00211684 doi: 10.1007/BF00211684

Matsuzaki, K. M., Suzuki, N., & Tada, R. (2020, June). An intensified East Asian winter monsoon in the Japan Sea between 7.9 and 3.6 Ma. *Geology*, *48*(9), 919–923. Retrieved 2022-12-20, from https://doi.org/10.1130/G47393.1 doi: 10.1130/G47393.1

Maurin, T., & Rangin, C. (2009). Structure and kinematics of the Indo-BurmeseWedge: Recent and fast growth of the outer wedge. *Tectonics*, *28*(2). Retrieved 2021-03-29, from http://agupubs.onlinelibrary.wiley.com/doi/abs/10.1029/2008TC002276 (eprint: https://onlinelibrary.wiley.com/doi/pdf/10.1029/2008TC002276) doi: https://doi.org/10.1029/2008TC002276

McQuarrie, N., & Hinsbergen, D. J. J. v. (2013, March). Retrodeforming the Arabia-Eurasia collision zone: Age of collision versus magnitude of continental subduction. *Geology*, *41*(3), 315–318. Retrieved 2021-04-06, from http://pubs.geoscienceworld.org/gsa/geology/article-abstrac

t/41/3/315/131120/Retrodeforming-the-Arabia-Eurasia-collision-zone (Publisher: GeoScienceWorld) doi: 10.1130/G33591.1

Meijer, N., Dupont-Nivet, G., Abels, H. A., Kaya, M. Y., Licht, A., Xiao, M., . . . Guo, Z. (2019, March). Central Asian moisture modulated by proto-Paratethys Sea incursions since the early Eocene. *Earth and Planetary Science Letters*, *510*, 73–84. Retrieved 2019-04-25, from https://linkinghub.elsevier.com/retrieve/pii/S0012821X19300019 doi: 10.1016/j.epsl.2018.12.031

Meijer, N., Dupont-Nivet, G., Barbolini, N., Woutersen, A., Rohrmann, A., Yang, Z., . . . Nowaczyk, N. (2021, February). Loess-Like Dust Appearance at 40 Ma in Central China. *Paleoceanography and Paleoclimatology*, 36. doi: 10.1029/2020PA003993

Meng, Q.-t., Bruch, A. A., Sun, G., Liu, Z. j., Liu, F., & Sun, P.-c. (2018, December). Quantitative reconstruction of Middle and Late Eocene paleoclimate based on palynological records from the Huadian Basin, northeastern China: Evidence for monsoonal influence on oil shale formation. *Palaeogeography, Palaeoclimatology, Palaeoecology*, *510*, 63–77. Retrieved 2020-07-10, from https://linkinghub.elsevier.com/retrieve/pii/S0031018217304741 doi: 10.1016/j.palaeo.2017.11.036

Merlis, T. M., Schneider, T., Bordoni, S., & Eisenman, I. (2013, February). HadleyII Circulation Response to Orbital Precession. Part II: Subtropical Continent. *Journal of Climate*, *26*(3), 754–771. Retrieved 2020-09-07, from https://journals.ametsoc.org/jcli/article/26/3/754/33493/Ha

dley-Circulation-Response-to-Orbital-Precession (Publisher: American Meteorological Society) doi: 10.1175/JCLI-D-12-00149.1

Metcalfe, I. (2013, April). Gondwana dispersion and Asian accretion: Tectonic and palaeogeographic evolution of eastern Tethys. *Journal of Asian Earth Sciences*, *66*, 1–33. Retrieved 2020-10-14, from https://linkinghub.elsevier.com/retrieve/pii/S1367912012005779 doi: 10.1016/j.jseaes.2012.12.020

Meulenkamp, J. E., & Sissingh, W. (2003, July). Tertiary palaeogeography and tectonostratigraphic evolution of the Northern and Southern Peri-Tethys platforms and the intermediate domains of the African–Eurasian convergent plate boundary zone. *Palaeogeography, Palaeoclimatology, Palaeoecology*, *196*(1), 209–228. Retrieved 2021-04-06, from https://www.sciencedirect.com/science/article/pii/S0031018203003195 doi: 10.1016/S0031-0182(03)00319-5

Miao, Y., Fang, X., Herrmann, M., Wu, F., Zhang, Y., & Liu, D. (2011, January). Miocene pollen record of KC-1 core in the Qaidam Basin, NE Tibetan Plateau and implications for evolution of the East Asian monsoon. *Palaeogeography, Palaeoclimatology, Palaeoecology*, *299*(1-2), 30–38. Retrieved 2022-05-04, from https://linkinghub.elsevier.com/retrieve/pii/S0031018210006425 doi: 10.1016/j.palaeo.2010.10.026

Miao, Y., Herrmann, M., Wu, F., Yan, X., & Yang, S. (2012, May). What controlled Mid–Late Miocene long-term aridification in Central Asia? — Global cooling or Tibetan Plateau uplift: A review. *Earth-Science Reviews*, *112*(3), 155–172. Retrieved 2022-03-22, from

https://www.sciencedirect.com/science/article/pii/S0012825212000141 doi: 10.1016/j.earscirev.2012.02.003

Miao, Y., Song, C., Fang, X., Meng, Q., Zhang, P., Wu, F., & Yan, X. (2016, January). Late Cenozoic genus Fupingopollenites development and its implications for the Asian summer monsoon evolution. *Gondwana Research*, *29*(1), 320–333. Retrieved 2017-10-09, from http://linkinghub.elsevier.com/retrieve/pii/S1342937X15000040 doi: 10.1016/j.gr.2014.12.007

Miao, Y., Warny, S., Clift, P. D., Liu, C., & Gregory, M. (2017, December). Evidence of continuous Asian summer monsoon weakening as a response to global cooling over the last 8 Ma. *Gondwana Research*, *52*, 48–58. Retrieved 2022-07-05, from https://linkinghub.elsevier.com/retrieve/pii/S1342937X16304294 doi: 10.1016/j.gr.2017.09.003

Miao, Y., Wu, F., Chang, H., Fang, X., Deng, T., Sun, J., & Jin, C. (2016, March). A Late-Eocene palynological record from the Hoh Xil Basin, northern Tibetan Plateau, and its implications for stratigraphic age, paleoclimate and paleoelevation. *Gondwana Research*, *31*, 241–252. Retrieved 2017-10-09, from http://linkinghub.elsevier.com/retrieve/pii/S1342937X15000374 doi: 10.1016/j.gr.2015.01.007

Miao, Y., Wu, F., Herrmann, M., Yan, X., & Meng, Q. (2013, October). Late early Oligocene East Asian summer monsoon in the NE Tibetan Plateau: Evidence from a palynological record from the Lanzhou Basin, China. *Journal of Asian Earth Sciences*, *75*, 46–57. Retrieved 2022-04-14, from

https://www.sciencedirect.com/science/article/pii/S1367912013003507 doi: 10.1016/j.jseaes.2013.07.003

Miller, K. G., Browning, J. V., Schmelz, W. J., Kopp, R. E., Mountain, G. S., &Wright, J. D. (2020, May). Cenozoic sea-level and cryospheric evolution from deep-sea geochemical and continental margin records. *Science Advances*, *6*(20), eaaz1346. Retrieved 2021-03-09, from https://advances.sciencemag.org/content/6/20/eaaz1346 (Publisher: American Association for the Advancement of Science Section: Review) doi: 10.1126/sciadv.aaz1346

Molnar, P., Boos, W. R., & Battisti, D. S. (2010, April). Orographic Controls on Climate and Paleoclimate of Asia: Thermal and Mechanical Roles for the Tibetan Plateau. *Annual Review of Earth and Planetary Sciences*, *38*(1), 77–102. Retrieved 2018-03-09, from http://www.annualreviews.org/doi/10.1146/annurev-earth-040809-152456 doi: 10.1146/annurev-earth-040809-152456

Molnar, P., England, P., & Martinod, J. (1993). Mantle dynamics, uplift of the Tibetan Plateau, and the Indian Monsoon. *Reviews of Geophysics*, *31*(4), 357. Retrieved 2020-07-27, from http://doi.wiley.com/10.1029/93RG02030 doi: 10.1029/93RG02030

Morley, R. J. (2018, July). Assembly and division of the South and South-East Asian flora in relation to tectonics and climate change. *Journal of Tropical Ecology*, *34*(4), 209–234. Retrieved 2022-06-23, from https://www.cambridge.org/core/product/identifier/S0266467418000202/type/journal_article doi: 10.1017/S0266467418000202

Moucha, R., & Forte, A. M. (2011, October). Changes in African topography driven by mantle convection. *Nature Geoscience*, *4*(10), 707–712. Retrieved 2021-04-07, from http://www.nature.com/articles/ngeo1235 (Number: 10 Publisher: Nature Publishing Group) doi: 10.1038/ngeo1235

Mouthereau, F. (2011, November). Timing of uplift in the Zagros belt/Iranian plateau and accommodation of late Cenozoic Arabia–Eurasia convergence. *Geological Magazine*, *148*(5-6), 726–738. Retrieved 2020-06-22, from https://www.cambridge.org/core/product/identifier/S0016756811000306/type/journal_article doi: 10.1017/S0016756811000306

Mouthereau, F., Lacombe, O., & Vergés, J. (2012, April). Building the Zagros collisional orogen: Timing, strain distribution and the dynamics of Arabia/Eurasia plate convergence. *Tectonophysics*, *532-535*, 27–60. Retrieved 2021-09-15, from https://www.sciencedirect.com/science/article/pii/S0040195112000509 doi: 10.1016/j.tecto.2012.01.022

Najman, Y., Sobel, E. R., Millar, I., Stockli, D. F., Govin, G., Lisker, F., . . . Kahn, A. (2020, January). The exhumation of the Indo-Burman Ranges, Myanmar. *Earth and Planetary Science Letters*, *530*, 115948. Retrieved 2021-03-29, from https://www.sciencedirect.com/science/article/pii/S0012821X19306405 doi: 10.1016/j.epsl.2019.115948

Ninomiya, K., & Shibagaki, Y. (2007). Multi-Scale Features of the Meiyu-Baiu Front and Associated Precipitation Systems. *Journal of the Meteorological Society of Japan. Ser. II*, *85B*, 103–122. Retrieved 2022-09-13, from

http://www.jstage.jst.go.jp/article/jmsj/85B/0/85B_0_103/_article doi: 10.2151/jmsj.85B.103

Okay, A. I., Zattin, M., & Cavazza, W. (2010, January). Apatite fission-track data for the Miocene Arabia-Eurasia collision. *Geology*, *38*(1), 35–38. Retrieved 2022-03-04, from https://doi.org/10.1130/G30234.1 doi: 10.1130/G30234.1

Otero, O., & Gayet, M. (2001, January). Palaeoichthyofaunas from the Lower Oligocene and Miocene of the Arabian Plate: palaeoecological and palaeobiogeographical implications. *Palaeogeography, Palaeoclimatology, Palaeoecology*, *165*(1), 141–169. Retrieved 2021-04-06, from https://www.sciencedirect.com/science/article/pii/S0031018200001589 doi: 10.1016/S0031-0182(00)00158-9

Ozsvárt, P., Kocsis, L., Nyerges, A., Győri, O., & Pálfy, J. (2016, October). The Eocene-Oligocene climate transition in the Central Paratethys. *Palaeogeography, Palaeoclimatology, Palaeoecology*, *459*, 471–487. Retrieved 2021-04-01, from https://www.sciencedirect.com/science/article/pii/S0031018216302899 doi: 10.1016/j.palaeo.2016.07.034

Page, M., Licht, A., Dupont-Nivet, G., Meijer, N., Barbolini, N., Hoorn, C., . . . Guo, Z. (2019, March). Synchronous cooling and decline in monsoonal rainfall in northeastern Tibet during the fall into the Oligocene icehouse. *Geology*, *47*(3), 203–206. Retrieved 2020-01-21, from https://pubs.geoscienceworld.org/gsa/geology/article/47/3/203/568396/Synchronous-cooling-and-decline-in-monsoonal doi: 10.1130/G45480.1

Palcu, D. V., Patina, I. S., Şandric, I., Lazarev, S., Vasiliev, I., Stoica, M., & Krijgsman, W. (2021, December). Late Miocene megalake regressions in Eurasia. *Scientific Reports*, *11*(1), 11471. Retrieved 2021-06-11, from http://www.nature.com/articles/s41598-021-91001-z doi: 10.1038/s41598-021-91001-z

Peng, T., Li, J., Song, C., Guo, B., Liu, J., Zhao, Z., & Zhang, J. (2016, April). An integrated biomarker perspective on Neogene–Quaternary climatic evolution in NE Tibetan Plateau: Implications for the Asian aridification. *Quaternary International*, *399*, 174–182. Retrieved 2022-06-09, from https://www.sciencedirect.com/science/article/pii/S1040618215004220 doi: 10.1016/j.quaint.2015.04.020

Pettke, T., Halliday, A. N., & Rea, D. K. (2002). Cenozoic evolution of Asian climate and sources of Pacific seawater Pb and Nd derived from eolian dust of sediment core LL44-GPC3. *Paleoceanography*, *17*(3), 3-1–3-13. Retrieved 2022-03-25, from http://onlinelibrary.wiley.com/doi/abs/10.1029/2001PA000673 (eprint: https://agupubs.onlinelibrary.wiley.com/doi/pdf/10.1029/2001PA000673) doi: 10.1029/2001PA000673

Pillot, Q., Donnadieu, Y., Sarr, A.-C., Ladant, J.-B., & Suchéras-Marx, B. (2022). Evolution of Ocean Circulation in the North Atlantic Ocean During the Miocene: Impact of the Greenland Ice Sheet and the Eastern Tethys Seaway. *Paleoceanography and Paleoclimatology*, *37*(8), e2022PA004415. Retrieved 2022-09-13, from http://onlinelibrary.wiley.com/doi/abs/10.1029/2022PA004415

(eprint: https://agupubs.onlinelibrary.wiley.com/doi/pdf/10.1029/2022PA004415) doi: 10.1029/2022PA004415

Pirouz, M., Avouac, J.-P., Hassanzadeh, J., Kirschvink, J. L., & Bahroudi, A. (2017, November). Early Neogene foreland of the Zagros, implications for the initial closure of the Neo-Tethys and kinematics of crustal shortening. *Earth and Planetary Science Letters*, *477*, 168–182. Retrieved 2020-10-20, from https://linkinghub.elsevier.com/retrieve/pii/S0012821X17304302 doi: 10.1016/j.epsl.2017.07.046

Poblete, F., Dupont-Nivet, G., Licht, A., van Hinsbergen, D. J. J., Roperch, P., Mihalynuk, M. G., . . . Baatsen, M. L. J. (2021, March). Towards interactive global paleogeographic maps, new reconstructions at 60, 40 and 20Ma. *Earth-Science Reviews*, *214*, 103508. Retrieved 2021-04-07, from https://www.sciencedirect.com/science/article/pii/S0012825221000076 doi: 10.1016/j.earscirev.2021.103508

Polissar, P. J., Uno, K. T., Phelps, S. R., Karp, A. T., Freeman, K. H., & Pensky, J. L. (2021). Hydrologic Changes Drive the Late Miocene Expansion of C4 Grasslands on the Northern Indian Subcontinent. *Paleoceanography and Paleoclimatology*, *36*(4), e2020PA004108. Retrieved 2022-06-07, from http://onlinelibrary.wiley.com/doi/abs/10.1029/2020PA004108 (eprint: https://agupubs.onlinelibrary.wiley.com/doi/pdf/10.1029/2020PA004108) doi: 10.1029/2020PA004108

Poulsen, C. J., & Jeffery, M. L. (2011, June). Climate change imprinting on stable isotopic compositions of high-elevation meteoric water cloaks past surface elevations of major

orogens. *Geology*, *39*(6), 595–598. Retrieved 2022-04-11, from http://pubs.geoscienceworld.org/geology/article/39/6/595/130636/Climate-change-imprinting-on-stable-isotopic doi: 10.1130/G32052.1

Pound, M. J., & Salzmann, U. (2017, February). Heterogeneity in global vegetation and terrestrial climate change during the late Eocene to early Oligocene transition. *Scientific Reports*, *7*, 43386. Retrieved 2017-11-23, from http://www.nature.com/articles/srep43386 doi: 10.1038/srep43386

Prabhat, P., Rahaman, W., Lathika, N., Tarique, M., Mishra, R., & Thamban, M. (2022, December). Modern-like deep water circulation in Indian Ocean caused by Central American Seaway closure. *Nature Communications*, *13*(1), 7561. Retrieved 2022-12-09, from https://www.nature.com/articles/s41467-022-35145-0 doi: 10.1038/s41467-022-35145-0

Prell, W. L., & Kutzbach, J. E. (1992). Sensitivity of the Indian monsoon to forcing parameters and implications for its evolution. *Nature*, *360*(6405), 647–652.

Qiang, X., An, Z., Song, Y., Chang, H., Sun, Y., Liu, W., . . . Ai, L. (2011, January). New eolian red clay sequence on the western Chinese Loess Plateau linked to onset of Asian desertification about 25 Ma ago. *Science China Earth Sciences*, *54*(1), 136–144. Retrieved 2017-10-09, from http://link.springer.com/10.1007/s11430-010-4126-5 doi: 10.1007/s11430-010-4126-5

Rae, J. W., Zhang, Y. G., Liu, X., Foster, G. L., Stoll, H. M., & Whiteford, R. D. (2021, May). Atmospheric CO 2 over the Past 66 Million Years from Marine Archives. *Annual Review*

of Earth and Planetary Sciences, *49*(1), 609–641. Retrieved 2021-06-01, from https://www.annualreviews.org/doi/10.1146/annurev-earth-082420-063026 doi: 10.1146/annurev-earth-082420-063026

Ramstein, G., Fluteau, F., Besse, J., & Joussaume, S. (1997, April). Effect of orogeny, plate motion and land–sea distribution on Eurasian climate change over the past 30 million years. *Nature*, *386*(6627), 788–795. Retrieved 2017-12-05, from http://www.nature.com/doifinder/10.1038/386788a0 doi: 10.1038/386788a0

Rea, D., Leinen, M., & Janecek, T. (1985, March). Geologic Approach to the Long-Term History of Atmospheric Circulation. *Science (New York, N.Y.)*, *227*, 721–5. doi: 10.1126/science.227.4688.721

Rea, D. K. (1994). The paleoclimatic record provided by eolian deposition in the deep sea: The geologic history of wind. *Reviews of Geophysics*, *32*(2), 159–195. Retrieved 2022-05-16, from http://onlinelibrary.wiley.com/doi/abs/10.1029/93RG03257 (eprint: https://agupubs.onlinelibrary.wiley.com/doi/pdf/10.1029/93RG03257) doi: 10.1029/93RG03257

Ren, J., Schubert, B. A., Lukens, W. E., & Quan, C. (2021, September). Low oxygen isotope values of fossil cellulose indicate an intense monsoon in East Asia during the late Oligocene. *Palaeogeography, Palaeoclimatology, Palaeoecology*, *577*, 110556. Retrieved 2022-02-22, from https://linkinghub.elsevier.com/retrieve/pii/S0031018221003412 doi: 10.1016/j.palaeo.2021.110556

Ren, X., Nie, J., Saylor, J. E., Wang, X., Liu, F., & Horton, B. K. (2020). Temperature Control on SilicateWeathering Intensity and Evolution of the Neogene East Asian Summer Monsoon. *Geophysical Research Letters*, *47*(15), e2020GL088808. Retrieved 2022-06-09, from http://onlinelibrary.wiley.com/doi/abs/10.1029/2020GL088808 (eprint: https://agupubs.onlinelibrary.wiley.com/doi/pdf/10.1029/2020GL088808) doi: 10.1029/2020GL088808

Roberts, E. M., Stevens, N. J., O'Connor, P. M., Dirks, P. H. G. M., Gottfried, M. D., Clyde, W. C., . . . Hemming, S. (2012, April). Initiation of the western branch of the East African Rift coeval with the eastern branch. *Nature Geoscience*, *5*(4), 289–294. Retrieved 2021-04-07, from http://www.nature.com/articles/ngeo1432 (Number: 4 Publisher: Nature Publishing Group) doi: 10.1038/ngeo1432

Rodwell, M. J., & Hoskins, B. J. (1995, May). A Model of the Asian Summer Monsoon.Part II: Cross-Equatorial Flow and PV Behavior. *Journal of the Atmospheric Sciences*, *52*(9), 1341–1356. Retrieved 2019-07-05, from http://journals.ametsoc.org/doi/abs/10.1175/1520-0469%281995%29052%3C1341%3AAMOTAS%3E2.0.CO%3B2 doi: 10.1175/1520-0469(1995)052h1341:AMOTASi2.0.CO;2

Rodwell, M. J., & Hoskins, B. J. (1996, July). Monsoons and the dynamics of deserts. Quarterly *Journal of the Royal Meteorological Society*, *122*(534), 1385–1404. Retrieved 2019-07-03, from http://doi.wiley.com/10.1002/qj.49712253408 doi: 10.1002/qj.49712253408

Roe, G. H., Ding, Q., Battisti, D. S., Molnar, P., Clark, M. K., & Garzione, C. N. (2016, May). A modeling study of the response of Asian summertime climate to the largest geologic

forcings of the past 50 Ma: geological controls on Asian climate. *Journal of Geophysical Research: Atmospheres*, *121*(10), 5453–5470. Retrieved 2018-01-11, from http://doi.wiley.com/10.1002/2015JD024370 doi: 10.1002/2015JD024370

Rowley, D. B., & Currie, B. S. (2006, February). Palaeo-altimetry of the late Eocene to Miocene Lunpola basin, central Tibet. *Nature*, *439*(7077), 677–681. Retrieved 2020-10-17, from https://www.nature.com/articles/nature04506 (Number: 7077 Publisher: Nature Publishing Group) doi: 10.1038/nature04506

Rögl, F. (1997). Palaeogeographic Considerations for Mediterranean and Paratethys Seaways (Oligocene to Miocene). *Annalen des Naturhistorischen Museums in Wien. Serie A für Mineralogie und Petrographie, Geologie und Paläontologie, Anthropologie und Prähistorie*, *99*, 279–310. Retrieved 2021-03-09, from http://www.jstor.org/stable/41702129 (Publisher: Naturhistorisches Museum)

Rögl, F. (1999). MEDITERRANEAN AND PARATETHYS. FACTS AND HYPOTHESES OF AN OLIGOCENE TO MIOCENE PALEOGEOGRAPHY (SHORT OVERVIEW). *Geologica carpathica*, *50*(4), 339–349.

Sampe, T., & Xie, S.-P. (2010, January). Large-Scale Dynamics of the Meiyu-Baiu Rainband: Environmental Forcing by the Westerly Jet*. *Journal of Climate*, *23*(1), 113–134. Retrieved 2020-07-25, from https://journals.ametsoc.org/jcli/article/23/1/113/32279/LargeScale-Dynamics-of-the-MeiyuBaiu-Rainband doi: 10.1175/2009JCLI3128.1

Sanyal, P., Bhattacharya, S., Kumar, R., Ghosh, S., & Sangode, S. (2004, March). Mio–Pliocene monsoonal record from Himalayan foreland basin (Indian Siwalik) and its relation to vegetational change. *Palaeogeography, Palaeoclimatology, Palaeoecology*, *205*, 23–41. doi: 10.1016/j.palaeo.2003.11.013

Sarr, A.-C., Donnadieu, Y., Bolton, C. T., Ladant, J.-B., Licht, A., Fluteau, F., . . . Dupont-Nivet, G. (2022, April). Neogene South Asian monsoon rainfall and wind histories diverged due to topographic effects. *Nature Geoscience*, *1–6*. Retrieved 2022-04-12, from http://www.nature.com/articles/s41561-022-00919-0 (Publisher: Nature Publishing Group) doi: 10.1038/s41561-022-00919-0

Sato, T. (2009, February). Influences of subtropical jet and Tibetan Plateau on precipitation pattern in Asia: Insights from regional climate modeling. *Quaternary International*, *194*(1-2), 148–158. Retrieved 2022-02-21, from https://linkinghub.elsevier.com/retrieve/pii/S1040618208002176 doi: 10.1016/j.quaint.2008.07.008

Saxena, R. K., & Trivedi, G. K. (2009). Palynological investigation of the Kopili Formation (Late Eocene) in North Cachar Hills, Assam, India. *Acta Palaeobotanica*, *49*(2), 25.

Scher, H. D., Whittaker, J. M., Williams, S. E., Latimer, J. C., Kordesch, W. E. C., & Delaney, M. L. (2015, July). Onset of Antarctic Circumpolar Current 30 million years ago as Tasmanian Gateway aligned with westerlies. *Nature*, *523*(7562), 580–583. Retrieved 2022-12-09, from http://www.nature.com/articles/nature14598 (Number: 7562 Publisher: Nature Publishing Group) doi: 10.1038/nature14598

Schiemann, R., Lüthi, D., & Schär, C. (2009, June). Seasonality and Interannual Variability of the Westerly Jet in the Tibetan Plateau Region. *Journal of Climate*, *22*(11), 2940–2957.

Retrieved 2022-12-09, from https://journals.ametsoc.org/view/journals/clim/22/11/2008jcli2625.1.xml (Publisher: American Meteorological Society Section: Journal of Climate) doi: 10.1175/2008JCLI2625.1

Schott, F. A., & McCreary, J. P. (2001, January). The monsoon circulation of the Indian Ocean. *Progress in Oceanography*, *51*(1), 1–123. Retrieved 2020-07-23, from https://linkinghub.elsevier.com/retrieve/pii/S0079661101000830 doi: 10.1016/S0079-6611(01)00083-0

Sembroni, A., Faccenna, C., Becker, T. W., Molin, P., & Abebe, B. (2016). Long-term, deep-mantle support of the Ethiopia-Yemen Plateau. *Tectonics*, *35*(2), 469–488. Retrieved 2021-09-02, from http://agupubs.onlinelibrary.wiley.com/doi/abs/10.1002/2015TC004000 (eprint: https://onlinelibrary.wiley.com/doi/pdf/10.1002/2015TC004000) doi: 10.1002/2015TC004000

Sepulchre, P., Caubel, A., Ladant, J.-B., Bopp, L., Boucher, O., Braconnot, P., . . . Tardif, D. (2020, July). IPSL-CM5A2 – an Earth system model designed for multi-millennial climate simulations. *Geoscientific Model Development*, *13*(7), 3011–3053. Retrieved 2020-11-27, from https://gmd.copernicus.org/articles/13/3011/2020/ doi: 10.5194/gmd-13-3011-2020

Sepulchre, P., Ramstein, G., Fluteau, F., Schuster, M., Tiercelin, J.-J., & Brunet, M. (2006, September). Tectonic Uplift and Eastern Africa Aridification. *Science*, *313*(5792), 1419–1423. Retrieved 2020-06-22, from

https://www.sciencemag.org/lookup/doi/10.1126/science.1129158 doi: 10.1126/science.1129158

Sha, Y., Ren, X., Shi, Z., Zhou, P., Li, X., & Liu, X. (2020, April). Influence of the Tibetan Plateau and its northern margins on the mid-latitude Westerly Jet over Central Asia in summer. *Palaeogeography, Palaeoclimatology, Palaeoecology*, *544*, 109611. Retrieved 2022-06-27, from https://linkinghub.elsevier.com/retrieve/pii/S0031018219306819 doi: 10.1016/j.palaeo.2020.109611

Sha, Y., Shi, Z., Liu, X., & An, Z. (2015). Distinct impacts of the Mongolian and Tibetan Plateaus on the evolution of the East Asian monsoon. *Journal of Geophysical Research: Atmospheres*, *120*(10), 4764–4782. Retrieved 2021-04-19, from http://agupubs.onlinelibrary.wiley.com/doi/abs/10.1002/2014JD022880 (eprint: https://onlinelibrary.wiley.com/doi/pdf/10.1002/2014JD022880) doi: https://doi.org/10.1002/2014JD022880

Shen, X., Wan, S., France-Lanord, C., Clift, P. D., Tada, R., Révillon, S., . . . Li, A. (2017, September). History of Asian eolian input to the Sea of Japan since 15 Ma: Links to Tibetan uplift or global cooling? *Earth and Planetary Science Letters*, *474*, 296–308. Retrieved 2017-10-09, from http://linkinghub.elsevier.com/retrieve/pii/S0012821X17303771 doi: 10.1016/j.epsl.2017.06.053

Shi, Z., Liu, X., Liu, Y., Sha, Y., & Xu, T. (2015). Impact of Mongolian Plateau versus Tibetan Plateau on the westerly jet over North Pacific Ocean. *Climate Dynamics*, *44*(11-12), 3067–3076. (ISBN: 0930-7575 Publisher: Springer2)

Shukla, A., Mehrotra, R. C., Spicer, R. A., Spicer, T. E., & Kumar, M. (2014, October). Cool equatorial terrestrial temperatures and the South Asian monsoon in the Early Eocene: Evidence from the Gurha Mine, Rajasthan, India. *Palaeogeography, Palaeoclimatology, Palaeoecology*, *412*, 187–198. Retrieved 2017-10-09, from http://linkinghub.elsevier.com/retrieve/pii/S00310182140039 9X doi:10.1016/j.palaeo.2014.08.004

Smith, S. G., Wegmann, K. W., Ancuta, L. D., Gosse, J. C., & Hopkins, C. E. (2016, August). Paleotopography and erosion rates in the central Hangay Dome, Mongolia: Landscape evolution since the mid-Miocene. *Journal of Asian Earth Sciences*, *125*, 37–57. Retrieved 2021-03-29, from https://www.sciencedirect.com/science/article/pii/S13679120 16301274 doi: 10.1016/j.jseaes.2016.05.013

Song, B., Spicer, R. A., Zhang, K., Ji, J., Farnsworth, A., Hughes, A. C., . . . Shi, G. (2020, May). Qaidam Basin leaf fossils show northeastern Tibet was high, wet and cool in the early Oligocene. *Earth and Planetary Science Letters*, *537*, 116175. Retrieved 2021-05-27, from https://www.sciencedirect.com/science/article/pii/S0012821X 20301187 doi: 10.1016/j.epsl.2020.116175

Sorrel, P., Eymard, I., Leloup, P.-H., Maheo, G., Olivier, N., Sterb, M., . . . Replumaz, A. (2017, December). Wet tropical climate in SE Tibet during the Late Eocene. *Scientific Reports*, *7*(1). Retrieved 2018-04-03, from http://www.nature.com/articles/s41598-017-07766-9 doi: 10.1038/s41598-017-07766-9

Sosdian, S. M., & Lear, C. H. (2020). Initiation of the Western Pacific Warm Pool at the Middle Miocene Climate Transition? *Paleoceanography and Paleoclimatology*, *35*(12), e2020PA003920. Retrieved 2021-09-20, from http://onlinelibrary.wiley.com/doi/abs/10.1029/2020PA003920 (eprint: https://onlinelibrary.wiley.com/doi/pdf/10.1029/2020PA003920) doi: 10.1029/2020PA003920

Spicer, R., Su, T., Valdes, P. J., Farnsworth, A., Wu, F.-X., Shi, G., . . . Zhou, Z. (2020, May). Why `the uplift of the Tibetan Plateau' is a myth? *National Science Review*, 19. Retrieved 2020-11-27, from https://academic.oup.com/nsr/advance-article/doi/10.1093/nsr/nwaa091/5829861 doi: 10.1093/nsr/nwaa091

Spicer, R., Yang, J., Herman, A., Kodrul, T., Aleksandrova, G., Maslova, N., . . . Jin, J.-H. (2017, September). Paleogene monsoons across India and South China: Drivers of biotic change. *Gondwana Research*, *49*, 350–363. Retrieved 2022-05-03, from https://linkinghub.elsevier.com/retrieve/pii/S1342937X16304385 doi: 10.1016/j.gr.2017.06.006

Spicer, R., Yang, J., Herman, A. B., Kodrul, T., Maslova, N., Spicer, T. E., . . . Jin, J. (2016, September). Asian Eocene monsoons as revealed by leaf architectural signatures. *Earth and Planetary Science Letters*, *449*, 61–68. Retrieved 2017-10-09, from http://linkinghub.elsevier.com/retrieve/pii/S0012821X16302618 doi: 10.1016/j.epsl.2016.05.036

Srivastava, G., Paudayal, K. N., Utescher, T., & Mehrotra, R. (2018, February). Miocene vegetation shift and climate change: Evidence from the Siwalik of Nepal. *Global and*

Planetary Change, *161*, 108–120. Retrieved 2022-05-30, from https://linkinghub.elsevier.com/retrieve/pii/S092181811730317X doi: 10.1016/j.gloplacha.2017.12.001

Srivastava, G., Spicer, R. A., Spicer, T. E., Yang, J., Kumar, M., Mehrotra, R., & Mehrotra, N. (2012, July). Megaora and palaeoclimate of a Late Oligocene tropical delta, Makum Coalfield, Assam: Evidence for the early development of the South Asia Monsoon. *Palaeogeography, Palaeoclimatology, Palaeoecology*, *342-343*, 130–142. Retrieved 2018-06-22, from http://linkinghub.elsevier.com/retrieve/pii/S0031018212002532 doi: 10.1016/j.palaeo.2012.05.002

Straume, E. O., Gaina, C., Medvedev, S., & Nisancioglu, K. H. (2020, October). Global Cenozoic Paleobathymetry with a focus on the Northern Hemisphere Oceanic Gateways. *Gondwana Research*, *86*, 126–143. Retrieved 2021-04-08, from https://www.sciencedirect.com/science/article/pii/S1342937X20301659 doi: 10.1016/j.gr.2020.05.011

Su, H., & Zhou, J. (2020, June). Timing of Arabia-Eurasia collision: Constraints from restoration of crustal-scale cross-sections. *Journal of Structural Geology*, *135*, 104041. Retrieved 2022-03-04, from https://www.sciencedirect.com/science/article/pii/S0191814119304456 doi: 10.1016/j.jsg.2020.104041

Su, Q., Nie, J., Meng, Q., Heermance, R., Gong, L., Luo, Z., . . . Garzione, C. (2019, September). Central Asian Drying at 3.3 Ma Linked to Tropical Forcing? *Geophysical Research Letters*, *46*. doi: 10.1029/2019GL084648

Su, T., Farnsworth, A., Spicer, R., & Huang, J. (2019). No high Tibetan Plateau until the Neogene. *Science Advances*, 9.

Su, T., Spicer, R. A., Li, S.-H., Xu, H., Huang, J., Sherlock, S., . . . Zhou, Z.-K. (2019, May). Uplift, climate and biotic changes at the Eocene–Oligocene transition in south-eastern Tibet. *National Science Review*, *6*(3), 495–504. Retrieved 2019-10-24, from https://academic.oup.com/nsr/article/6/3/495/5036537 doi: 10.1093/nsr/nwy062

Su, T., Spicer, R. A., Wu, F.-X., Farnsworth, A., Huang, J., Del Rio, C., . . . Zhou, Z.-K. (2020, December). A Middle Eocene lowland humid subtropical "Shangri-La" ecosystem in central Tibet. *Proceedings of the National Academy of Sciences*, *117*(52), 32989–32995. Retrieved 2021-02-01, from http://www.pnas.org/lookup/doi/10.1073/pnas.2012647117 doi: 10.1073/pnas.2012647117

Suarez, M. B., Passey, B. H., & Kadinsky, A. (2011, December). Paleosol carbonate multiple isotopologue signature of active East Asian summer monsoons during the late Miocene and Pliocene. *Geology*, *39*(12), 1151–1154. Retrieved 2022-06-09, from http://pubs.geoscienceworld.org/geology/article/39/12/1151/130458/Paleosol-carbonate-multiple-isotopologue-signature doi: 10.1130/G32350.1

Sun, J., Liu, W., Guo, Z., Qi, L., & Zhang, Z. (2022, April). Enhanced aridification across the Eocene/Oligocene transition evidenced by geochemical record in the Tajik Basin, Central Asia. *Global and Planetary Change*, *211*, 103789. Retrieved 2022-03-22, from

https://www.sciencedirect.com/science/article/pii/S0921818122000056X doi: 10.1016/j.gloplacha.2022.103789

Sun, J., Sheykh, M., Ahmadi, N., Cao, M., Zhang, Z., Tian, S., . . . Talebian, M. (2021, February). Permanent closure of the Tethyan Seaway in the northwestern Iranian Plateau driven by cyclic sea-level fluctuations in the late Middle Miocene. *Palaeogeography, Palaeoclimatology, Palaeoecology*, *564*, 110172. Retrieved 2021-05-03, from https://www.sciencedirect.com/science/article/pii/S0031018220306209 doi: 10.1016/j.palaeo.2020.110172

Sun, J., & Windley, B. (2015, October). Onset of aridification by 34 Ma across the Eocene-Oligocene transition in Central Asia. *Geology*, *43*, G37165.1. doi: 10.1130/G37165.1

Sun, J., Ye, J., Wu, W., Ni, X., Bi, S., Zhang, Z., . . . Meng, J. (2010, June). Late Oligocene–Miocene mid-latitude aridification and wind patterns in the Asian interior. *Geology*, *38*(6), 515–518. Retrieved 2022-04-06, from https://doi.org/10.1130/G30776.1 doi: 10.1130/G30776.1

Sun, J., Zhang, L., Deng, C., & Zhu, R. (2008, May). Evidence for enhanced aridity in the Tarim Basin of China since 5.3Ma. *Quaternary Science Reviews*, *27*(9-10), 1012–1023. Retrieved 2022-06-16, from https://linkinghub.elsevier.com/retrieve/pii/S0277379108000310 doi: 10.1016/j.quascirev.2008.01.011

Sun, J., & Zhang, Z. (2008, November). Palynological evidence for the Mid-Miocene Climatic Optimum recorded in Cenozoic sediments of the Tian Shan Range, northwestern China. *Global and Planetary Change*, *64*(1-2), 53–68. Retrieved 2022-05-04, from

https://linkinghub.elsevier.com/retrieve/pii/S0921818108001045 doi: 10.1016/j.gloplacha.2008.09.001

Sun, J., Zhang, Z., Cao, M., Windley, B. F., Tian, S., Sha, J., . . . Oimahmadov, I. (2020, May). Timing of seawater retreat from proto-Paratethys, sedimentary provenance, and tectonic rotations in the late Eocene-early Oligocene in the Tajik Basin, Central Asia. *Palaeogeography, Palaeoclimatology, Palaeoecology*, *545*, 109657. Retrieved 2020-11-02, from http://www.sciencedirect.com/science/article/pii/S0031018220301024 doi: 10.1016/j.palaeo.2020.109657

Sun, Q.-g., Collinson, M. E., Li, C.-S., Wang, Y.-f., & Beerling, D. J. (2002). Quantitative reconstruction of palaeoclimate from the Middle Miocene Shanwang ora, eastern China. *Palaeogeography, Palaeoclimatology, Palaeoecology*, 15. doi: 10.1016/S0031-0182(01)00433-3

Sun, X., & Wang, P. (2005, July). How old is the Asian monsoon system?|Palaeobotanical records from China. *Palaeogeography, Palaeoclimatology, Palaeoecology*, *222*(3-4), 181–222. Retrieved 2017-10-09, from http://linkinghub.elsevier.com/retrieve/pii/S0031018205001203 doi: 10.1016/j.palaeo.2005.03.005

Sun, Y., Liu, J., Liang, Y., Ji, J., Liu, W., Aitchison, J. C., . . . Liu, Z. (2020, September). Cenozoic moisture uctuations on the northeastern Tibetan Plateau and association with global climatic conditions. *Journal of Asian Earth Sciences*, *200*, 104490. Retrieved 2022-05-12, from

https://www.sciencedirect.com/science/article/pii/S1367912020302832 doi: 10.1016/j.jseaes.2020.104490

Tada, R., Zheng, H., & Clift, P. D. (2016, December). Evolution and variability of the Asian monsoon and its potential linkage with uplift of the Himalaya and Tibetan Plateau. *Progress in Earth and Planetary Science*, *3*(1). Retrieved 2017-10-09, from http://www.progearthplanetsci.com/content/3/1/4 doi: 10.1186/s40645-016-0080-y

Tan, N., Zhang, Z. S., Guo, Z. T., Guo, C. C., Zhang, Z. J., He, Z. L., & Ramstein, G. (2022). Recognizing the Role of Tropical Seaways in Modulating the Pacific Circulation. *Geophysical Research Letters*, *49*(19), e2022GL099674. Retrieved 2022-10-04, from http://onlinelibrary.wiley.com/doi/abs/10.1029/2022GL099674 (eprint: https://agupubs.onlinelibrary.wiley.com/doi/pdf/10.1029/2022GL099674) doi: 10.1029/2022GL099674

Tang, H., Li, S.-F., Su, T., Spicer, R. A., Zhang, S.-T., Li, S.-H., . . . Zhou, Z.-K. (2020, December). Early Oligocene vegetation and climate of southwestern China inferred from palynology. *Palaeogeography, Palaeoclimatology, Palaeoecology*, *560*, 109988. Retrieved 2022-03-11, from https://www.sciencedirect.com/science/article/pii/S0031018220304338 doi: 10.1016/j.palaeo.2020.109988

Tang, H., Micheels, A., Eronen, J. T., Ahrens, B., & Fortelius, M. (2013, March). Asynchronous responses of East Asian and Indian summer monsoons to mountain uplift shown by regional climate modelling experiments. *Climate Dynamics*, *40*(5), 1531–1549. Retrieved

2021-03-10, from https://doi.org/10.1007/s00382-012-1603-x doi: 10.1007/s00382-012-1603-x

Tang, Z.-H., & Ding, Z.-L. (2013, December). A palynological insight into the Miocene aridification in the Eurasian interior. *Palaeoworld*, *22*(3-4), 77–85. Retrieved 2022-06-23, from https://linkinghub.elsevier.com/retrieve/pii/S1871174X13000073 doi: 10.1016/j.palwor.2013.05.001

Tardif, D., Fluteau, F., Donnadieu, Y., Le Hir, G., Ladant, J.-B., Sepulchre, P., . . . Dupont-Nivet, G. (2020, May). The origin of Asian monsoons: a modelling perspective. *Climate of the Past*, *16*(3), 847–865. Retrieved 2020-05-08, from https://www.clim-past.net/16/847/2020/ doi: 10.5194/cp-16-847-2020

Tardif, D., Toumoulin, A., Fluteau, F., Donnadieu, Y., Le Hir, G., Barbolini, N., . . . Dupont-Nivet, G. (2021, October). Orbital variations as a major driver of climate and biome distribution during the greenhouse to icehouse transition. *Science Advances*, *7*(43), eabh2819. Retrieved 2021-10-25, from https://www.science.org/doi/10.1126/sciadv.abh2819 doi: 10.1126/sciadv.abh2819

Tauxe, L., & Feakins, S. J. (2020). A Reassessment of the Chronostratigraphy of Late Miocene C3–C4 Transitions. *Paleoceanography and Paleoclimatology*, *35*(7), e2020PA003857. Retrieved 2022-06-07, from http://onlinelibrary.wiley.com/doi/abs/10.1029/2020PA003857 (eprint: https://agupubs.onlinelibrary.wiley.com/doi/pdf/10.1029/2020PA003857) doi:10.1029/2020PA003857

Thomson, J. R., Holden, P. B., Anand, P., Edwards, N. R., Porchier, C. A., & Harris, N. B. W. (2021, June). Tectonic and climatic drivers of Asian monsoon evolution. *Nature Communications*, *12*(1), 4022. Retrieved 2021-10-05, from http://www.nature.com/articles/s41467-021-24244-z (Bandiera abtest: a Cc license type: cc by Cg type: Nature Research Journals Number: 1 Primary atype: Research Publisher: Nature Publishing Group Subject term: Climate change;Palaeoclimate Subject term id: climate-change;palaeoclimate) doi: 10.1038/s41467-021-24244-z

Torsvik, T. H., Müller, R. D., Van der Voo, R., Steinberger, B., & Gaina, C. (2008). Global plate motion frames: Toward a unified model. *Reviews of Geophysics*, *46*(3). Retrieved 2022-10-24, from http://onlinelibrary.wiley.com/doi/abs/10.1029/2007RG000227 (eprint: https://agupubs.onlinelibrary.wiley.com/doi/pdf/10.1029/2007RG000227) doi: 10.1029/2007RG000227

Toumoulin, A., Donnadieu, Y., Ladant, J., Batenburg, S. J., Poblete, F., & Dupont-Nivet, G. (2020, August). Quantifying the Effect of the Drake Passage Opening on the Eocene Ocean. *Paleoceanography and Paleoclimatology*, *35*(8). Retrieved 2020-08-13, from https://onlinelibrary.wiley.com/doi/abs/10.1029/2020PA003889 doi: 10.1029/2020PA003889

Toumoulin, A., Tardif, D., Donnadieu, Y., Licht, A., Ladant, J.-B., Kunzmann, L., & Dupont-Nivet, G. (2022, February). Evolution of continental temperature seasonality from the Eocene greenhouse to the Oligocene icehouse –a model–data comparison. *Climate of the Past*, *18*(2), 341–362. Retrieved 2022-02-28, from

https://cp.copernicus.org/articles/18/341/2022/ (Publisher: Copernicus GmbH) doi: 10.5194/cp-18-341-2022

Tripathi, S., Tiwari, M., Lee, J., & Khim, B.-K. (2017, February). First evidence of denitrification vis-á-vis monsoon in the Arabian Sea since Late Miocene. *Scientific Reports*, *7*(1), 43056. Retrieved 2022-06-02, from http://www.nature.com/articles/srep43056 (Number: 1 Publisher: Nature Publishing Group) doi: 10.1038/srep43056

Valcke, S., Budich, R., Carter, M., Guilyardi, E., Lautenschlager, M., Redler, R., & Steenman-Clark, L. (2006). The PRISM software framework and the OASIS coupler. *Annual BMRC Modelling Workshop'The Australian Community Climate and Earth System Simulator (ACCESS)-challenges and opportunities*, 10.

van Hinsbergen, D. J. J., Lippert, P. C., Dupont-Nivet, G., McQuarrie, N., Doubrovine, P. V., Spakman, W., & Torsvik, T. H. (2012, May). Greater India Basin hypothesis and a two-stage Cenozoic collision between India and Asia. *Proceedings of the National Academy of Sciences*, *109*(20), 7659–7664. Retrieved from http://www.pnas.org/content/109/20/7659.abstract doi: 10.1073/pnas.1117262109

van Hinsbergen, D. J. J., Lippert, P. C., Li, S., Huang, W., Advokaat, E. L., & Spakman, W. (2019, June). Reconstructing Greater India: Paleogeographic, kinematic, and geodynamic perspectives. *Tectonophysics*, *760*, 69–94. Retrieved 2020-10-15, from https://linkinghub.elsevier.com/retrieve/pii/S0040195118301331 doi: 10.1016/j.tecto.2018.04.006

Vassallo, R., Jolivet, M., Ritz, J. F., Braucher, R., Larroque, C., Sue, C., . . . Javkhlanbold, D. (2007, July). Uplift age and rates of the Gurvan Bogd system (Gobi-Altay) by apatite

fission track analysis. *Earth and Planetary Science Letters*, *259*(3), 333–346. Retrieved 2021-04-20, from https://www.sciencedirect.com/science/article/pii/S0012821X07002853 doi: 10.1016/j.epsl.2007.04.047

Vicente de Gouveia, S., Besse, J., Frizon de Lamotte, D., Greff-Lefftz, M., Lescanne, M., Gueydan, F., & Leparmentier, F. (2018, April). Evidence of hotspot paths below Arabia and the Horn of Africa and consequences on the Red Sea opening. *Earth and Planetary Science Letters*, *487*, 210–220. Retrieved 2021-10-13, from https://www.sciencedirect.com/science/article/pii/S0012821X18300487 doi: 10.1016/j.epsl.2018.01.030

Vornlocher, J., Lukens, W., Schubert, B., & Quan, C. (2021, April). Late Oligocene Precipitation Seasonality in East Asia Based on δ13C Profiles in Fossil Wood. *Paleo-ceanography and Paleoclimatology*, *36*. doi: 10.1029/2021PA004229

Vögeli, N., Najman, Y., van der Beek, P., Huyghe, P., Wynn, P. M., Govin, G., . . . Sachse, D. (2017, August). Lateral variations in vegetation in the Himalaya since the Miocene and implications for climate evolution. *Earth and Planetary Science Letters*, *471*, 1–9. Retrieved 2022-05-02, from https://www.sciencedirect.com/science/article/pii/S0012821X17302315 doi: 10.1016/j.epsl.2017.04.037

Wan, S., Li, A., Clift, P. D., & Stuut, J.-B. W. (2007, October). Development of the East Asian monsoon: Mineralogical and sedimentologic records in the northern South China Sea since 20 Ma. *Palaeogeography, Palaeoclimatology, Palaeoecology*, *254*(3-4), 561–582. Retrieved 2022-05-03, from

https://linkinghub.elsevier.com/retrieve/pii/S0031018207003963 doi: 10.1016/j.palaeo.2007.07.009

Wang, B., & Ding, Q. (2008, March). Global monsoon: Dominant mode of annual variation in the tropics. *Dynamics of Atmospheres and Oceans*, *44*(3-4), 165–183. Retrieved 2019-05-16, from https://linkinghub.elsevier.com/retrieve/pii/S0377026508000055 doi: 10.1016/j.dynatmoce.2007.05.002

Wang, B., Shi, G., Xu, C., Spicer, R. A., Perrichot, V., Schmidt, A. R., . . . Engel, M. S. (2021). The mid-Miocene Zhangpu biota reveals an outstandingly rich rainforest biome in East Asia. *Science Advances*, *7*(18), eabg0625. Retrieved 2022-05-03, from https://www.science.org/doi/full/10.1126/sciadv.abg0625 (Publisher: American Association for the Advancement of Science) doi: 10.1126/sciadv.abg0625

Wang, C., Dai, J., Zhao, X., Li, Y., Graham, S. A., He, D., . . . Meng, J. (2014, May). Outward-growth of the Tibetan Plateau during the Cenozoic: A review. *Tectonophysics*, *621*, 1–43. Retrieved 2017-10-09, from http://linkinghub.elsevier.com/retrieve/pii/S0040195114000729 doi: 10.1016/j.tecto.2014.01.036

Wang, D., Lu, S., Han, S., Sun, X., & Quan, C. (2013, January). Eocene prevalence of monsoon-like climate over eastern China reected by hydrological dynamics. *Journal of Asian Earth Sciences*, *62*, 776–787. Retrieved 2022-05-04, from https://linkinghub.elsevier.com/retrieve/pii/S1367912012005184 doi: 10.1016/j.jseaes.2012.11.032

Wang, H., Lu, H., Zhao, L., Zhang, H., Lei, F., & Wang, Y. (2019, November). Asian monsoon rainfall variation during the Pliocene forced by global temperature change. *Nature Communications*, *10*(1), 5272. Retrieved 2022-06-09, from https://www.nature.com/articles/s41467-019-13338-4 (Number: 1 Publisher: Nature Publishing Group) doi: 10.1038/s41467-019-13338-4

Wang, L., & Chen, W. (2014, March). An Intensity Index for the East Asian Winter Monsoon. *Journal of Climate*, *27*(6), 2361–2374. Retrieved 2021-10-13, from https://journals.ametsoc.org/view/journals/clim/27/6/jcli-d-13-00086.1.xml (Publisher: American Meteorological Society Section: Journal of Climate) doi: 10.1175/JCLI-D-13-00086.1

Wang, L., Kunzmann, L., Su, T., Xing, Y.-W., Zhang, S.-T., Wang, Y.-Q., & Zhou, Z.-K. (2019, May). The disappearance of Metasequoia (Cupressaceae) after the middle Miocene in Yunnan, Southwest China: Evidences for evolutionary stasis and intensification of the Asian monsoon. *Review of Palaeobotany and Palynology*, *264*, 64–74. Retrieved 2023-04-14, from https://linkinghub.elsevier.com/retrieve/pii/S0034666718301246 doi: 10.1016/j.revpalbo.2018.12.007

Wang, P., Clemens, S., Beaufort, L., Braconnot, P., Ganssen, G., Jian, Z., . . . Sarnthein, M. (2005, March). Evolution and variability of the Asian monsoon system: state of the art and outstanding issues. *Quaternary Science Reviews*, *24*(5-6), 595–629. Retrieved 2020-10-11, from https://linkinghub.elsevier.com/retrieve/pii/S0277379104002975 doi: 10.1016/j.quascirev.2004.10.002

Wang, Q., Li, Y., Ferguson, D. K., Mo, W.-B., & Yang, N. (2021, July). An equable subtropical climate throughout China in the Miocene based on palaeooral evidence. *Earth-Science Reviews*, *218*, 103649. Retrieved 2022-05-03, from https://www.sciencedirect.com/science/article/pii/S0012825221001501 doi: 10.1016/j.earscirev.2021.103649

Wang, X., Carrapa, B., Sun, Y., Dettman, D. L., Chapman, J. B., Caves Rugenstein, J. K., . . . Chen, F. (2020, July). The role of the westerlies and orography in Asian hydroclimate since the late Oligocene. *Geology*, *48*(7), 728–732. Retrieved 2020-10-11, from https://pubs.geoscienceworld.org/gsa/geology/article/48/7/728/584578/The-role-of-the-westerlies-and-orography-in-Asian doi: 10.1130/G47400.1

Wang, X., Qiu, Z., Li, Q., Wang, B., Qiu, Z., Downs, W. R., . . . Meng, Q. (2007, October). Vertebrate paleontology, biostratigraphy, geochronology, and paleoenvironment of Qaidam Basin in northern Tibetan Plateau. *Palaeogeography, Palaeoclimatology, Palaeoecology*, *254*(3-4), 363–385. Retrieved 2023-01-03, from https://linkinghub.elsevier.com/retrieve/pii/S0031018207003057 doi: 10.1016/j.palaeo.2007.06.007

Wang, Y., & Deng, T. (2005, July). A 25 m.y. isotopic record of paleodiet and environmental change from fossil mammals and paleosols from the NE margin of the Tibetan Plateau. *Earth and Planetary Science Letters*, *236*(1-2), 322–338. Retrieved 2022-06-16, from https://linkinghub.elsevier.com/retrieve/pii/S0012821X0500316X doi: 10.1016/j.epsl.2005.05.006

Wasiljeff, J., Salminen, J. M., Stenman, J., Zhang, Z., & Kaakinen, A. (2022, April). Oligocene moisture variations as evidenced by an aeolian dust sequence in Inner Mongolia, China. *Scientific Reports*, *12*. doi: 10.1038/s41598-022-09362-y

Webb, A. A. G., Guo, H., Clift, P. D., Husson, L., Müller, T., Costantino, D., . . . Wang, Q. (2017, April). The Himalaya in 3D: Slab dynamics controlled mountain building and monsoon intensification. *Lithosphere*, *9*(4), 637–651. Retrieved 2022-06-07, from https://doi.org/10.1130/L636.1 doi: 10.1130/L636.1

Webster, P. J., Magan~a, V. O., Palmer, T. N., Shukla, J., Tomas, R. A., Yanai, M., & Yasunari, T. (1998, June). Monsoons: Processes, predictability, and the prospects for prediction. *Journal of Geophysical Research: Oceans*, *103*(C7), 14451–14510. Retrieved 2020-06-19, from http://doi.wiley.com/10.1029/97JC02719 doi: 10.1029/97JC02719

Webster, P. J., & Yang, S. (1992, July). Monsoon and Enso: Selectively Interactive Systems. *Quarterly Journal of the Royal Meteorological Society*, *118*(507), 877–926. Retrieved 2019-07-05, from http://doi.wiley.com/10.1002/qj.49711850705 doi: 10.1002/qj.49711850705

Wei, G., Li, X.-H., Liu, Y., Shao, L., & Liang, X. (2006). Geochemical record of chemical weathering and monsoon climate change since the early Miocene in the South China Sea. *Paleoceanography*, *21*(4). Retrieved 2022-05-03, from https://onlinelibrary.wiley.com/doi/abs/10.1029/2006PA001300 (eprint: https://onlinelibrary.wiley.com/doi/pdf/10.1029/2006PA001300) doi: 10.1029/2006PA001300

Wei, H.-H., & Bordoni, S. (2016, August). On the Role of the African Topography in the South Asian Monsoon. *Journal of the Atmospheric Sciences*, *73*(8), 3197–3212. Retrieved

2019-11-15, from http://journals.ametsoc.org/doi/10.1175/JAS-D-15-0182.1 doi: 10.1175/JAS-D-15-0182.1

Wei, J., Wang, Y., Wang, G., Wei, Z., Wei, H., Zhang, T., . . . Li, L. (2022, April). Biomarker Records From Eocene Lacustrine Sequence in the Eastern Tibet Plateau and Its Implication for Organic Matter Sources. *Frontiers in Earth Science*, *10*, 849041. doi: 10.3389/feart.2022.849041

Westerhold, T., Marwan, N., Drury, A. J., Liebrand, D., Agnini, C., Anagnostou, E., . . . Zachos, J. C. (2020, September). An astronomically dated record of Earth's climate and its predictability over the last 66 million years. *Science*, *369*(6509), 1383–1387. Retrieved 2020-09-12, from https://www.sciencemag.org/lookup/doi/10.1126/science.aba6853 doi: 10.1126/science.aba6853

Westerweel, J., Licht, A., Cogné, N., Roperch, P., Dupont-Nivet, G., Thi, M. K., . . . Aung, D. W. (2020). Burma Terrane Collision and Northward Indentation in the Eastern Himalayas Recorded in the Eocene-Miocene Chindwin Basin (Myanmar). *Tectonics*, *39*(10), e2020TC006413. Retrieved 2021-03-29, from http://agupubs.onlinelibrary.wiley.com/doi/abs/10.1029/2020TC006413 (eprint: https://onlinelibrary.wiley.com/doi/pdf/10.1029/2020TC006413) doi: https://doi.org/10.1029/2020TC006413

Westerweel, J., Roperch, P., Licht, A., Dupont-Nivet, G., Win, Z., Poblete, F., . . . Aung, D. W. (2019, October). Burma Terrane part of the Trans-Tethyan arc during collision with India according to palaeomagnetic data. *Nature Geoscience*, *12*(10), 863–868. Retrieved

2019-10-17, from http://www.nature.com/articles/s41561-019-0443-2 doi: 10.1038/s41561-019-0443-2

White, R. H., Battisti, D. S., & Roe, G. H. (2017). Mongolian Mountains Matter Most: Impacts of the Latitude and Height of Asian Orography on Pacific Wintertime Atmospheric Circulation. *JOURNAL OF CLIMATE*, *30*, 18.

Wichura, H., Jacobs, L. L., Lin, A., Polcyn, M. J., Manthi, F. K., Winkler, D. A., . . . Clemens, M. (2015, March). A 17-My-old whale constrains onset of uplift and climate change in east Africa. *Proceedings of the National Academy of Sciences*, *112*(13), 3910–3915. Retrieved 2021-04-07, from http://www.pnas.org/content/112/13/3910 (Publisher: National Academy of Sciences Section: Physical Sciences) doi: 10.1073/pnas.1421502112

Wolfe, J. (1993). A method of obtaining climatic parameters from leaf assemblages. *US Government Printing Office*.(2040 2041).

Wu, F., Fang, X., Yang, Y., Dupont-Nivet, G., Nie, J., Fluteau, F., . . . Han, W. (2022, October). Reorganization of Asian climate in relation to Tibetan Plateau uplift. *Nature Reviews Earth & Environment*, *3*(10), 684–700. Retrieved 2022-10-24, from http://www.nature.com/articles/s43017-022-00331-7 (Number: 10 Publisher: Nature Publishing Group) doi: 10.1038/s43017-022-00331-7

Wu, G., Liu, Y., He, B., Bao, Q., Duan, A., & Jin, F.-F. (2012, May). Thermal Controls on the Asian Summer Monsoon. *Scientific Reports*, *2*(1), 404. Retrieved 2023-03-31, from https://www.nature.com/articles/srep00404 doi: 10.1038/srep00404

Wu, M., Zhuang, G., Hou, M., & Liu, Z. (2021, July). Expanded lacustrine sedimentation in the Qaidam Basin on the northern Tibetan Plateau: Manifestation of climatic wetting during

the Oligocene icehouse. *Earth and Planetary Science Letters*, *565*, 116935. Retrieved 2022-05-04, from https://linkinghub.elsevier.com/retrieve/pii/S0012821X21001941 doi: 10.1016/j.epsl.2021.116935

Xia, K., Su, T., Liu, Y.-S. C., Xing, Y.-W., Jacques, F. M., & Zhou, Z.-K. (2009, May). Quantitative climate reconstructions of the late Miocene Xiaolongtan megaora from Yunnan, southwest China. *Palaeogeography, Palaeoclimatology, Palaeoecology*, *276*(1-4), 80–86. Retrieved 2022-03-22, from https://linkinghub.elsevier.com/retrieve/pii/S0031018209000819 doi: 10.1016/j.palaeo.2009.02.024

Xiao, G. Q., Abels, H. A., Yao, Z. Q., Dupont-Nivet, G., & Hilgen, F. J. (2010, July). Asian aridification linked to the first step of the Eocene-Oligocene climate Transition (EOT) in obliquity-dominated terrestrial records (Xining Basin, China). *Climate of the Past*, *6*(4), 501–513. Retrieved 2017-10-09, from http://www.clim-past.net/6/501/2010/ doi: 10.5194/cp-6-501-2010

Xie, S.-P., Xu, H., Saji, N. H., Wang, Y., & Liu, W. T. (2006, July). Role of Narrow Mountains in Large-Scale Organization of Asian Monsoon Convection*. *Journal of Climate*, *19*(14), 3420–3429. Retrieved 2022-07-08, from http://journals.ametsoc.org/doi/10.1175/JCLI3777.1 doi: 10.1175/JCLI3777.1

Xie, Y., Wu, F., Fang, X., Song, J., & Niu, Z. (2022, August). Late Eocene onset of the East Asian Monsoon in the Qingjiang Basin of Central Jiangxi Province (Southeast China) revealed

by a major vegetation transition from desert to forest. *Palaeogeography, Palaeoclimatology, Palaeoecology*, *602*, 111179. doi: 10.1016/j.palaeo.2022.111179

Xing, Y., Utescher, T., Jacques, F. M., Su, T., Liu, Y. C., Huang, Y., & Zhou, Z. (2012, November). Paleoclimatic estimation reveals a weak winter monsoon in southwestern China during the late Miocene: Evidence from plant macrofossils. *Palaeogeography, Palaeoclimatology, Palaeoecology*, *358-360*, 19–26. Retrieved 2022-05-04, from https://linkinghub.elsevier.com/retrieve/pii/S0031018212004129 doi: 10.1016/j.palaeo.2012.07.011

Xiong, Z., Ding, L., Spicer, R. A., Farnsworth, A.,Wang, X., Valdes, P. J., . . . Yue, Y. (2020, August). The early Eocene rise of the Gonjo Basin, SE Tibet: From low desert to high forest. *Earth and Planetary Science Letters*, *543*, 116312. Retrieved 2020-10-12, from https://linkinghub.elsevier.com/retrieve/pii/S0012821X20302569 doi: 10.1016/j.epsl.2020.116312

Xiong, Z., Liu, X., Ding, L., Farnsworth, A., Spicer, R. A., Xu, Q., . . . Yue, Y. (2022). The rise and demise of the Paleogene Central Tibetan Valley. *Science Advances*, *8*(6), eabj0944. Retrieved 2022-02-10, from http://www.science.org/doi/10.1126/sciadv.abj0944 (Publisher: American Association for the Advancement of Science) doi: 10.1126/sciadv.abj0944

Xu, Q., Ding, L., Spicer, R. A., Liu, X., Li, S., & Wang, H. (2018, February). Stable isotopes reveal southward growth of the Himalayan-Tibetan Plateau since the Paleocene. *Gondwana Research*, *54*, 50–61. Retrieved 2020-10-20, from https://linkinghub.elsevier.com/retrieve/pii/S1342937X17303295 doi: 10.1016/j.gr.2017.10.005

Xu, Q., Ding, L., Zhang, L., Cai, F., Lai, Q., Yang, D., & Liu-Zeng, J. (2013, January). Paleogene high elevations in the Qiangtang Terrane, central Tibetan Plateau. *Earth and Planetary Science Letters*, *362*, 31–42. Retrieved 2020-10-17, from http://www.sciencedirect.com/science/article/pii/S0012821X1200684X doi: 10.1016/j.epsl.2012.11.058

Yang, C., Dang, H., Zhou, X., Zhang, H., Wang, X., Wang, Y., . . . Jian, Z. (2021, April). Upper ocean hydrographic changes in response to the evolution of the East Asian monsoon in the northern South China Sea during the middle to late Miocene. *Global and Planetary Change*, *201*, 103478. doi: 10.1016/j.gloplacha.2021.103478

Yang, W., Zuo, R., Wang, X., Song, Y., Jiang, Z., Luo, Q., . . . Zhang, Z. (2019, January). Sensitivity of lacustrine stromatolites to Cenozoic tectonic and climatic forcing in the southern Junggar Basin, NW China: New insights from mineralogical, stable and clumped isotope compositions. *Palaeogeography, Palaeoclimatology, Palaeoecology*, *514*, 109–123. Retrieved 2022-06-17, from https://linkinghub.elsevier.com/retrieve/pii/S0031018218303985 doi: 10.1016/j.palaeo.2018.10.011

Yang, X., Groeneveld, J., Jian, Z., Steinke, S., & Giosan, L. (2020). Middle Miocene Intensification of South Asian Monsoonal Rainfall. *Paleoceanography and Paleoclimatology*, *35*(12), e2020PA003853. Retrieved 2021-03-17, from http://agupubs.onlinelibrary.wiley.com/doi/abs/10.1029/2020PA003853 (eprint: https://onlinelibrary.wiley.com/doi/pdf/10.1029/2020PA003853) doi: https://doi.org/10.1029/2020PA003853

Yao, Y.-F., Bruch, A. A., Mosbrugger, V., & Li, C.-S. (2011, May). Quantitative reconstruction of Miocene climate patterns and evolution in Southern China based on plant fossils. *Palaeogeography, Palaeoclimatology, Palaeoecology*, *304*(3-4), 291–307. Retrieved 2022-05-06, from https://linkinghub.elsevier.com/retrieve/pii/S003101821000221X doi: 10.1016/j.palaeo.2010.04.012

Yarmolyuk, V. V., Kudryashova, E. A., Kozlovsky, A. M., & Lebedev, V. A. (2008, October). Late Cenozoic volcanism of Khangai (Central Mongolia): Evidence for recent orogeny in Central Asia. *Doklady Earth Sciences*, *422*(1), 1032–1036. Retrieved 2021-03-29, from http://link.springer.com/10.1134/S1028334X08070064 doi: 10.1134/S1028334X08070064

Yu, E., Zhang, R., Jiang, D., Ramstein, G., Zhang, Z., & Sun, J. (2018, October). High-resolution simulation of Asian monsoon response to regional uplift of the Tibetan Plateau with regional climate model nested with global climate model. *Global and Planetary Change*, *169*, 34–47. Retrieved 2021-09-24, from https://linkinghub.elsevier.com/retrieve/pii/S0921818118300407 doi: 10.1016/j.gloplacha.2018.07.002

Yuan, Q., Barbolini, N., Ashworth, L., Rydin, C., Gao, D.-L., Shan, F.-S., . . . Vajda, V. (2021, July). Palaeoenvironmental changes in Eocene Tibetan lake systems traced by geochemistry, sedimentology and palynofacies. *Journal of Asian Earth Sciences*, *214*, 104778. Retrieved 2022-05-04, from https://linkinghub.elsevier.com/retrieve/pii/S1367912021001164 doi: 10.1016/j.jseaes.2021.104778

Yuan, Q., Barbolini, N., Rydin, C., Gao, D.-L., Wei, H.-C., Fan, Q.-S., . . . Vajda, V. (2020, November). Aridification signatures from fossil pollen indicate a drying climate in east-central Tibet during the late Eocene. *Climate of the Past*, *16* (6), 2255–2273. Retrieved 2022-05-04, from https://cp.copernicus.org/articles/16/2255/2020/ doi: 10.5194/cp-16-2255-2020

Yuan, W., Carter, A., Dong, J., Bao, Z., An, Y., & Guo, Z. (2006, January). Mesozoic–Tertiary exhumation history of the Altai Mountains, northern Xinjiang, China: New constraints from apatite fission track data. *Tectonophysics*, *412*(3), 183–193. Retrieved 2021-03-26, from https://www.sciencedirect.com/science/article/pii/S00401951 0500449X doi: 10.1016/j.tecto.2005.09.007

Zhang, R., Jiang, D., Liu, X., & Tian, Z. (2012, December). Modeling the climate effects of different subregional uplifts within the Himalaya-Tibetan Plateau on Asian summer monsoon evolution. *Chinese Science Bulletin*, *57*(35), 4617–4626. Retrieved 2017-10-09, from http://link.springer.com/10.1007/s11434-012-5284-y doi: 10.1007/s11434-012-5284-y

Zhang, R., Jiang, D., Ramstein, G., Zhang, Z., Lippert, P. C., & Yu, E. (2018, February). Changes in Tibetan Plateau latitude as an important factor for understanding East Asian climate since the Eocene: A modeling study. *Earth and Planetary Science Letters*, *484*, 295–308. Retrieved 2018-01-16, from http://linkinghub.elsevier.com/retrieve/pii/S0012821X173074 6X doi: 10.1016/j.epsl.2017.12.034

Zhang, R., Jiang, D., & Zhang, Z. (2017, December). Effects of the uplifts of the main and marginal Tibetan Plateau on the Asian climate under modern and ~30 Ma boundary conditions. *Palaeogeography, Palaeoclimatology, Palaeoecology*. Retrieved 2018-01-16, from http://linkinghub.elsevier.com/retrieve/pii/S0031018217308866 doi: 10.1016/j.palaeo.2017.12.022

Zhang, R., Jiang, D., Zhang, Z., Cheng, Z., & Zhang, Q. (2017). Comparison of the climate effects of surface uplifts from the northern Tibetan Plateau, the Tianshan, and the Mongolian Plateau on the East Asian climate. *Journal of Geophysical Research: Atmospheres*, *122*(15), 7949–7970. Retrieved 2022-12-19, from https://onlinelibrary.wiley.com/doi/abs/10.1002/2017JD026470 (eprint: https://onlinelibrary.wiley.com/doi/pdf/10.1002/2017JD026470) doi: 10.1002/2017JD026470

Zhang, R., Jiang, D., Zhang, Z., & Zhang, C. (2021). Effects of Tibetan Plateau Growth, Paratethys Sea Retreat and Global Cooling on the East Asian Climate by the Early Miocene. *Geochemistry, Geophysics, Geosystems*, *22*(6), e2021GC009655. Retrieved 2021-09-24, from http://onlinelibrary.wiley.com/doi/abs/10.1029/2021GC009655 (eprint: https://agupubs.onlinelibrary.wiley.com/doi/pdf/10.1029/2021GC009655) doi: 10.1029/2021GC009655

Zhang, Z., Flatøy, F., Wang, H., Bethke, I., Bentsen, M., & Guo, Z. (2012, January). Early Eocene Asian climate dominated by desert and steppe with limited monsoons. *Journal of Asian Earth Sciences*, *44*, 24–35. Retrieved 2017-10-09, from

http://linkinghub.elsevier.com/retrieve/pii/S1367912011002148 doi: 10.1016/j.jseaes.2011.05.013

Zhang, Z., Ramstein, G., Schuster, M., Li, C., Contoux, C., & Yan, Q. (2014, September). Aridification of the Sahara desert caused by Tethys Sea shrinkage during the Late Miocene. *Nature*, *513*(7518), 401–404. Retrieved 2019-09-06, from http://www.nature.com/articles/nature13705 doi: 10.1038/nature13705

Zhang, Z., & Sun, J. (2011, January). Palynological evidence for Neogene environmental change in the foreland basin of the southern Tianshan range, northwestern China. *Global and Planetary Change*, *75*(1-2), 56–66. Retrieved 2022-05-04, from https://linkinghub.elsevier.com/retrieve/pii/S0921818110002304 doi:10.1016/j.gloplacha.2010.10.006

Zhang, Z., Wang, H., Guo, Z., & Jiang, D. (2007, March). What triggers the transition of palaeoenvironmental patterns in China, the Tibetan Plateau uplift or the Paratethys Sea retreat? *Palaeogeography, Palaeoclimatology, Palaeoecology*, *245*(3-4), 317–331. Retrieved 2017-10-09, from http://linkinghub.elsevier.com/retrieve/pii/S0031018206004469 doi: 10.1016/j.palaeo.2006.08.003

Zhang, Z., Xiao, W., Majidifard, M. R., Zhu, R., Wan, B., Ao, S., . . . Esmaeili, R. (2017, June). Detrital zircon provenance analysis in the Zagros Orogen, SW Iran: implications for the amalgamation history of the Neo-Tethys. *International Journal of Earth Sciences*, *106*(4), 1223–1238. Retrieved 2022-03-04, from https://doi.org/10.1007/s00531-016-1314-3 doi: 10.1007/s00531-016-1314-3

Zhang, Z., Zhang, Z., He, Z., Tan, N., Guo, Z., Zhu, J., . . . de Boer, A. M. (2022). Impact of Mountains in Southern China on the Eocene Climates of East Asia. *Journal of Geophysical Research: Atmospheres*, *127*(17), e2022JD036510. Retrieved 2022-12-05, from http://onlinelibrary.wiley.com/doi/abs/10.1029/2022JD036510 (eprint: https://agupubs.onlinelibrary.wiley.com/doi/pdf/10.1029/2022JD036510) doi: 10.1029/2022JD036510

Zhao, H., Qiang, X., Xu, X., & Sun, Y. (2020, April). Iron oxide characteristics of the Chinese loess-red clay sequences and their implications for the evolution of the East Asian summer monsoon since the Late Oligocene. *Palaeogeography, Palaeoclimatology, Palaeoecology*, *543*, 109604. Retrieved 2022-06-09, from https://linkinghub.elsevier.com/retrieve/pii/S0031018219308995 doi: 10.1016/j.palaeo.2020.109604

Zhao, L., Lu, H., Wang, H., Meadows, M., Ma, C., Tang, L., . . . Zhang, H. (2020, October). Vegetation dynamics in response to evolution of the Asian Monsoon in a warm world: Pollen evidence from the Weihe Basin, central China. *Global and Planetary Change*, *193*, 103269. Retrieved 2022-06-09, from https://linkinghub.elsevier.com/retrieve/pii/S0921818120301600 doi: 10.1016/j.gloplacha.2020.103269

Zheng, H., Wei, X., Tada, R., Clift, P. D., Wang, B., Jourdan, F., . . . He, M. (2015, June). Late Oligocene–early Miocene birth of the Taklimakan Desert. *Proceedings of the National Academy of Sciences*, *112*(25), 7662–7667. Retrieved 2022-02-11, from http://www.pnas.org/lookup/doi/10.1073/pnas.1424487112 doi: 10.1073/pnas.1424487112

Zheng, H., Yang, Q., Cao, S., Clift, P. D., He, M., Kano, A., . . . Jourdan, F. (2022, December). From desert to monsoon: irreversible climatic transition at ~ 36 Ma in southeastern Tibetan Plateau. *Progress in Earth and Planetary Science*, *9*(1), 12. Retrieved 2022-05-02, from https://progearthplanetsci.springeropen.com/articles/10.1186/s40645-022-00470-x doi: 10.1186/s40645-022-00470-x

Zhisheng, A., Guoxiong, W., Jianping, L., Youbin, S., Yimin, L., Weijian, Z., . . . Juan, F. (2015, May). Global Monsoon Dynamics and Climate Change. *Annual Review of Earth and Planetary Sciences*, *43*(1), 29–77. Retrieved 2017-10-02, from http://www.annualreviews.org/doi/10.1146/annurev-earth-060313-054623 doi: 10.1146/annurev-earth-060313-054623

Zhisheng, A., Kutzbach, J. E., Prell, W. L., & Porter, S. C. (2001, May). Evolution of Asian monsoons and phased uplift of the Himalaya–Tibetan plateau since Late Miocene times. *Nature*, *411*(6833), 62–66. Retrieved 2021-09-16, from http://www.nature.com/articles/35075035 (Bandiera abtest: a Cg type: Nature Research Journals Number: 6833 Primary atype: Research Publisher: Nature Publishing Group) doi: 10.1038/35075035

Zhou, P., Ireland, T., Murray, R. W., & Clift, P. D. (2021, June). Marine sedimentary records of chemical weathering evolution in the western Himalaya since 17 Ma. *Geosphere*, *17*(3), 824–853. Retrieved 2022-09-13, from https://pubs.geoscienceworld.org/gsa/geosphere/article/17/3/824/595660/Marine-sedimentary-records-of-chemical-weathering doi: 10.1130/GES02211.1

Zhuang, G., Pagani, M., & Zhang, Y. G. (2017, July). Monsoonal upwelling in the western Arabian Sea since the middle Miocene. *Geology*, *45*(7), 655–658. Retrieved 2022-05-02, from https://doi.org/10.1130/G39013.1 doi: 10.1130/G39013.1

Ziegler, C. L., Murray, R. W., Hovan, S. A., & Rea, D. K. (2007, February). Resolving eolian, volcanogenic, and authigenic components in pelagic sediment from the Pacific Ocean. *Earth and Planetary Science Letters*, *254*(3), 416–432. Retrieved 2022-03-25, from https://www.sciencedirect.com/science/article/pii/S0012821X06008661 doi: 10.1016/j.epsl.2006.11.049

Zoura, D., Hill, D., Dolan, A., Hunter, S., Tang, Z., & Haywood, A. (2019, August). Atmospheric carbon dioxide, ice sheet and topographic constraints on palaeo moisture availability in Asia. *Earth and Planetary Science Letters*, *519*, 12–27. Retrieved 2019-09-12, from https://linkinghub.elsevier.com/retrieve/pii/S0012821X19302390 doi: 10.1016/j.epsl.2019.04.035

8 Supplementary

Table 3: (suite) List of references used in Figure 2 for paleoclimate indicators compilation

Figure 14. Comparison of monsoon diagnostics obtained in our control historical simulation (**Left column**) with modern observations and reanalysis (**Right column**). **(a, b)** Mean Annual Precipitations (shading, mm/yr), and regions where the Monsoon Precipitation Index is over 0.5 (thin red dots) and 0.75 (thick red dots) ; **(c, d)** JJA mean 2 m temperature (shading, Celsius) and 300 hPa atmospheric temperature (white contour, Kelvin) ; **(e, f)** JJA normalized Sea Level Pressure anomalies (shading, hPa) and 850 hPa winds (vectors over 4 m/s); **(g, h)** DJF mean 2 m

temperature (shading, Celsius) ; **(i, j)** DJF normalized Sea Level Pressure anomalies (shading, hPa) and 850 hPa winds (vectors over 4 m/s). In all captions, topography in gray contour, each 1000 m. On the right column, precipitation are from GPCP, pressure and 300hPa temperature from ERAINT, 850hPa winds and surface temperature from ERA40.

Figure 15. Mean Annual Precipitation (shading, mm/yr), overlain with regions where the Monsoon Precipitation Index (B. Wang & Ding, 2008) is over 0.5 (thin red dots) and 0.75 (thick red dots), for all reference and sensitivity experiments.

Figure 16. June-August (JJA) normalized Sea Level Pressure anomalies (shading, hPa) and 850 hPa winds over 4 m/s (vectors), for all reference and sensitivity experiments.

Figure 17. December-February (DJF) normalized Sea Level Pressure anomalies (shading, hPa) and 850 hPa winds over 4 m/s (vectors), for all reference and sensitivity experiments.

Figure 18. Jet Stream velocity and localization over Asia in August (purple outline), for all sensitivity experiments and precipitation for the month of August (shading, mm/month).

Key Points:

- Modern Asian monsoonal characteristics appeared sequentially during the Cenozoic, driven by distinct paleogeographic and climatic forcing factors.
- Model results depict monsoon-like precipitation seasonality in parts of Southern and Eastern Asia since the Paleogene.
- Monsoon-like rainfall regime in Paleogene eastern Asia is triggered by the proto-Tibetan Plateau uplift.
- Increasing continentality, due to the retreat of the Paratethys Sea and the emergence of the Arabian Platform above sea level, are instrumental in the establishment of surface temperature gradients that promote moist air advection from the Indian Ocean towards Asia in summer.
- The Anatolian-Iranian and East African landforms contribute to reinforcing the Somali Jet that brings moisture to Southeastern Asia in summer.
- The uplift of the Mongolian Plateau drives the formation of the Siberian High in winter, which broadly reinforces the East Asian winter monsoon and induces aridification of the Gobi region.
- The uplift of the Tian Shan and Pamir mountain ranges blocks the westerly moisture flux, forces the northward migration of the Jet Stream in summer, and enhances inland Asian aridification. Their effect on the South Asian monsoon is likely dependent on the paleoelevation of neighboring landforms, especially the Anatolian-Iranian Plateau.
- Additional constraints on the respective timing of uplift and paleoelevation are key to improving our understanding of monsoon establishment.

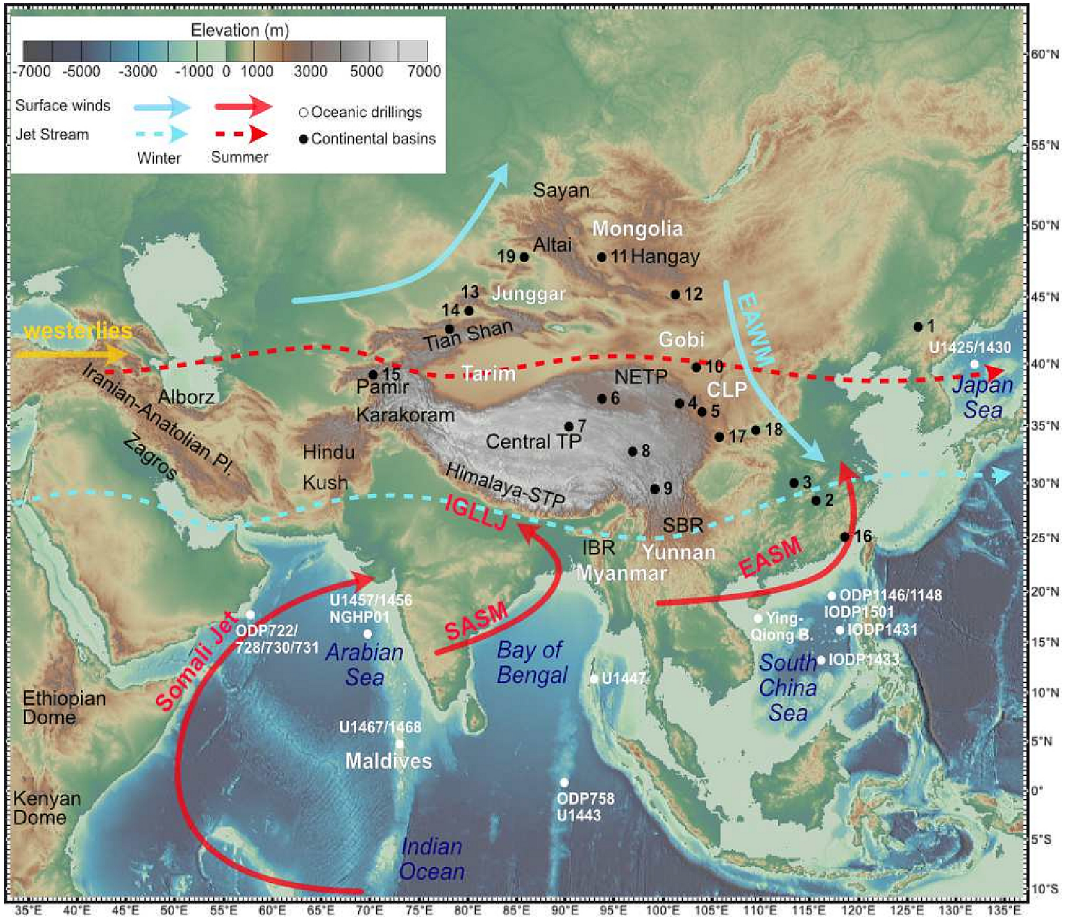
Elevation (m)
-7000 -5000 -3000 -1000 0 1000 3000 5000 7000
Surface winds
Jet Stream
Winter
Summer
Oceanic drillings
Continental basins
Sayan
Mongolia
19 Altai
11 Hangay
13 Junggar
14
12
Tian Shan
EAWM
westerlies
Gobi
1
U1425/1430
Tarim
NETP
10
15
Pamir
6
4
5
CLP
Japan Sea
Iranian-Anatolian Pl.
Alborz
Karakoram
7
Central TP
17
18
Zagros
Hindu
Kush
8
Himalaya-STP
3
2
9
IGLLJ
SBR
16
IBR
Yunnan
Myanmar
EASM
ODP1146/1148
IODP1501
IODP1431
U1457/1456
NGHP01
ODP722/
728/730/731
Somali Jet
SASM
Arabian
Sea
Bay of
Bengal
Ying-
Qiong B.
South
China
Sea
IODP1433
U1447
Ethiopian
Dome
U1467/1468
Maldives
ODP758
U1443
Kenyan
Dome
Indian
Ocean
60°N
55°N
50°N
45°N
40°N
35°N
30°N
25°N
20°N
15°N
10°N
5°N
0°
5°S
10°S
35°E
40°E
45°E
50°E
55°E
60°E
65°E
70°E
75°E
80°E
85°E
90°E
95°E
100°E
105°E
110°E
115°E
120°E
125°E
130°E
135°E

Figure 1

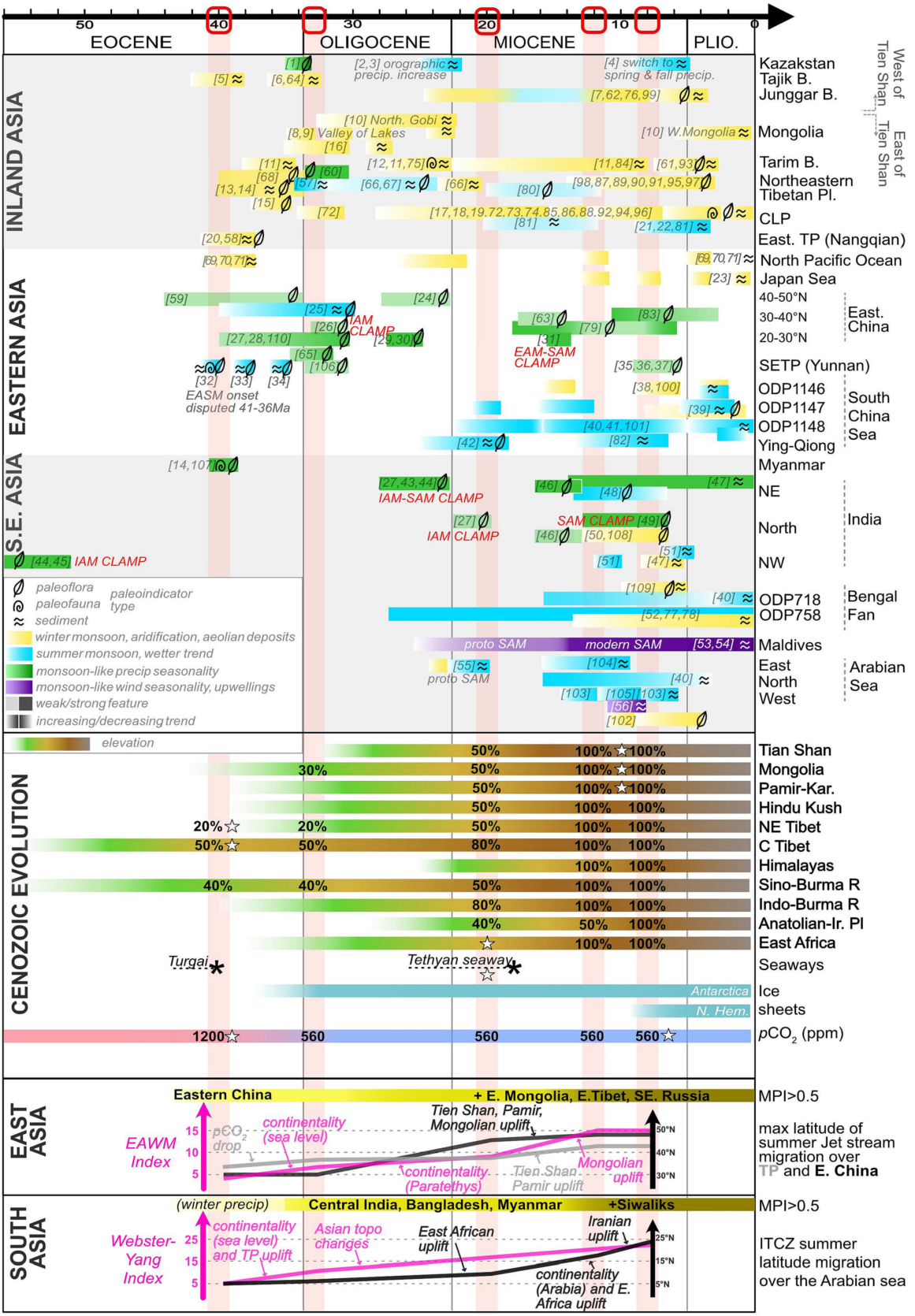
50
40
30
20
10
0
EOCENE
OLIGOCENE
MIOCENE
PLIO.
PALEOCLIMATE INDICATORS
INLAND ASIA
EASTERN ASIA
S.E. ASIA
[1]
[5]
[6,64]
[2,3] orographic precip. increase
[4] switch to spring & fall precip.
[7,62,76,99]
[10] North. Gobi
[8,9] Valley of Lakes
[16]
[10] W.Mongolia
[11]
[68]
[60]
[13,14]
[57]
[12,11,75]
[11,84]
[61,93]
[66,67]
[66]
[80]
[98,87,89,90,91,95,97]
[15]
[72]
[17,18,19,72,73,74,85,86,88,92,94,96]
[81]
[21,22,81]
[20,58]
[69,70,71]
[23]
[59]
[24]
[25]
[26]
IAM CLAMP
[29,30]
[27,28,110]
[65]
[106]
[63]
[79]
[83]
[31]
EAM-SAM CLAMP
[35,36,37]
[32]
[33]
[34]
EASM onset disputed 41-36Ma
[38,100]
[39]
[40,41,101]
[42]
[82]
[14,107]
[27,43,44]
IAM-SAM CLAMP
[46]
[47]
[48]
[27]
IAM CLAMP
SAM CLAMP [49]
[46]
[50,108]
[51]
[47]
[44,45] IAM CLAMP
[109]
[40]
[52,77,78]
proto SAM
modern SAM
[53,54]
[55]
proto SAM
[104]
[40]
[103]
[105]
[103]
[56]
[102]
paleoflora
paleofauna
paleoindicator type
sediment
winter monsoon, aridification, aeolian deposits
summer monsoon, wetter trend
monsoon-like precip seasonality
monsoon-like wind seasonality, upwellings
weak/strong feature
increasing/decreasing trend
elevation
Kazakstan
Tajik B.
Junggar B.
West of Tien Shan
East of Tien Shan
Mongolia
Tarim B.
Northeastern Tibetan Pl.
CLP
East. TP (Nangqian)
North Pacific Ocean
Japan Sea
40-50°N
30-40°N
20-30°N
East. China
SETP (Yunnan)
ODP1146
ODP1147
ODP1148
Ying-Qiong
South China Sea
Myanmar
NE
North
NW
India
ODP718
ODP758
Bengal Fan
Maldives
East
North
West
Arabian Sea
BOUNDARY CONDITIONS
CENOZOIC EVOLUTION
Tian Shan
Mongolia
Pamir-Kar.
Hindu Kush
NE Tibet
C Tibet
Himalayas
Sino-Burma R
Indo-Burma R
Anatolian-Ir. Pl
East Africa
Seaways
Turgai
Tethyan seaway
Ice sheets
Antarctica
N. Hem.
pCO2 (ppm)
MODELLING RESULTS
EAST ASIA
Eastern China
+ E. Mongolia, E.Tibet, SE. Russia
MPI>0.5
EAWM Index
pCO2 drop
continentality (sea level)
Tien Shan, Pamir, Mongolian uplift
continentality (Paratethys)
Tien Shan-Pamir uplift
Mongolian uplift
max latitude of summer Jet stream migration over TP and E. China
SOUTH ASIA
(winter precip)
Central India, Bangladesh, Myanmar
+Siwaliks
MPI>0.5
Webster-Yang Index
continentality (sea level) and TP uplift
Asian topo changes
East African uplift
Iranian uplift
continentality (Arabia) and E. Africa uplift
ITCZ summer latitude migration over the Arabian sea

Figure 2

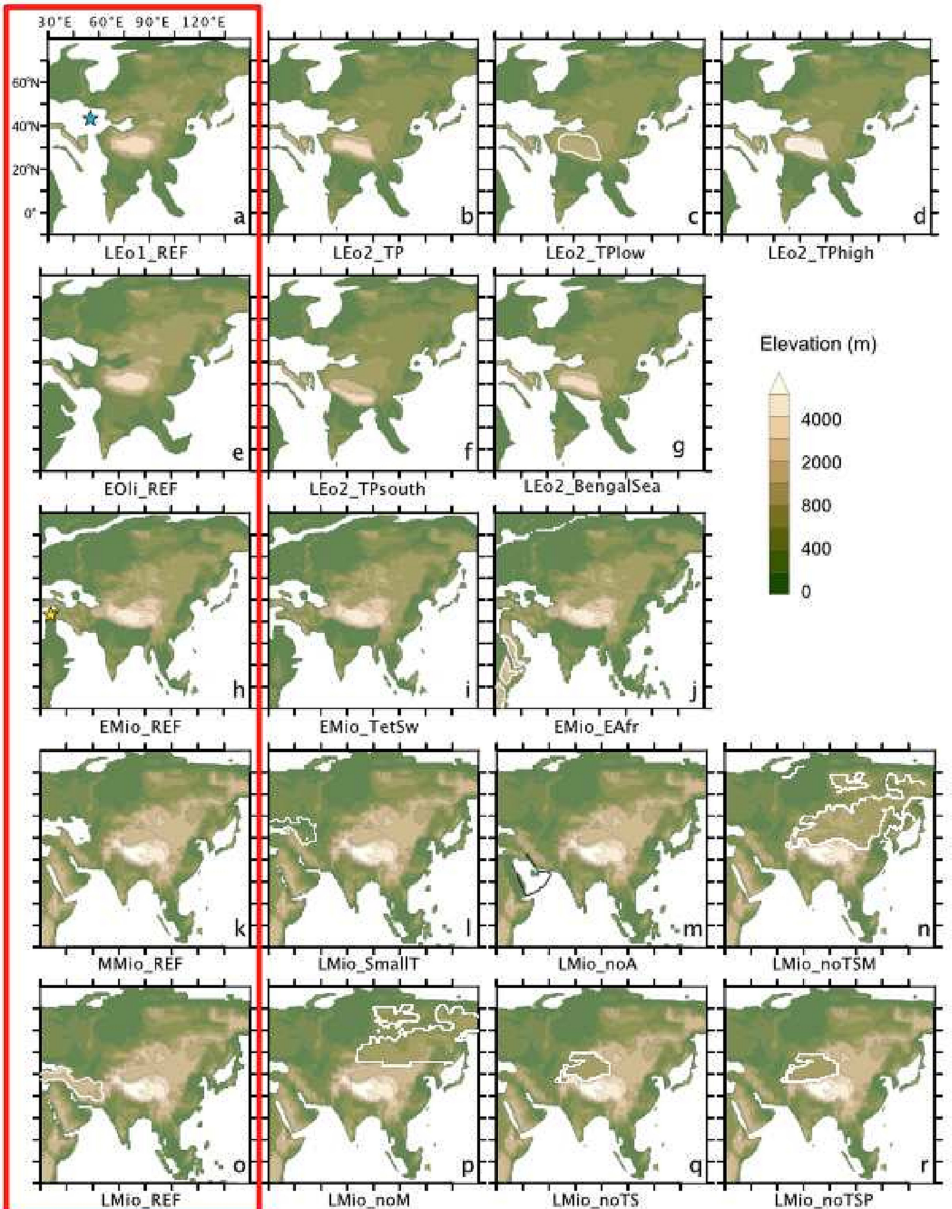
30°E
60°E
90°E
120°E
60°N
40°N
20°N
0°
a
b
c
d
LEo1_REF
LEo2_TP
LEo2_TPlow
LEo2_TPhigh
e
f
g
EOli_REF
LEo2_TPsouth
LEo2_BengalSea
Elevation (m)
4000
2000
800
400
0
h
i
j
EMio_REF
EMio_TetSw
EMio_EAfr
k
l
m
n
MMio_REF
LMio_SmallT
LMio_noA
LMio_noTSM
o
p
q
r
LMio_REF
LMio_noM
LMio_noTS
LMio_noTSP

Figure 3

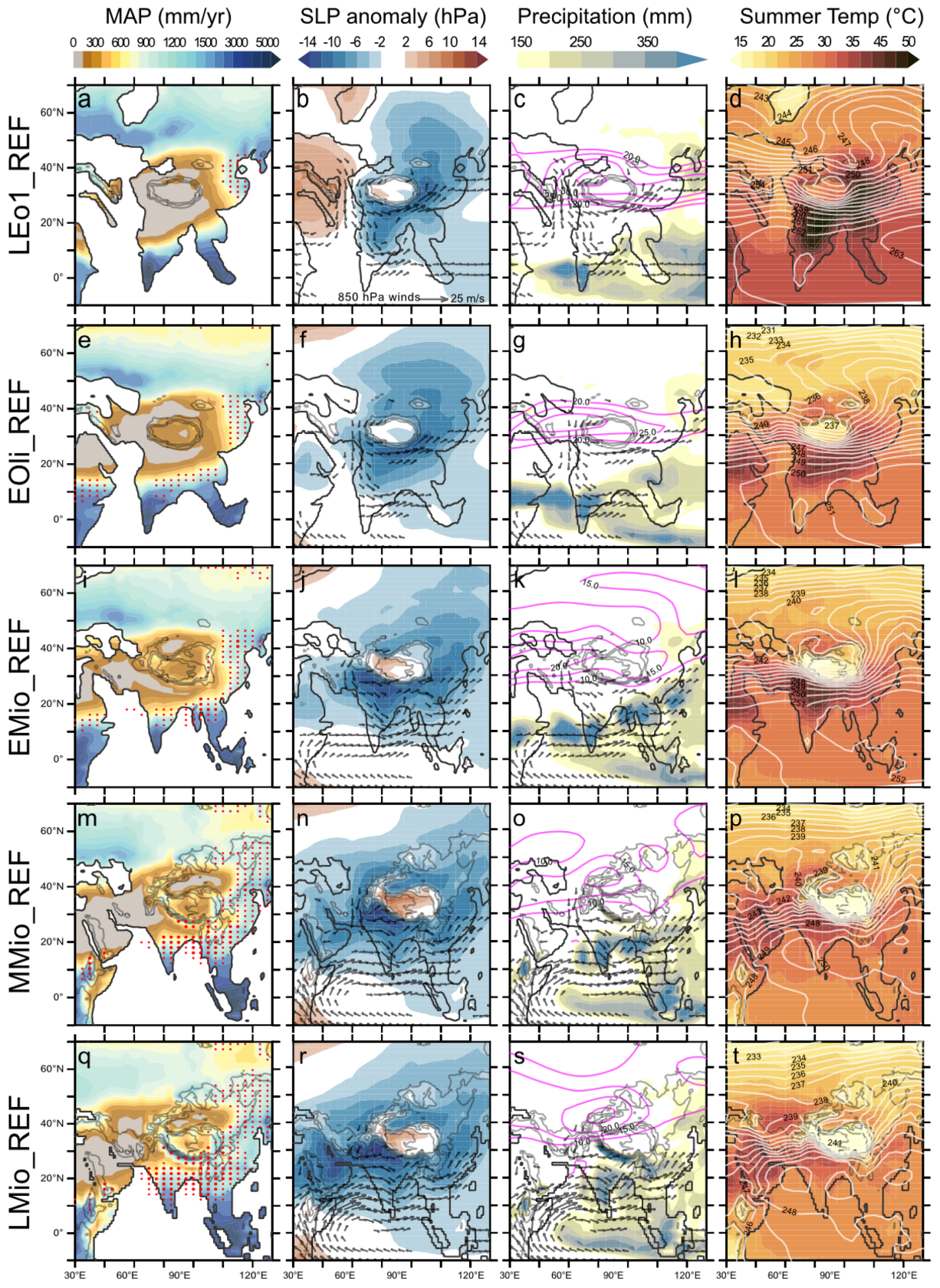
MAP (mm/yr)
0 300 600 900 1200 1500 3000 5000
SLP anomaly (hPa)
-14 -10 -6 -2 2 6 10 14
Precipitation (mm)
150 250 350
Summer Temp (°C)
15 20 25 30 35 45 50
LEo1_REF
EOli_REF
EMio_REF
MMio_REF
LMio_REF
850 hPa winds
25 m/s
60°N
40°N
20°N
0°
30°E
60°E
90°E
120°E

Figure 4

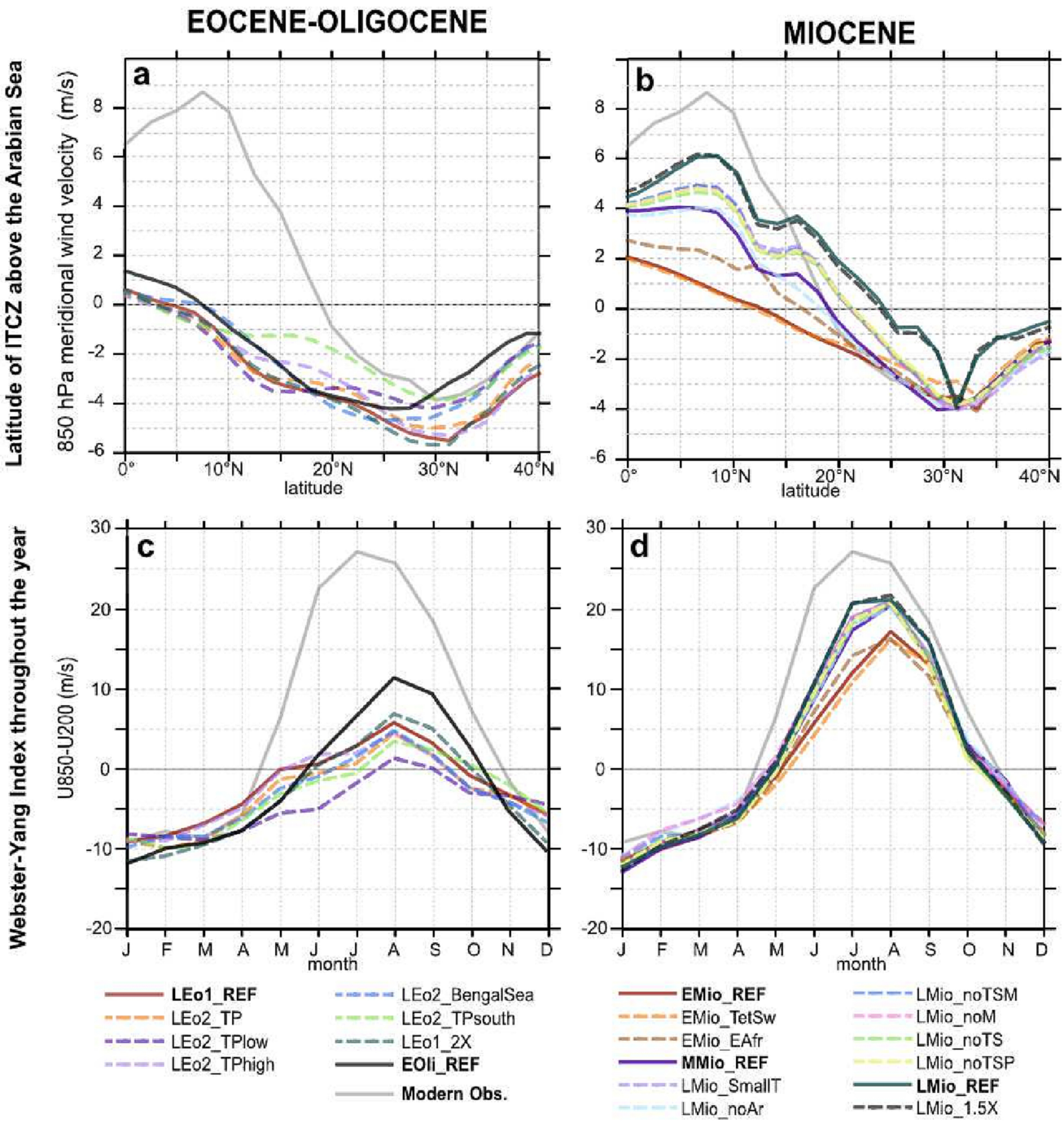
EOCENE-OLIGOCENE
MIOCENE
Latitude of ITCZ above the Arabian Sea
850 hPa meridional wind velocity (m/s)
a
b
latitude
Webster-Yang Index throughout the year
U850-U200 (m/s)
c
d
month
LEo1_REF
LEo2_TP
LEo2_TPlow
LEo2_TPhigh
LEo2_BengalSea
LEo2_TPsouth
LEo1_2X
EOli_REF
Modern Obs.
EMio_REF
EMio_TetSw
EMio_EAfr
MMio_REF
LMio_SmallT
LMio_noAr
LMio_noTSM
LMio_noM
LMio_noTS
LMio_noTSP
LMio_REF
LMio_1.5X

Figure 5

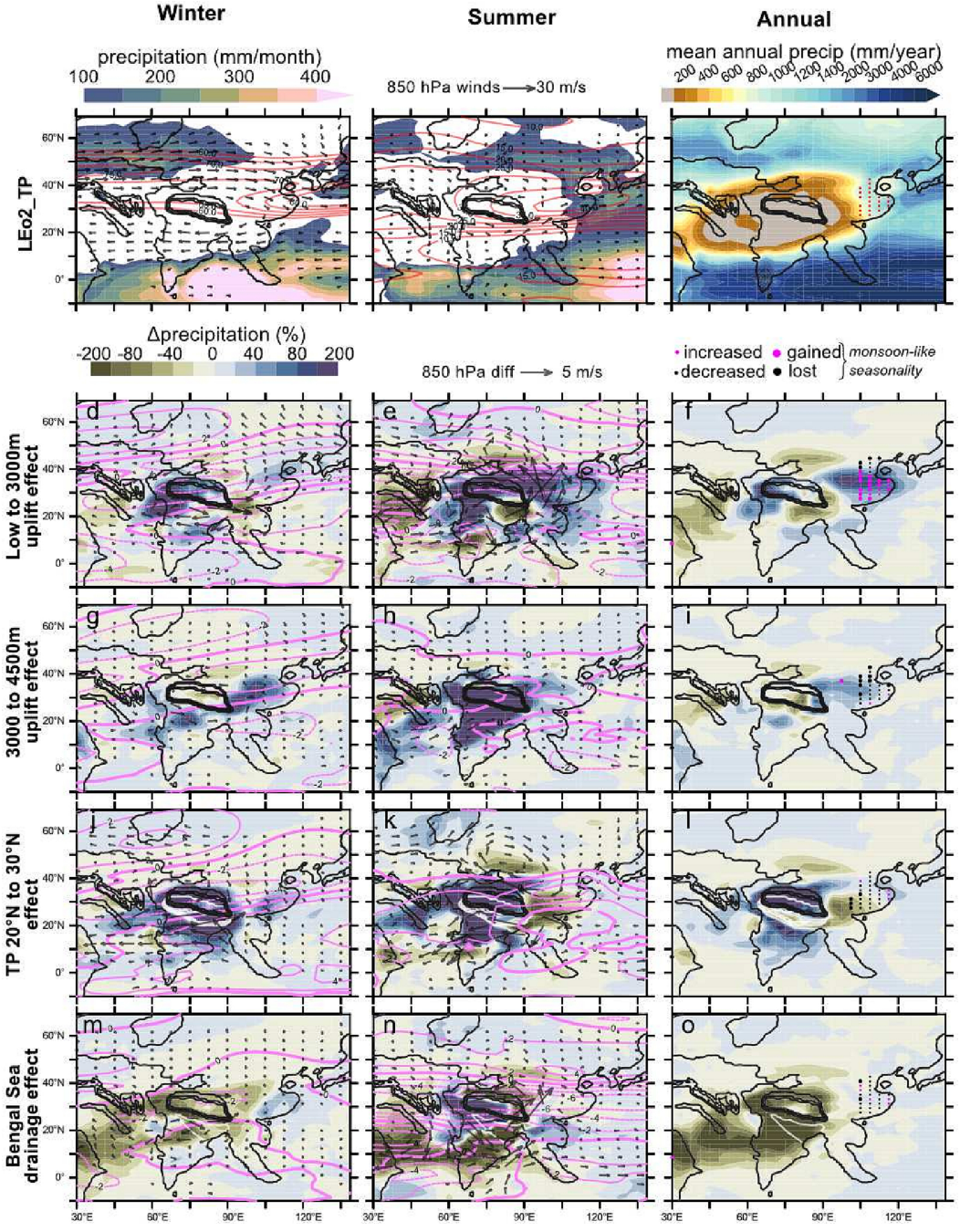
Winter
Summer
Annual
precipitation (mm/month)
100 200 300 400
850 hPa winds ⟶ 30 m/s
mean annual precip (mm/year)
200 400 600 800 1000 1200 1400 2000 3000 4000 6000
LEo2_TP
Δprecipitation (%)
-200 -80 -40 0 40 80 200
850 hPa diff ⟶ 5 m/s
increased
decreased
gained
lost
monsoon-like
seasonality
Low to 3000m uplift effect
3000 to 4500m uplift effect
TP 20°N to 30°N effect
Bengal Sea drainage effect
60°N
40°N
20°N
0°
30°E
60°E
90°E
120°E

Figure 6

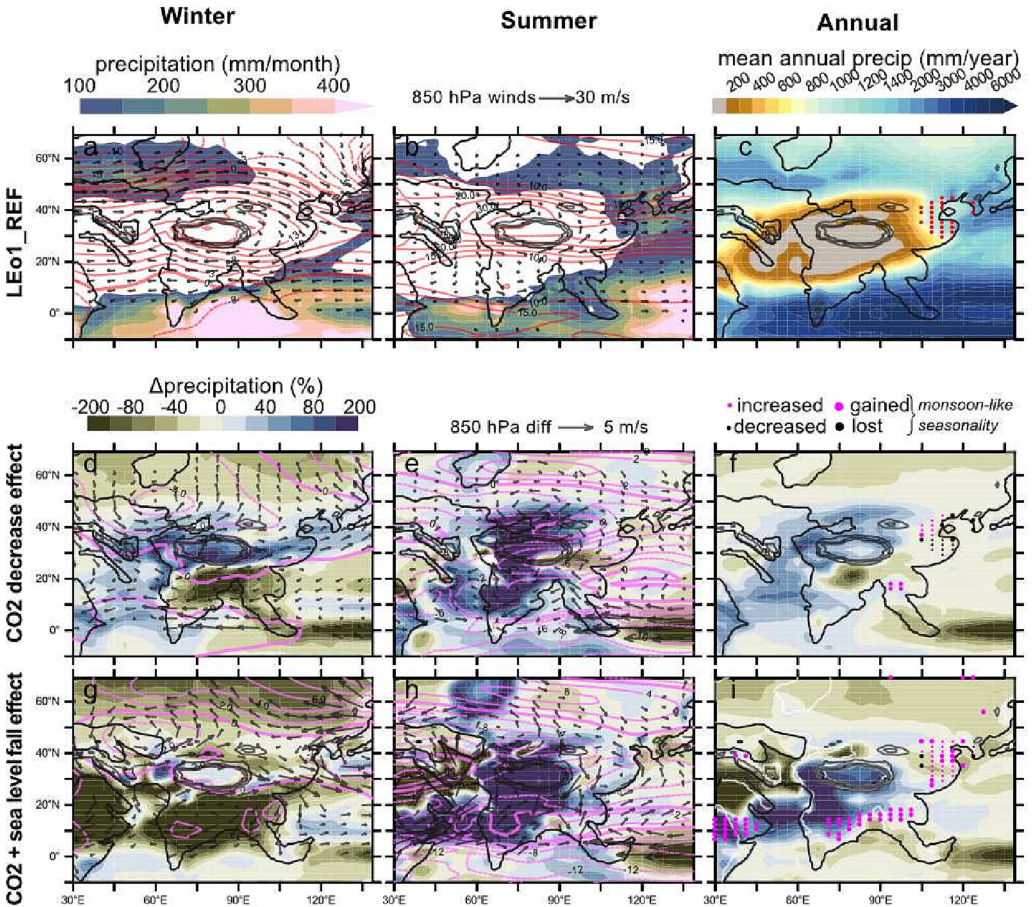
Winter
Summer
Annual
precipitation (mm/month)
100 200 300 400
850 hPa winds ⟶ 30 m/s
mean annual precip (mm/year)
200 400 600 800 1000 1200 1400 2000 3000 4000 6000
LEo1_REF
a
b
c
Δprecipitation (%)
-200 -80 -40 0 40 80 200
850 hPa diff ⟶ 5 m/s
increased
decreased
gained
lost
monsoon-like seasonality
CO2 decrease effect
CO2 + sea level fall effect
d
e
f
g
h
i
60°N
40°N
20°N
0°
30°E
60°E
90°E
120°E

Figure 7

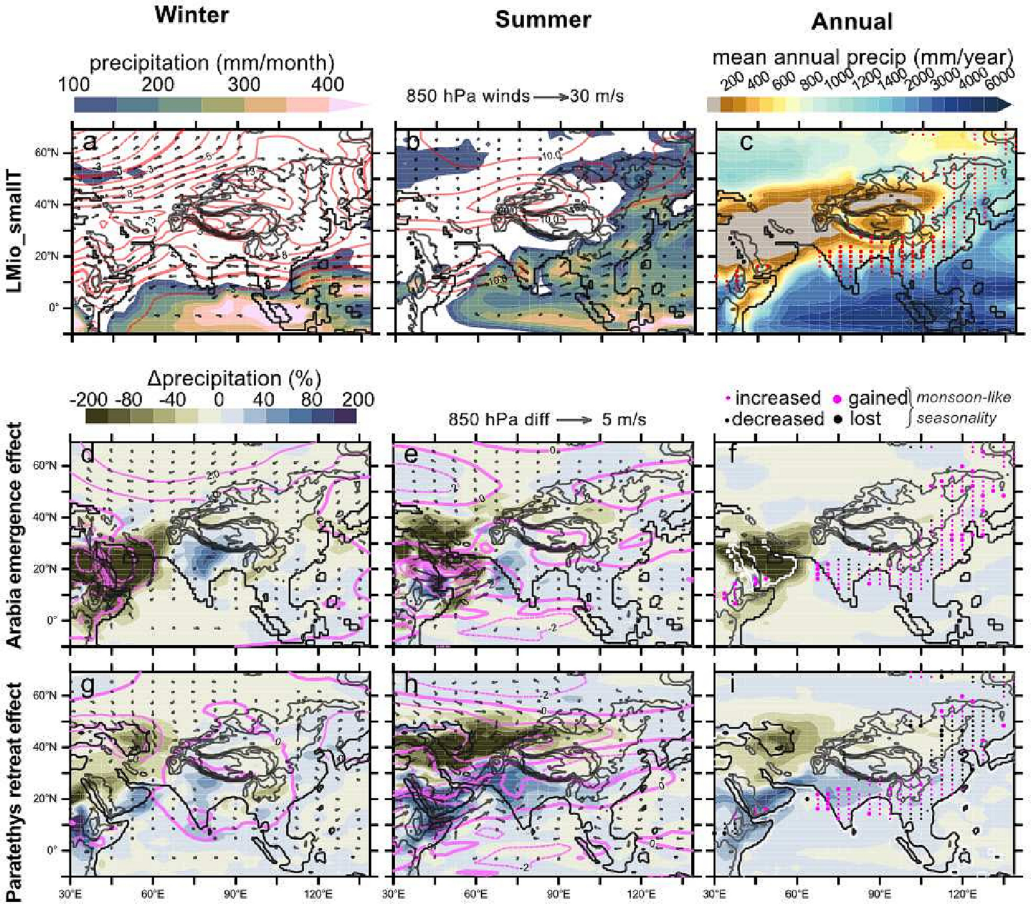
Winter
Summer
Annual
precipitation (mm/month)
100 200 300 400
850 hPa winds → 30 m/s
mean annual precip (mm/year)
200 400 600 800 1000 1200 1400 2000 3000 4000 6000
LMio_smallT
a
b
c
Δprecipitation (%)
-200 -80 -40 0 40 80 200
850 hPa diff → 5 m/s
increased
decreased
gained
lost
monsoon-like
seasonality
Arabia emergence effect
Paratethys retreat effect
d
e
f
g
h
i
60°N
40°N
20°N
0°
30°E
60°E
90°E
120°E

Figure 8

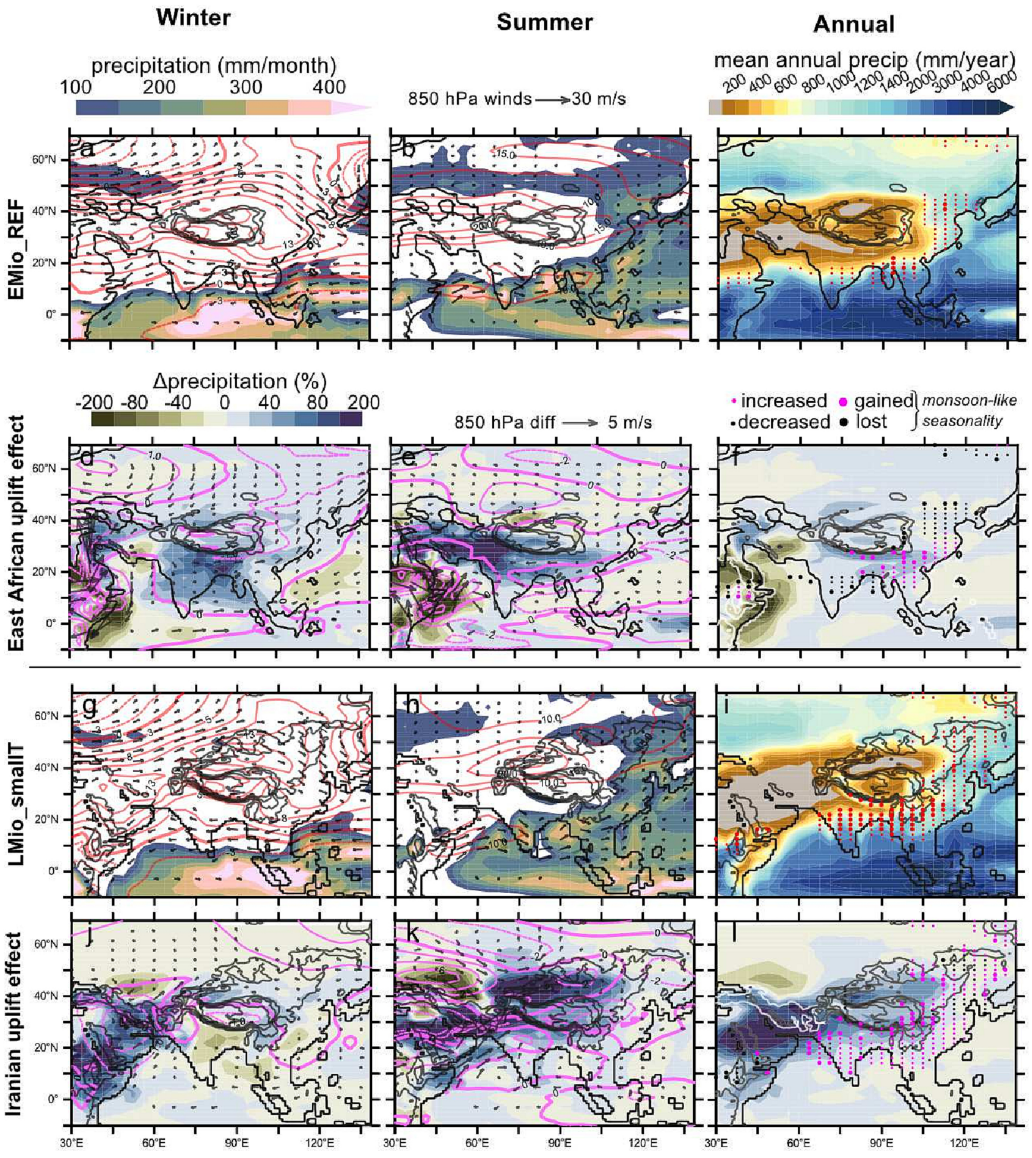
Winter
Summer
Annual
precipitation (mm/month)
100 200 300 400
850 hPa winds ⟶ 30 m/s
mean annual precip (mm/year)
200 400 600 800 1000 1200 1400 2000 3000 4000 6000
EMio_REF
Δprecipitation (%)
-200 -80 -40 0 40 80 200
850 hPa diff ⟶ 5 m/s
increased
decreased
gained
lost
monsoon-like seasonality
East African uplift effect
LMio_smallT
Iranian uplift effect
60°N
40°N
20°N
0°
30°E
60°E
90°E
120°E

Figure 9

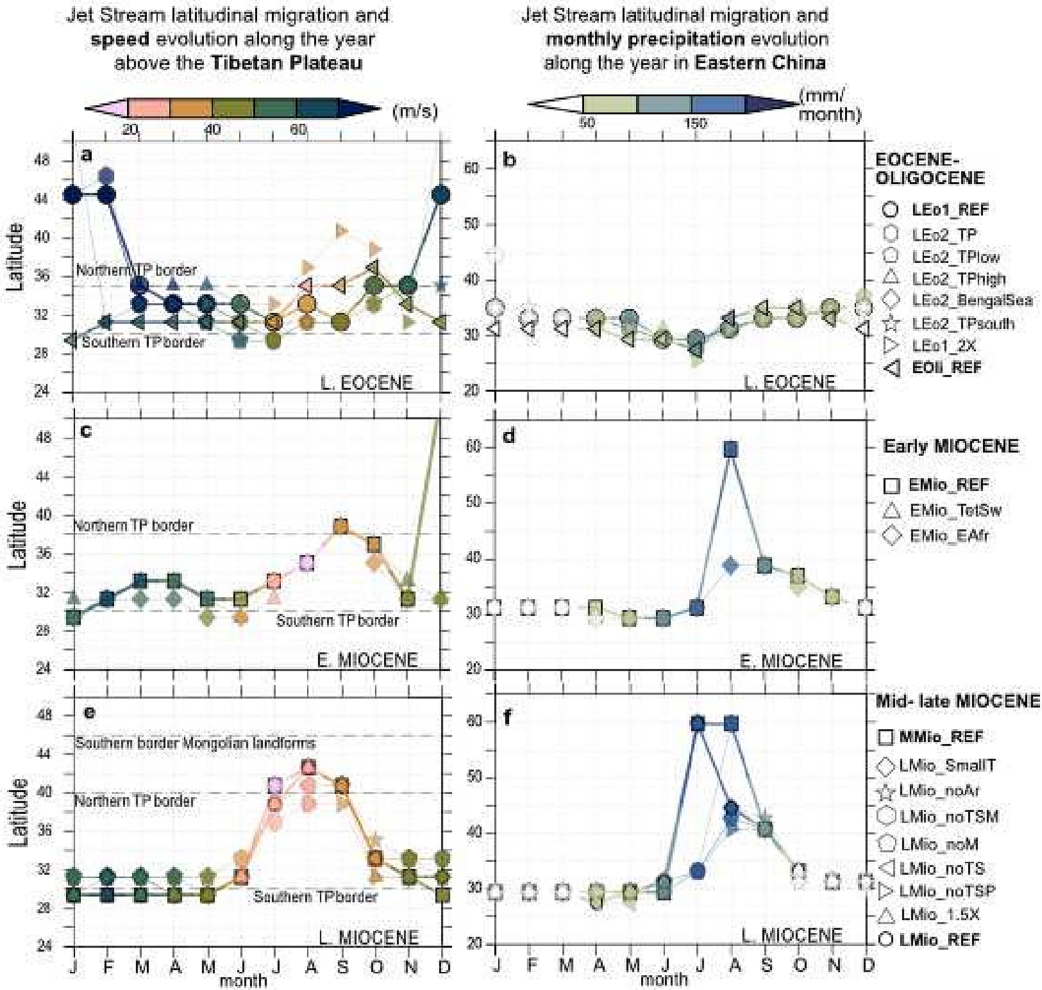
Jet Stream latitudinal migration and
speed evolution along the year
above the Tibetan Plateau
(m/s)
20
40
60
Jet Stream latitudinal migration and
monthly precipitation evolution
along the year in Eastern China
(mm/
month)
50
150
a
b
c
d
e
f
Latitude
Northern TP border
Southern TP border
Southern border Mongolian landforms
L. EOCENE
E. MIOCENE
L. MIOCENE
J F M A M J J A S O N D
month
EOCENE-
OLIGOCENE
LEo1_REF
LEo2_TP
LEo2_TPlow
LEo2_TPhigh
LEo2_BengalSea
LEo2_TPsouth
LEo1_2X
EOII_REF
Early MIOCENE
EMio_REF
EMio_TetSw
EMio_EAfr
Mid- late MIOCENE
MMio_REF
LMio_SmallT
LMio_noAr
LMio_noTSM
LMio_noM
LMio_noTS
LMio_noTSP
LMio_1.5X
LMio_REF

Figure 10

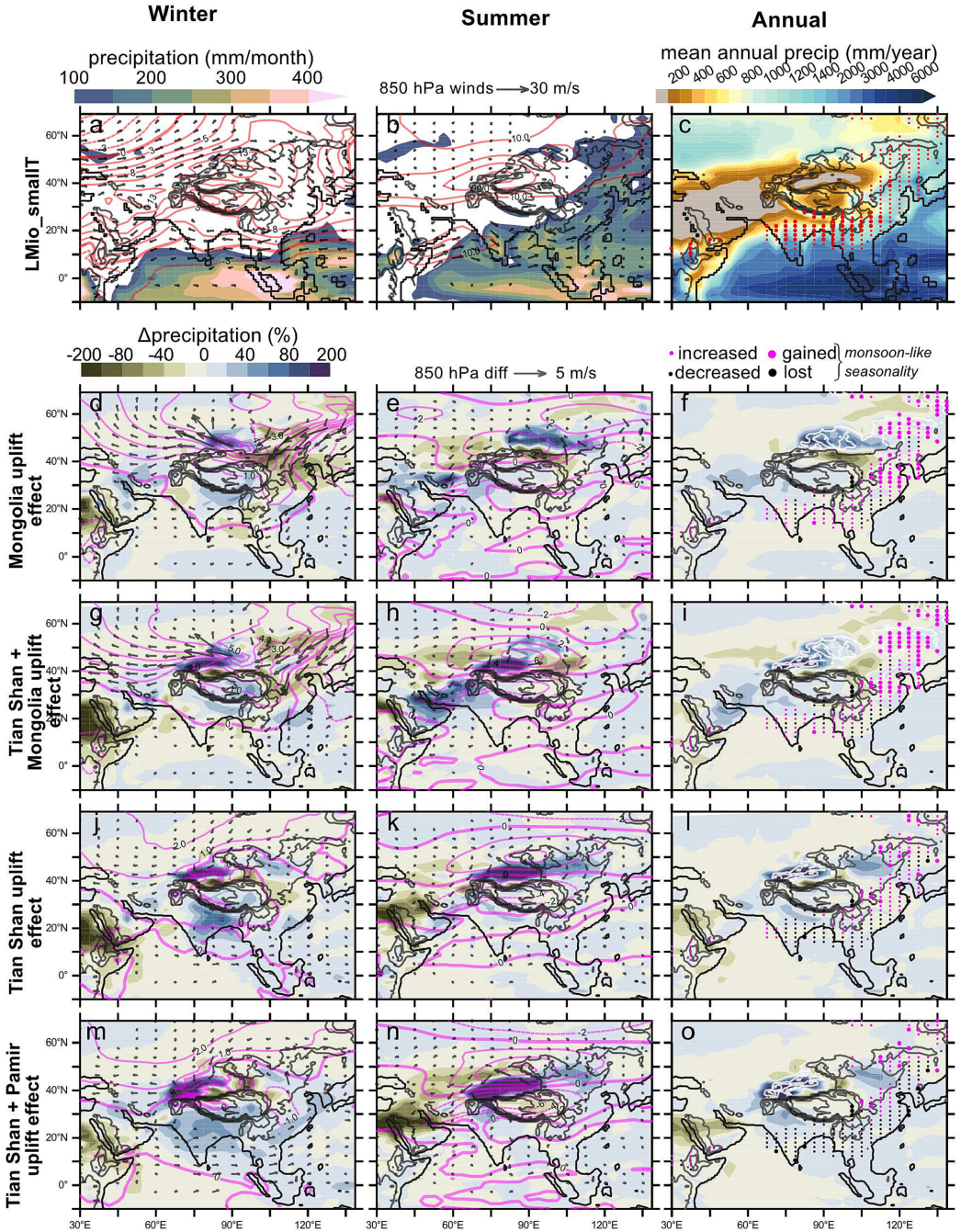
Winter
Summer
Annual
precipitation (mm/month)
100 200 300 400
850 hPa winds → 30 m/s
mean annual precip (mm/year)
200 400 600 800 1000 1200 1400 2000 3000 4000 6000
LMio_smallT
Δprecipitation (%)
-200 -80 -40 0 40 80 200
850 hPa diff → 5 m/s
increased
decreased
gained
lost
monsoon-like
seasonality
Mongolia uplift effect
Tian Shan + Mongolia uplift effect
Tian Shan uplift effect
Tian Shan + Pamir uplift effect
a
b
c
d
e
f
g
h
i
j
k
l
m
n
o
60°N
40°N
20°N
0°
30°E
60°E
90°E
120°E

Figure 11

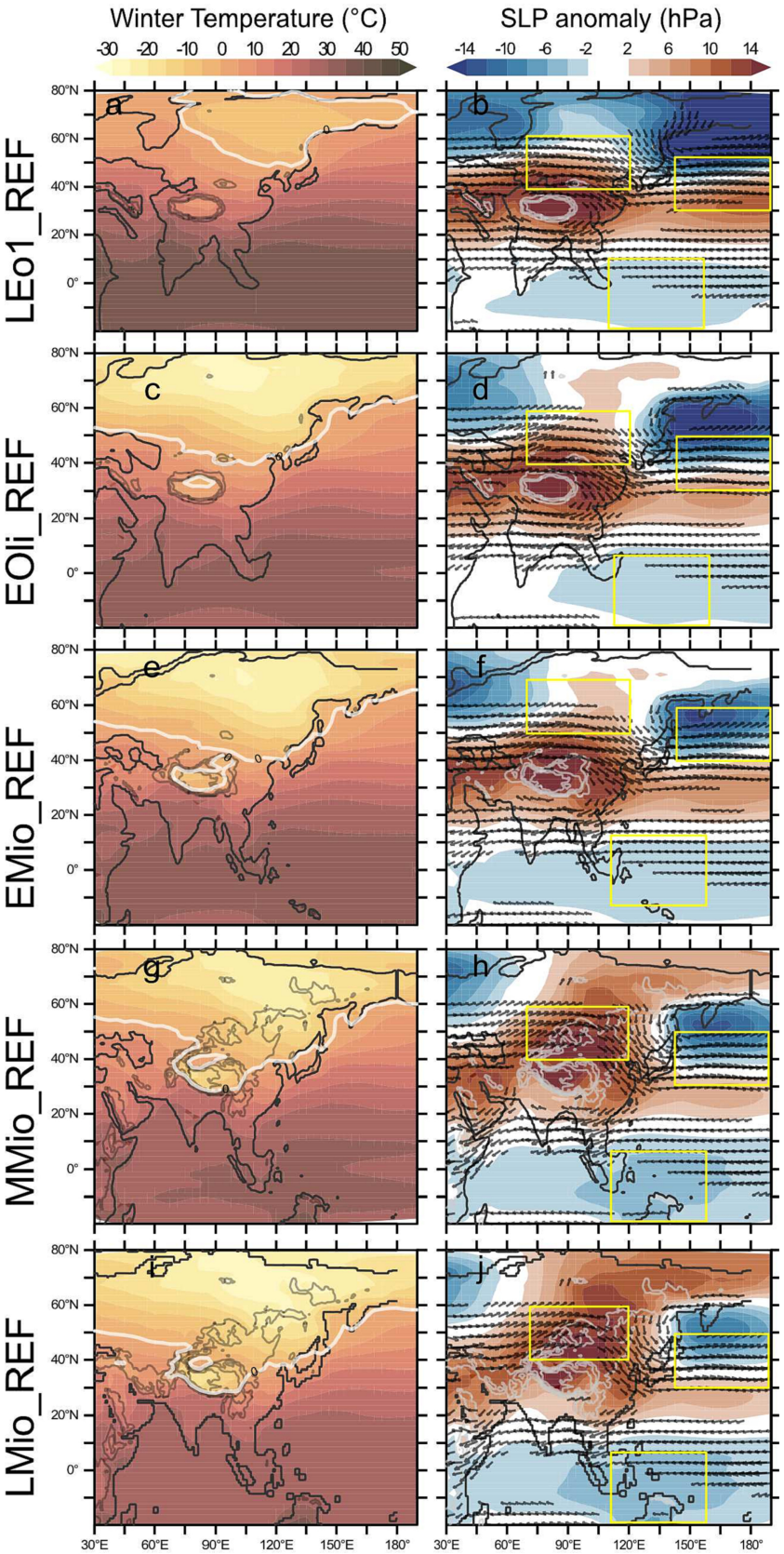
Winter Temperature (°C)
-30 -20 -10 0 10 20 30 40 50
SLP anomaly (hPa)
-14 -10 -6 -2 2 6 10 14
LEo1_REF
EOli_REF
EMio_REF
MMio_REF
LMio_REF
a
b
c
d
e
f
g
h
i
j
80°N
60°N
40°N
20°N
0°
30°E
60°E
90°E
120°E
150°E
180°

Figure 12

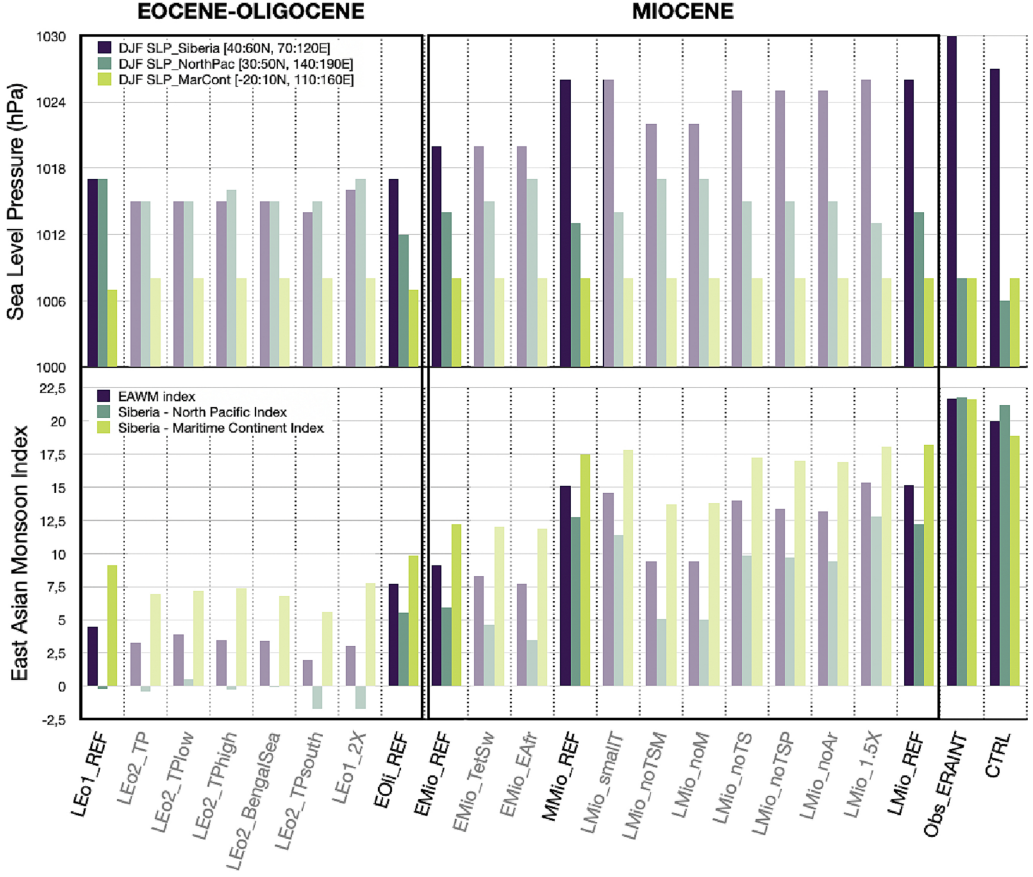
EOCENE-OLIGOCENE
MIOCENE
DJF SLP_Siberia [40:60N, 70:120E]
DJF SLP_NorthPac [30:50N, 140:190E]
DJF SLP_MarCont [-20:10N, 110:160E]
Sea Level Pressure (hPa)
1030
1024
1018
1012
1006
1000
EAWM index
Siberia - North Pacific Index
Siberia - Maritime Continent Index
East Asian Monsoon Index
22,5
20
17,5
15
12,5
10
7,5
5
2,5
0
-2,5
LEo1_REF
LEo2_TP
LEo2_TPlow
LEo2_TPhigh
LEo2_BengalSea
LEo2_TPsouth
LEo1_2X
EOli_REF
EMio_REF
EMio_TetSw
EMio_EAfr
MMio_REF
LMio_smallT
LMio_noTSM
LMio_noM
LMio_noTS
LMio_noTSP
LMio_noAr
LMio_1.5X
LMio_REF
Obs_ERAINT
CTRL

Figure 13